(2)

A STUDY OF THE EFFECT OF NITROGEN AND MOLYBDENUM IN THE CORROSION INHIBITION OF AUSTENITIC STAINLESS STEEL

by

Donggil Kim

Doctor of Philosophy

in

Materials Science and Engineering

State University of New York at Stony Brook

1992

SECURITY CLASSIFICATION OF THIS PAGE

REPORT DOCUMENTATION PAGE

1a REPORT SECURITY CLASSIFICATION: Unclassified	1b. RESTRICTIVE MARKINGS
2a SECURITY CLASSIFICATION AUTHORITY	3. DISTRIBUTION/AVAILABILITY OF REPORT
2b DECLASSIFICATION/DOWNGRADING SCHEDULE	
4. PERFORMING ORGANIZATION REPORT NUMBER(S)	5. MONITORING ORGANIZATION REPORT NUMBER(S)
6a NAME OF PERFORMING ORGANIZATION / 6b. OFFICE SYMBOL (If applicable)	7a. NAME OF MONITORING ORGANIZATION
6c. ADDRESS (City, State and ZIP Code)	7b. ADDRESS (City, State and ZIP Code)
8a. NAME OF FUNDING/SPONSORING ORGANIZATION: Dept. of Matls. Sci.& Eng. SUNY / 8b. OFFICE SYMBOL (If applicable)	9. PROCUREMENT INSTRUMENT IDENTIFICATION NUMBER
8c. ADDRESS (City, State and ZIP Code): Dept. of Matls. Sci. and Eng. SUNY, Stony Brook, NY 11794-2275	10 SOURCE OF FUNDING NOS. — PROGRAM ELEMENT NO. / PROJECT NO. / TASK NO. / WORK UNIT NO.
11 TITLE (Include Security Classification)	

12. PERSONAL AUTHOR(S): CLIVE R. CLAYTON AND DONGGIL KIM

13a TYPE OF REPORT	13b. TIME COVERED	14. DATE OF REPORT (Yr., Mo., Day)	15. PAGE COUNT
FINAL	FROM _____ TO _____	1992 July, 10,	197

16. SUPPLEMENTARY NOTATION

17. COSATI CODES			18. SUBJECT TERMS (Continue on reverse if necessary and identify by block number)
FIELD	GROUP	SUB GR.	

19. ABSTRACT (Continue on reverse if necessary and identify by block number)

The synergistic effect of N and Mo in remarkably improving the corrosion resistance of austenitic stainless steels in Cl^- containing solution has been investigated. Electrochemical techniques in conjunction with X-ray photoelectron spectroscopy (XPS) were utilized to elucidate the mechanism by which N and Mo influence the passivation behavior of austenitic stainless steel.

Since nitrates and nitrites are known to be powerful corrosion inhibitors, the possibility that alloyed nitrogen was capable of oxidizing to either of these species was considered. While no evidence could be found of NO_3^- formation by XPS, it was decided to further clarify this issue by considering the stability of NO_3^- ions on the surface of pure Cr and a variety of Mo bearing stainless steels polarized through an extensive range of

20 DISTRIBUTION/AVAILABILITY OF ABSTRACT: UNCLASSIFIED/UNLIMITED ☐ SAME AS RPT. ☐ DTIC USERS ☐	21. ABSTRACT SECURITY CLASSIFICATION
22a NAME OF RESPONSIBLE INDIVIDUAL	22b TELEPHONE NUMBER (Include Area Code) / 22c OFFICE SYMBOL

DD FORM 1473, 83 APR — EDITION OF 1 JAN 73 IS OBSOLETE.

SECURITY CLASSIFICATION OF THIS PAGE

potentials. Nitrate was found to be unstable at all potentials considered provided that the metal was exposed directly to the solution. This resulted in clear evidence that alloyed nitrogen does not oxidize to NO_3^- or NO_2^-. Indeed a new mechanism by which nitrates inhibit corrosion was uncovered.

The apparent synergistic effect of Mo-N in improving the corrosion of austenitic stainless steels has been investigated from two points of view: (1) the influence on N and Mo on the composition of the alloy just beneath the passive film and (2) the influence of N and Mo on the structure and function of the passive film.

Enrichment of metallic Ni beneath the passive films of austenitic stainless steels was observed. This enrichment increased with a small addition of Mo with N. Evidence was found of the formation of stable intermetallic phase consisting of a mixed Mo-Ni nitride. The phase appeared to result from a tendency of N to selectively enhance the anodic dissolution of Fe and to render conditions favorable for stronger atomic interactions between Ni and Mo, according to the Engel-Brewer model of intermetallic bonding. The metallic phase was seen as a component to the passivation process in a manner not considered previously.

The passive films of Mo bearing austenitic stainless steels polarized in acidic Cl^- solution exhibited a bipolar structure with MoO_4^{-2} providing a cation selective property to the outer region of the intrinsically anodically selective passive film. Improved resistance to Cl^- ion attack was attained by increasing the cation selective effectiveness of the outer portion of the passive film by enhancing the formation of MoO_4^{-2} instead of MoO_3 by lowering interfacial pH as a result of the protonation of nitrogen.

The nitrogen species observed in the passive films of all austenitic stainless steels studied were a surface nitride and NH_3. In 18-8 stainless steel, it was shown that NH_3 enhanced passivity by forming a more Cr-enriched passive film due to the increased selective dissolution of Fe ions. Evidence from pitting incubation time measurements suggested that the NH_3 improved the resistance to Cl^- ion attack. This is postulated to be due to NH_3 operating as a solid-state buffer to local acidification resulting from hydrolysis.

FINAL REPORT

TO

OFFICE OF RESEARCH

CONTRACT NO. N0001485K0437

A STUDY OF THE EFFECT OF NITROGEN AND MOLYBDENUM IN THE CORROSION INHIBITION OF AUSTENITIC STAINLESS STEEL

BY

CLIVE R. CLAYTON AND DONGGIL KIM

DEPARTMENT OF MATERIALS SCIENCE AND ENGINEERING

STATE UNIVERSITY OF NEW YORK

STONY BROOK, NY 11794-2275

Abstract of the Dissertation

A STUDY OF THE EFFECT OF NITROGEN AND MOLYBDENUM IN THE CORROSION INHIBITION OF AUSTENITIC STAINLESS STEEL

by

Donggil Kim

Doctor of Philosophy

in

Materials Science and Engineering

State University of New York at Stony Brook

1992

The synergistic effect of N and Mo in remarkably improving the corrosion resistance of austenitic stainless steels in Cl^- containing solution has been investigated. Electrochemical techniques in conjunction with X-ray photoelectron spectroscopy (XPS) were utilized to elucidate the mechanism by which N and Mo influence the passivation behavior of austenitic stainless steel.

Since nitrates and nitrites are known to be powerful corrosion inhibitors, the possibility that alloyed nitrogen was capable of oxidizing to either of

these species was considered. While no evidence could be found of NO_3^- formation by XPS, it was decided to further clarify this issue by considering the stability of NO_3^- ions on the surface of pure Cr and a variety of Mo bearing stainless steels polarized through an extensive range of potentials. Nitrate was found to be unstable at all potentials considered provided that the metal was exposed directly to the solution. This resulted in clear evidence that alloyed nitrogen does not oxidize to NO_3^- or NO_2^-. Indeed a new mechanism by which nitrates inhibit corrosion was uncovered.

The apparent synergistic effect of Mo-N in improving the corrosion of austenitic stainless steels has been investigated from two points of view: (1) the influence on N and Mo on the composition of the alloy just beneath the passive film and (2) the influence of N and Mo on the structure and function of the passive film.

Enrichment of metallic Ni beneath the passive films of austenitic stainless steels was observed. This enrichment increased with a small addition of Mo with N. Evidence was found of the formation of stable intermetallic phase consisting of a mixed Mo-Ni nitride.

The phase appeared to result from a tendency of N to selectively enhance the anodic dissolution of Fe and to render conditions favorable for stronger atomic interactions between Ni and Mo, according to the Engel-Brewer model of intermetallic bonding. The metallic phase was seen as a component to the passivation process in a manner not considered previously.

The passive films of Mo bearing austenitic stainless steels polarized in acidic Cl^- solution exhibited a bipolar structure with MoO_4^{-2} providing a cation selective property to the outer region of the intrinsically anodically selective passive film. Improved resistance to Cl^- ion attack was attained by increasing the cation selective effectiveness of the outer portion of the passive film by enhancing the formation of MoO_4^{-2} instead of MoO_3 by lowering interfacial pH as a result of the protonation of nitrogen.

The nitrogen species observed in the passive films of all austenitic stainless steels studied were a surface nitride and NH_3. In 18-8 stainless steel, it was shown that NH_3 enhanced passivity by forming a more Cr-enriched passive film due to the increased selective dissolution of Fe ions. Evidence from pitting incubation time

measurements suggested that the NH_3 improved the resistance to Cl^- ion attack. This is postulated to be due to NH_3 operating as a solid-state buffer to local acidification resulting from hydrolysis.

Table of Contents

List of Tables

Table 5.7 Thickness(Å) of the passive films of 18-8 alloys polarized at -180 mV.

List of Figures

Figure 8.2 Salient electrochemical characteristics vs. temperature for AL6X and AL6XN alloys polarized in 0.5M H_2SO_4. (a) Potentials(E_{br}, E_{pp} and E_{ocp}), (b) Critical current density(I_{crit}) and (c) Passivation current density(I_{pass})

1. INTRODUCTION

1.1 Statement of the Problem

Nitrogen, a powerful austenite stabilizer[1,2], has been shown to inhibit the precipitation of secondary phases[3-5], improves mechanical properties and enhances the effect of chromium and molybdenum in improving localized corrosion resistance and the passivation characteristics of stainless steels.[2,3-8] During anodic dissolution of high N austenitic stainless steels, it has been shown, in this laboratory, that nitrogen is segregated to the passive film-metal interface where it forms a relatively stable surface nitride phase. This stable nitride is associated with improvements in passivation (reduction in active corrosion) and pitting resistance.[3,5-11] Such improvements are found to be greatest when Mo is present in the steel.

A major question addressed in this dissertation is whether during passivation alloyed N becomes oxidized to NO_2^- or NO_3^- at anodic potentials, which are effective corrosion inhibitors. This issue has been considered from the perspective of the stability of NO_3^- ions on metal

surface at anodic potentials. One aspect of this research is to compare the influence of N alloying and nitrate inhibitors on passivity of stainless steels. Also NH_3 have been reported to be observed in the passive film of stainless steel polarized in a Cl^- containing solution. The role of bound NH_3 on the passivity of stainless steel has not been considered previously.

It is well known that molybdenum has a very strong effect on improving pitting resistance and lowering the rate of anodic dissolution of stainless steel.[8,12] In addition, a small amount of added nitrogen improves the effects of molybdenum through an apparent synergism which has not hitherto been explained.[10,13-15] The Mo-N synergism was evaluated from two perspectives: (1) the role of Mo and N in determining the structure and function of the passive oxide film, (2) the influence of Mo and N on the alloy composition at the interface and within the passive oxide film. The influence of N on the local pH and the pH sensitive formation of MoO_4^{-2} in the passive film was evaluated in the special cases of Mo_2N and Mo bearing steels. In each case, it was observed that the MoO_4^{-2} species of the passive film increased in the presence of N additions. Even though metallic Ni enrichment

underneath the passive film has been reported by many studies,[9,16-19] no mechanism by which Ni enrichment may influence on the passivity has been reported. In this work, we have considered the possible metal phase contribution to the apparent Mo-N synergism.

We have, for the first time, determined the existence of Mo^{+5} as a constituent of the passive film of Mo-bearing steel polarized in Cl^- solution through various experiments for Mo^{+5} standards.

1.2 Experimental Methodology

The primary experimental techniques for this research were electrochemical and XPS analysis. Electrochemical analysis was utilized to investigate the general corrosion behavior of the materials considered. Individual specimens were prepared under specific electrochemical conditions for XPS analysis to aid in interpreting the electrochemical behavior. Using variable angle X-ray photoelectron spectroscopy which provides in-depth non-destructive analysis, the structure and the composition of the passive layers and the substrate were investigated. X-ray diffraction was only utilized for

identifying various synthesized Mo compounds, needed for spectral analysis of standards.

1.3 Summary of the Results

Surface nitrides were formed under conditions leading to the direct exposure of metal surface to the electrolyte, by the direct reduction of NO_3^- ions regardless of applied potentials. The role of the surface nitride formed cathodically from NO_3^- ions, is analogous to that formed from anodic segregation of nitrogen in a N alloyed steel. The surface nitride enhances the pitting resistance of stainless steels, because the nitride acts as (a) a precursor to the passive film (b) a buffer to local acidity, thus stabilizing the first formed layers of the passive film.

Mo additions to stainless steel improve pitting resistance and lowered the rate of active dissolution. The N in Mo bearing steel was segregated as a surface nitride phase and further suppressed active dissolution through an apparent Mo-N synergism. For Fe20Cr20Ni steel, only metallic Cr enrichment was observed underneath the passive film. Comparison of Fe20Cr20Ni6Mo and Fe20Cr20Ni,

showed that metallic Ni and Mo enrichment in the former increased by the apparent formation of a Mo-Ni intermetallic phase, while metallic Cr enrichment decreased. With 0.2 wt%N addition to the Fe20Cr20Ni6Mo alloy, a subsequent decrease in Cr enrichment and increase in Ni and Mo enrichments were observed. Also N in Mo bearing alloys enhances the passivity in Cl^- solution by increasing the bipolarity of the passive film due to the preferred formation of MoO_4^{-2} rather than MoO_3.

Increasing the N content of an 18-8 stainless steel improves the pitting resistance and reduces the critical current density and the passive current density by making NH_3 complex with Cr^{+3} to form $[Cr(NH_3)_5OH_2]^{+3}$. The NH_3 complex in the passive film reduces the packing density, enhances the selective dissolution of Fe^{+2} and Fe^{+3} in the passive film rendering a more Cr-enriched passive film. This Cr-enriched film improves the pitting resistance and reduces the passive current density.

The passive film of pure Mo and Mo_2N, polarized in Cl^- contained solution, were comprised of Mo^{+4} and Mo^{+5} cations. It has been observed that N also enhances the passivity of pure Mo by increasing the local pH and suppressing the formation of MoO_3, which is the main

species in the transpassive region.

According to an extensive investigation in separated work presented in the Appendix, the existence of Mo^{+5} in the passive film of pure Mo and stainless steel is proved and the binding energy of Mo^{+5} 3p photoelectrons is determined.

1.4 Outline of the Dissertation

A literature survey of the studies of the effect of Mo and N on the corrosion behavior of austenitic stainless steel is presented in Chapter 2. The principles of XPS including the variable angle technique and the quantitative analysis methods are reviewed in Chapter 3. The experimental details are supplied in Chapter 4. The results and a discussion of the findings of this research effort are presented in Chapter 5 and 6, respectively. The conclusions and recommendations for future investigations appear in Chapter 7 and 8, respectively. The extensive work, in which the binding energy of Mo^{+5} 3d spectra was determined, is added in the Appendix.

2. LITERATURE SURVEY

2.1 The Study of NO_3^- Stability and Its Corrosion Inhibition Property

Nitrate anions are known to have strong inhibitive effects on the corrosion rate of many metals and alloys. Numerous papers have been devoted to understanding the mechanism by which NO_3^- operates. Kouldelkova and Augustynski[20] have studied the behavior of NO_3^- on an aluminum alloy polarized from -340 mV (Open Circuit Potential) to 1490 mV (SCE, passive region) in 1M NO_3^- /0.1M Cl^- solution. Their N1s XPS spectra of the passive film showed peaks at 399.8 eV and 407.0 eV. The position of the peak at 399.8 eV was the binding energy of the N1s electron of NH_4^+ formed by reduction of NO_3^-. McKissick et al.[21] studied weight loss of Al alloys as a function of NO_3^- concentration in Cl^- solutions. They found that, by varying the NO_3^- concentration from 0.0 up to 0.012N $NaNO_3$ in 0.01N NaCl, an initial parabolic increase in weight loss was yielded as the NO_3^- was increased to 0.006N. Upon increasing the NO_3^- concentration to 0.012N, they observed a decrease in weight loss of the Al alloy.

For NO_3^- concentrations higher than 0.01N, the weight loss observed was negligible. They attributed this parabolic weight loss behavior to NO_3^- being reduced to NO_2^-. Using cyclic voltammetery, Pletcher and Poorabedi[22] performed nitrate reduction studies on copper. From the solution analysis, they found that NH_3 was the predominant reduction species of nitrate and that the rate of NO_3^- reduction was proportional to the proton concentration in the solution. They proposed that protonation occurred prior to reduction of the NO_3^- ion. The reduction of NO_3^- to nitride has been reported by Datta et al.[23] They analyzed the transpassive dissolution of nickel in 6M $NaNO_3$ + 0.1M NaOH and have found that nitride corresponding to a N1s binding energy of 397.5 eV was retained at the metal-oxide interface. This surface nitride was conjectured as either resulting from a direct interaction between nitrate and the metal surface or a result of a NO_3^- reduction reaction that occurred after the anodic current was turned off. Newman et al.[24,25] reported that, when a nitrogen-free alloy was polarized in 4M HCl + 2M $NaNO_3$ solution, an effect of NO_3^- addition was similar to that of the alloyed N. This effect was attributed to the electroreduction of the NO_3^-

ions in solution. However the nature of the surface nitrogen was not explained. In previous studies performed in this laboratory,[10,26,27] NO_3^- reduction on pure metals and stainless steels and surface nitride formation at cathodic potential were reported using the XPS technique. That work has been further extended in this dissertation in order to elucidate the nature of the Mo-N synergism.

2.2 The Role of N and Mo on the Corrosion of Austenitic Stainless Steels

Nitrogen alloying has been successfully used to improve the mechanical properties of commonly used austenitic stainless steels commonly used. Early evidence of enhanced resistance to the initiation of pitting by alloying with nitrogen was reported by Uhlig[28] and Streicher[12]. By comparing weight loss, Uhlig[28] concluded that the corrosion resistance of 0.24 wt%N austenitic 18-8 stainless steel in ferric chloride solution was approximately double that of 0.165 wt%N 18-8 alloy. Streicher,[12] investigating pitting corrosion of 18-8 steels in NaCl solution as a function of nitrogen and other alloying additions, observed that increasing the

Mo, N and/or Si content and reducing the C content, improved the pitting resistance. Further that combined additions of Mo, N and Si provided superior behavior to individual additions of these elements.

According to polarization studies in 0.5M H_2SO_4 + 0.5M NaCl by Eckenrod and Kovach[3] of 18-8 stainless steels containing 0.04 wt%N - 0.24 wt%N, it was found that increasing the N content resulted in a significant reduction in the critical and the passive current densities and an increase in the pitting potentials. Chigal et al.[29] and Kolotyrkin et al.[30] reported on the anodic polarization of Fe20Cr20Ni stainless steels containing 0.05, 0.38 and 0.50 wt%N in 1M $HClO_4$ + 0.3M NaCl. Their work showed that increasing the N content also resulted in the lowering of the critical current density and the dissolution rate of the alloy.

Osozawa and Okato[8,31] have reported that, in deaerated 4 wt% NaCl solution at 30°C, a 0.2 wt%N addition to a 17Cr22Ni1.5Mo steel corresponded to approximately a 4 wt% increase of Cr as estimated by the pitting potential. In addition, the authors reported on the presence of NH_4^+ ions, by solution analysis after pitting corrosion tests. Therefore, it was suggested that

the formation of NH_4^+ ions reduced the local acidification within the pit, aiding repassivation before pit growth occurred. N as an alloying element to improve pitting corrosion resistance was also reported by Kearns et al.[5] and Truman et al.[2] Kearns et al.[5] reported that N additions to low carbon austenitic stainless steels containing molybdenum improved crevice corrosion resistance, intergranular corrosion resistance and passivation characteristics by electrochemical testing in acidic and chloride containing solutions. Newman[24,25,32,33] reported the effect of nitrogen on the anodic behavior of austenitic stainless steel in a Cl^- containing acidic solution. In that work, the reduction of anodic dissolution rate was observed during the polarization of N-bearing stainless steel in Cl^- solution or N-free steel in Cl^-/NO_3^- solution. These results were affected by the enrichment of surface nitrogen during the polarization. Truman et al.[2] showed that N was more effective in improving corrosion resistance in the presence of Mo, suggesting a possible synergism between Mo and N. In another study, Bandy and Van Rooyen[13] examined the pitting resistance of an experimental stainless steel(alloy 30-C) with a nominal composition

of 22Cr-21Ni-6Mo-0.49N. Comparative anodic polarization studies with the commercial alloy AL6X (20Cr-24Ni-6.5Mo-0.04N) in deaerated 0.5M HCl + 3M NaCl at 50°C showed immediate pitting of AL6X whereas alloy 30-C became fully passive after some incipient breakdown.

In a further study of 30-C, surface analysis by Auger electron spectroscopy(AES) and X-ray photoelectron spectroscopy(XPS) was performed in this laboratory after 24 hours passivation at 500 mV(SCE) in a deaerated SO_4^{-2} containing solution and in a Cl^- containing solution at 22°C.[6,7,14] It was observed that N as a surface nitride was enriched to about 7 times its bulk level at the oxide-metal interface. This excessive segregation of nitrogen was caused by selective dissolution of metal atoms at the surface. Recent studies[9,10,16-19,34] reported that Ni enrichment underneath the passive film of austenitic stainless steel was increased by raising the N content and that Ni appeared to play an important role in improving passivity and raising the pitting potential. Even though Ni nitride is unstable, a mixed nitride with Cr or Mo is very stable.[35] Therefore this surface nitride was conjectured to easily form at the oxide-metal interface and to improve passivation characteristics.

2.3 Models of the Effect of Nitrogen on Corrosion Resistance

Summarizing the earlier suggestions, the effects of nitrogen were grouped into three models:

(1) Consumption of protons in pit nuclei by nitrogen dissolution due to the reaction, $N + 4H^+ + 3e = NH_4^+$.[8] There are several apparent difficulties with this idea, but none is insuperable on closer examination. The beneficial effect of nitrogen often increases as other beneficial elements such as Mo are added, hence it is found that nitrogen is highly beneficial in alloys which already have rather high pitting potentials.[7,13] This appears to be inconsistent with a cathodic reaction (nitrogen dissolution) which is more rapid at low potential. Through the study of nitrate inhibition of pitting nitrogen stability on the surface and its related chemistry need to be reanalyzed.

(b) Enrichment of nitrogen below the passive film.[2,6,7,14] Many attempts have been made to related the surface compositions of passive alloys to their pitting behavior. On the basis of a uniform penetration of chloride ions, such compositional information would be

directly related to the resistance of the film to breakdown. Nitrogen has been shown to be strongly enriched under the passive film during prolonged passivation,[6,7,14] and one can therefore argue that a more rapid transient enrichment may occur at flaws where the local passive dissolution rate is much greater than that measured macroscopically. Such an enrichment might prevent rapid dissolution of the substrate following destruction of the film. This suggestion is not testable and it currently appears more profitable to explore effects of nitrogen in small, affectively dissolving pits. This approach is justified by the observation of unstable pitting at very low potentials[36] and by indications that alloyed nitrogen mainly affects the propagation rather than the initiation of pits.[31] In this model, the structure and compositions are not considered important. Therefore the relation between the stability of the passive film and the enrichment of nitrogen is not yet explained.

(3) Enrichment of nitrogen on an active surface.[9,14,16-19] This model offers the possibility of unifying the nitrogen effect with the molybdenum effect. The basis of this suggestion is that the dissolution of nitrogen to

ammonium, at sufficiently high positive potential, becomes too slow to keep up with the increasing rate of alloy dissolution. Nitrogen atoms will be enriched on the active surface and should have sufficient mobility to block some proportion of the mobile kink sites on the surface. A chemical interaction between N and metallic elements may be involved. In this research, analysis of the nature of this chemical interaction was attempted.

2.4 Passivation Behavior of Molybdenum

The literature on the passivity of Mo is quite mixed-especially those groups representing XPS data. However, on considering a range of electrochemical data for pure Mo,[10,18,26,37-40] it is apparent that pure Mo has a passive region in Cl^- containing solutions. In deaerated 0.1M HCl, for example, Mo is passive in the range between -396 mV to 125 mV(SCE). Many papers have contributed to the understanding of the nature of the passivity of molybdenum. Heumann and Hauck,[37] through the kinetics of dissolution of molybdenum in strong acid electrolytes (H_2SO_4, HCl, HNO_3, pH 0-2), observed that molybdenum dissolved with a valence of six and that the rate

controlling step is the transition from valence four to six. They concluded that MoO_2 was formed on the metal surface by anodic polarization and molybdenum dissolved from a passive state. This behavior was independently verified by Clayton and Lu[41] using a bipotentiostat. They found the evidence of MoO_4^{-2} release from pure Mo in 0.1M HCl, and subsequent deposition on a passive Cr electrode. Wikstrom and Nobe[42] measured capacitance values and reported that the passive film of pure Mo in 1N H_2SO_4 consisted of MoO_2. M. Hull[43] suggested that, by measuring the anodic dissolution current of molybdenum wire and disc electrodes in 1.0M H_2SO_4, the passive films had the composition MoO_2 and MoO_3.

Two groups, Kozhevnikov et al.[44] and Brox[45,46], analyzed the Mo surfaces passivated in 0.5M H_2SO_4 by XPS and concluded that no oxides of molybdenum were formed at potentials in the passive region. They concluded that the passive state was due to oxygen chemisorption. Ansell et al.[47] also examined the surface of molybdenum electrodes by XPS and found that Mo was slightly oxidized by deaerated water. Pozdeeva et al.[48] suggested that the passive film is a mixed oxide having an oxidation number ranging from 5.3 to 5.5. It was also suggested that, in

the transpassive region, the δ and Γ oxides i.e. $MoO_{1.97-2.06}$ and $MoO_{2.65-2.75}$ were formed and subsequently oxidized to the soluble product H_2MoO_4. At high potentials (>700 mV), a mixture of the β, β' and α phases, $MoO_{2.87}$-MoO_3, were considered to be formed. In another study, based on electrochemical data, König and Göhr[49] suggested that MoO_3 is formed in the transpassive region. Lu and Clayton[38] have reported that the passive film formed on molybdenum in deaerated 0.1M HCl is a compact thin film comprised of MoO_2 and $MoO(OH)_2$ and that the transpassive product of molybdenum is a mixture of MoO_2, $MoO(OH)_2$, Mo_2O_5 and MoO_3. However the existence of $MoO(OH)_2$ is brought into question in this dissertation due to a more extensive study of Mo^{+5} containing compounds, which is presented in the Appendix.

2.5 Bipolar Model of the Passivity of Stainless Steel

This model was proposed first by Sakashita and Sato[50] describing the ion-selective nature of porous bipolar product membranes. They suggested that passivity should, in principle, be reinforced when the film becomes bipolarized with an anion-selective inner layer and a

action-selective outer layer. Under these conditions, the outer layer would allow univalent cation such as H^+ to escape while inhibiting the ingress of anions such as OH^- and Cl^-. In another work by Sakashita and Sato,[51] hydrated Cr^{+3} and Fe^{+3} oxide membranes were found to be anion-selective in monovalent solutions but cation-selective in the presence of multivalent anions such as MoO_4^{-2} or CrO_4^{-2}. This indicated that the adsorption of molybdate on the membrane produced a cation-selective outer layer. Applying this model to the study of thin passive film, Clayton et al.[19,41,52-54] have shown that with the cation migration from the metal hindered by the anion-selective inner layer, a positive space charge will develope, causing the O^{-2} ions formed by deprotonation of OH^- to migrate to the metal surface and create a dehydrated oxide. Also, they have reported that the adsorption of molybdate on the film changes the inherent anion-selectivity of the outer region of the film to cation-selective. This produces effectively a bipolar film, which allows univalent cations to migrate out of the passive film while hindering the ingress of anions such as Cl^- and OH^-. Therefore this results in improving pitting resistance due to the reduction of Cl^-

adsorption. Schematic representation of the bipolar behavior of the passive film formed on stainless steel is presented in figure 2.1.

3. Variable Angle X-ray Photoelectron Spectroscopy

3.1 Introduction

Variable Angle X-ray Photoelectron Spectroscopy (VAXPS) has become a widely used tool for surface chemical analysis, because it supplies an abundance of surface chemical and in-depth elemental information non-destructively. Angular peak intensity distributions can yield information regarding the surface layer thickness,[55-66] the atomic profile,[61,66,67] the morphology of the overlayer coverage,[55-62,65,66] the photoelectron attenuation length[55-58,62,64,65,68,69] and the surface topography.[55-616] The non-destructive nature of XPS combined with the ability to investigate depth profiles makes VAXPS a preferable technique for passive film analysis in comparison with ion-etch profiling, as in AES or SIMS. The underlying principle of the VAXPS technique is the ability to selectively enhance the signal emanating from the top atomic layers by collecting photoelectrons from low- or grazing-electron exit angles. This effect is illustrated in figure 3.1, where the effective sampling depth is observed to decrease with the

sine of the photoelectron take-off angle.

3.2 Theoretical Considerations

A basic expression regarding photoemission from a solid was first described for UPS by Berglund and Spicer in 1964.[71] They arrived at a suitable equation by considering the emission as a three-step process; excitation, travel to the surface and escape from the surface, Their equation has been modified by a number of other workers for XPS. Fadley et al.[55,58] was the first to comprehensively treat angle resolved effects, theoretically and experimentally. Several other expressions of the photoemission process have also appeared in the literature.[71-75]

A basic feature of the photoemission experiment is indicated in figure 3.2.[53] X-rays with an angular divergence of ϕ_x are incident on the specimen surface at an angle ϕ_x. Refraction and reflection of the X-ray radiation may occur at the surface such that in general the internal propagation angle ϕ_x' need not to equal ϕ_x, and a fraction R_x of the X-ray intensity is reflected back from the surface. The X-rays are attenuated in

intensity due to absorption as they penetrate to some depth z below the surface. Photoelectrons produced at this depth travel toward the surface at an angle θ'. The no-loss component of this photoelectron flux is attenuated by inelastic scattering during this travel. The electrons also may be refracted and reflected at the surface, so that the measured external angle θ need not be equal to the internal angle θ', and a fraction of intensity R_e is internally reflected. The uncertainty in measured θ produced by the spectrometer is $\Delta\theta$. The electrons possess a kinetic energy E just outside the specimen surface. The angle between the X-ray and electron α propagation directions is assumed fixed. An expression for the number of photoelectrons in a certain no-loss peak that emitted from a differential volume element dxdydz can be written as:

$$dN(k,\theta,\phi_x,x,y,z) = [\text{X-ray flux at depth z}] \cdot [\text{Number of atoms in volume element}] \cdot [\text{Probability for k emission}] \cdot [\text{Fraction reach surface in no-loss peak}] \cdot [\text{Electron flux change in crossing surface}] \cdot [\text{Instrumental detection efficiency}] \quad (3.1)$$

In order to further derive equation 3.1, several simplifying assumption are made: (1) The specimen surface is flat, (2) The specimen is amorphous or polycrystalline, (3) The refraction and reflection of X-ray at the specimen surface is adequately described by classical electromagnetic theory, (4) The attenuation in the specimen of either X-rays or no-loss photoelectrons is described by an exponential decay along the path length, (5) Both attenuation lengths of X-ray(Γ_x) and photoelectron(Γ_e) are constants independent of electron emission depth, θ and ϕ_x, (6) Effect of electron refraction and reflection at the surface are negligible, and (7) Elastic electron scattering has negligible effects on angular distributions of photoelectrons. With the use of the above assumptions, equation 3.1 can be expressed in mathematical form:

$$\begin{aligned} dN(k,\theta,\phi_x,x,y,z) = {} & [I(\theta,x,y)(1-R_x)(\sin\phi_x/\sin\phi_x') \\ & \exp(-z/\Gamma_x\sin\phi_x')]\cdot[\delta(z)dxdydz] \\ & \cdot[d\sigma_k/d\Omega\{\Omega'(E,E_0,\theta,x,y)\}] \\ & \cdot[\exp(-z/\Gamma_e(E)\sin\theta')] \\ & \cdot[(1-R_e)\sin\theta'/\sin\theta] \\ & \cdot D_0(E,E_0) \end{aligned} \qquad (3.2)$$

Here, $\delta(z)$ represents the z-dependent atomic density (number/unit volume) associated with level k, $d\sigma/d\Omega'$ is the average bulk differential photoelectric cross section per atom for level k associated with emission into the internal solid angle Ω', $(1-R_e)$ represents intensity losses due to the surface reflection of X-rays and electrons, and $D_0(E,E_0)$ is used to denote an energy-dependent instrumental detection efficiency. If we assume the atomic density is constant with z, $\theta = \theta'$, $R_e = 0$, $\Omega = \Omega'$, and refraction and reflection of X-ray can be negligible, equation 3.2 can be integrated over the entire volume of a specimen of thickness t to yield for the total intensity in peak k:

$$N_t(k,\theta) = D(E,E_0)\cdot I_x\cdot\Omega_0(E,E_0)\cdot(A_0/\sin\theta)\cdot\delta\cdot(d\sigma/d\Omega') \cdot\Gamma_e(E)\cdot\sin\theta\cdot[1-\exp(-t/\Gamma_e(E)\sin\theta] \qquad (3.3)$$

Here, I_x is X-ray flux and A_0 is aperture area. For an infinitely thick specimen, equation 3.3 reduced to

$$N_\infty(k,\theta) = D(E,E_0)\cdot I_x\cdot\Omega_0(E,E_0)\cdot A_0\cdot\delta \cdot(d\sigma/d\Omega)\cdot\Gamma_e(E) \qquad (3.4)$$

The peak intensities forming multiple overlayer structures can be calculated by accounting for the attenuation from each successive layer and, also, the thickness of each layer can be calculated. A particularly useful method of data analysis may be accomplished by taking the ratio of the overlayer/substrate species. The overlayer and substrate peaks must occur at the same energies for ratio data to be meaningful, as in the case of metal and native oxide. The usefulness of ratio data arises because of several factors which include cancelation of the instrument response function, elimination of X-ray flux angular distribution factor, and elimination/cancelation of various specific spectrometer types and settings. Therefore ratio data can be compared between different spectrometers and laboratories without the addition of any correction factors. It is also assumed that the photoelectric cross-section, the asymmetric parameter and mean free paths for photoelectrons from the same core state of a given atomic species in the substrate and the overlayer are equal.

3.3 Quantitative Analysis

3.3.1 Sensitivity Factor

In XPS data, the peak area measures the total number of atoms emitting photoelectrons which are collected. We can restate equation 3.4 in its more commonly used form,

$$I = I_x \cdot R \cdot y \cdot \sigma \cdot D \cdot A \cdot \Gamma \qquad (3.5)$$

where I = number of photoelectrons detected/sec

I_x = incident X-ray flux (photons/sec.cm^2)

R = instrumental efficiency factor

y = efficiency of photoelectric process

σ = photoelectric cross section (cm^2/atom)

D = atomic density (atoms/cm^3)

A = analyzing area (cm^2)

Γ = inelastic mean free path

For a multicomponent homogeneous solid, the atomic density and the concentration of a component i can be expressed as:

$$D_i = I_i/I_x R_i y_i \sigma_i A_i \Gamma_i = I_i/S_i \qquad (3.6)$$

$$C_i = D_i/\Sigma D_i = (I_i/S_i)/\Sigma(I_i/S_i) \qquad (3.7)$$

where C is the concentration and S is the atomic sensitivity factor. Even for a given element, absolute

sensitivity factors depend on several factors: the spectrometer type and condition, vacuum level, and experimental condition etc. Therefore, in this study, relative sensitivity factors were obtained experimentally and used for calculating concentrations in surface oxide films.

3.3.2 Thickness Calculation

The presence of surface layers result in the intensities of the substrate and surface layer contributions varying as a function of $1/\sin\theta$. Using equation 3.3, 3.4 and 3.5, these intensities are defined as:

$$I_s^d = I_s \exp(-t_{ox}/\Gamma_{ox}\sin\theta) \qquad (3.8)$$

$$I_{ox}^d = I_{ox}(1-\exp(-t_{ox}/\Gamma_{ox}\sin\theta)) \qquad (3.9)$$

Thickness of the surface layer(e.g. oxide layer), t_{ox}, can be obtained by solving equation 3.8 and 3.9.

$$t_{ox} = \Gamma_{ox}\sin\theta \ln[(I_{ox}^d/I_{ox})(I_s/I_s^d) + 1]$$

$$= \Gamma_{ox}\sin\theta \ln[(I_{ox}^d S_s D_s/I_s^d S_{ox} D_{ox}) + 1] \qquad (3.10)$$

For a specimen with duplex overlayers (e.g. oxide and hydroxide layers), the thickness of the first overlayer, which is located between the substrate and the other overlayer (e.g. hydroxide layer), can be calculated using

equation 3.10. Thickness of the second overlayer, t_{OH}, can be obtained using equation 3.11, which is derived with similar method to equation 3.10.

$$t_{OH} = \Gamma_{OH}\sin\theta \ln[(I_{OH}S_sD_s/I_sS_{OH}D_{OH}) \cdot \exp(-t_{ox}/\Gamma_{ox}\sin\theta)+1] \quad (3.11)$$

4. EXPERIMENTAL

4.1 Materials

4.1.1 Pure Metals and Stainless Steels

Pure Metals - The electrode material for electrochemical analysis included a high purity (99.99%) Cr disc (r=5mm, t=1mm) and high purity (99.99%) Mo and Pt coupons (7mm x 10mm x 1mm).

Stainless Steels - Several kinds of austenitic stainless steels in coupon forms(7mm x 10mm x 1mm) used in this study are listed in table 4.1. These steel samples were annealed at 1100°C for 3 hours in an evacuated quartz tube and quenched in water. These steels were provided by Colt Industries(Eckenrod and Kovach), Allegheny Ludlum Steel Corp.(J. R. Kearns) and Sandvik AB(Sweden).

4.1.2 Molybdenum Nitride(Mo_2N)

Pure Mo in coupon form was nitrided in a quartz tube in an ammonia(NH_3) environment at 600°C for 48 hours by Y. Lu[39] in McMaster University. The structure of these nitrides has been characterized by X-ray diffraction and

found to be Mo_2N.

4.1.3 Electrolytes

All electrolytes were prepared from doubly distilled water and analytical reagent grade chemicals. All solutions were deaerated with Ar for at least 2 hours before using.

4.2 Electrochemical Analysis

4.2.1 Sample Preparation

Metal samples were ground using a 600 grit SiC paper disc and polished with 6μm and 0.25μm diamond paste. They were ultrasonically cleaned in acetone and in iso-propanol. Then, they were rinsed with doubly distilled water and mounted for polarization. As presented in figure 4.1, all specimens were mounted on holders constructed of borosilicate glass tube and plexiglas. An external electrical connection to the specimen was established by contacting a Cu wire to the specimen which exited the cell through a glass tube. Specimens were embedded in an epoxy resin and the specimen edges and exposed Cu were all masked with epoxy.

Thus only the specimen surface came into contact with the electrolyte.

4.2.2 Electrochemical Cell

A conventional[76] and a modified Greene cell constructed of borosilicate glass and fitted with ground seal was utilized for the electrochemical work. For the nitrate treatment in order to form a surface nitride on metal electrodes electrochemically, a modified Greene cell was used. The platinum counter electrodes were removed from the cell and placed in two separate compartments on the opposite sides of the cell to prevent plating of Pt on the working electrode during nitrate reduction process. A porous frit was placed between the compartment and the cell. A Saturated Calomel Electrode (SCE) was used for the reference electrode and all potentials are reported relative to the SCE. The reference electrode was placed in a solution of 1M KCl and separated from the cell by a glass frit and a Luggin-Haber capillary tube. The electrolyte in the cell was deaerated with Ar for at least 2 hours prior to start of the experiment. A magnetic stirring bar provided solution agitation throughout the experiment.

4.2.3 Instrumentation

Polarization experiments were performed with a model 173 potentiostat/galvanostat manufactured by the Princeton Applied Research corporation. The potentiostat was equipped with a model 276 IEEE 488 interface bus and an APPLE II personal computer for data acquisition. A block diagram of the apparatus is presented in figure 4.2.

4.2.4 Specimen Pretreatment

To remove the air-formed oxide film and to activate the surface of the working electrode, cathodic pretreatments were performed. The Cr specimens were pretreated in the cathodic range at -930 mV for 15 min and the Mo and the steel specimens were activated at -700 mV for 15 min. All cathodic pretreatment were conducted at ambient temperature of 22°C.

4.2.5 NO_3^- Stability Studies

After air-formed oxide removal, pure Cr samples were polarized in 0.1M HCl + 0.5M $NaNO_3$ at various conditions listed in table 4.2 in order to determine the stability on metal surface.

4.2.6 Cathodic Nitrate Treatment

For some specimens, nitrate treatments were performed after air-formed oxide removal in order to dope nitrogen in forms of nitride onto the metal surface electrochemically. A cathodic potential (-930 mV for the Cr and -700 mV for the Mo and the stainless steels) was applied to the working electrode with charging of ≈750 mC/cm^2 in a deaerated 0.1M HCl + 0.5M $NaNO_3$ solution. A modified Greene cell was used for this experiment and described in section 4.2.2. For the further polarization in 0.1M HCl after this treatment, the electrochemical cell was flushed and rinsed twice with 0.1M HCl to remove soluble reduction products. This is an essential step in this treatment.

4.2.7 Potentiodynamic Polarization

After the cathodic pretreatment or the nitrate treatment, potentiodynamic polarization was performed in a deaerated electrolyte at a scan rate of 1 mV/sec. Polarization started from 250 mV below the Open Circuit Potential (OCP). However, for the nitrate-treated samples, polarization started from the OCP to avoid any

loss of surface nitride from the metal substrate by the ammonia/ammonium formation.

4.2.8 Potentiostatic Polarization

To investigate the effect of each alloying element on the corrosion behavior with electrochemical and the XPS technique, potentiostatic polarizations were performed at various conditions, which are listed in table 4.3-4.4. Polarization was conducted by stepping the potential from the OCP to a potential of interest for a specific time and monitoring the current as a function of time. After electrochemical treatment, the specimens were immediately rinsed with deaerated doubly distilled water and transferred to the spectrometer under an Ar atmosphere.

4.3 Surface Analysis by Variable Angle X-ray Photoelectron Spectroscopy(VAXPS)

4.3.1 Instrumentation

The XPS measurements were performed using a commercially available spectrometer manufactured by V.G. Scientific Ltd., ESCA 3 MKII, controlled by a V.G. 1000

data system. The analytical system consists of a dual Al/Mg X-ray source, electron gun, ion gun and hemispherical electron analyzer. The dual X-ray source produces either Al $K\alpha_{1,2}$ (1486.6 eV, 0.85 eV FWHM) or Mg $K\alpha_{1,2}$ (1253.6 eV, 0.70 eV FWHM) irradiation. The X-ray source are separated from the analyzer chamber by a thin (2μm) Be window which screens out stray electrons and contamination. The ion gun used for surface etching was of the static type, producing a focusable ion beam with a maximum accelerating potential of 10 KeV. The landing current of the ion beam onto the sample was monitored with a micro-ammeter. The electron analyzer is of the electrostatic hemispherical type. Figure 4.3 is a schematic of the system.

4.3.2 Sample Preparation and Transfer

To investigate the passivation behavior for the stainless steels, XPS was used to analyze the surfaces of the various specimens following polarization at various conditions. After the polarization, the specimen was rinsed immediately with deaerated doubly distilled water and dried with an Ar jet. The entire procedure was performed inside an Ar purged glove box and the specimen

was transferred to the spectrometer under Ar atmosphere.

4.3.3 Operating Conditions

Since the Auger peaks of Ni generated by a Mg X-ray source (410 eV for $L_3M_{45}M_{45}$, 393 eV for $L_2M_{45}M_{45}$) appeared near the N1s spectrum (binding energy : ≈400 eV),[77-79] the Mg $K\alpha_{1,2}$ source could not be used in this study. Only an Al $K\alpha_{1,2}$ X-ray(1486.6 eV) source at 400 watts (Anode current=40 mA, Anode voltage=10 KV) was utilized. Measurements were performed at varying photoelectron take-off angles to observe the inner and outer layers of the surface film. XPS analysis was implemented by taking narrow scans (25 eV width, 250 channels) at a 20 eV pass energy. The analyzer was operated at a constant analyzer energy (CAE) mode. Base pressures during analysis were about 1×10^{-9} torr. As a reference, the binding energies of the $Au4f_{7/2}$ and the $Cu2p_{3/2}$ photoelectrons were found to be 83.8 eV and 932.5 eV, respectively. By taking the C1s spectrum from the adventitious carbon at 284.6 eV, all binding energies were corrected for charge shifting.

4.3.4 Data Analysis

The major merit of XPS is its sensitivity to variations in chemical state. An homogeneous chemical species will produce a well defined peak in the XPS spectrum. A specific element will very often be present in several different chemical and/or oxidation states within a single specimen. The binding energy shifts between these various species may be extremely small (≈0.1 eV). Curve fitting provides a method by which to separate out the individual chemical species from a complex spectra containing several different chemical states. The curve fitting program allows the operator to synthesize peaks by specifying the peak's position, height, width and shape. The shape parameters included the peak's Gaussian/Lorentzian ratio and tail characteristics such as height, slope and exponential-to-linear tail mix. The $K\alpha'$, $K\alpha_3$ and $K\alpha_4$ satellites were automatically included in the synthesis. A Shirley background subtraction[80] (non-linear background subtraction) was also conducted for each multiplet in the spectral region under analysis. Since curve fitting may provide several possible solutions to the same spectrum, variable angle XPS data, double differentiation and

measurement of spin-orbit splitting were employed in order to determine the most probable and accurate fit. For optimizing the fit, a non-linear least square algorithm developed by Sherwood[80] was utilized. In table 4.5, the binding energies and curve fitting parameters of all elements analyzed in this study are presented.

5. RESULTS

5.1 NO_3^- Stability on the Surface of Metallic Electrode

5.1.1 XPS Analysis of NO_3^- Stability on Pure Cr

From the polarization curve of pure Cr in figure 5.1, five potentials were chosen for the experiments in which possible NO_3^- reduction on the surface of a Cr electrode was investigated, -930 mV, -700 mV, 0 mV, 950 mV and 1300 mV corresponding respectively to cathodic, active, passive, passive-transpassive transient and transpassive regions. Figure 5.2 shows the N1s spectra for pure Cr samples treated as the conditions of table 4.2. According to the binding energies in table 4.5, four types of N compounds were consistently found throughout the experiments. These compounds corresponded to (1) nitride, (2) NH_3, (3) NH_4^+ and (4) NO_3^-. Based upon the peak area ratios at 20° and 50° take-off angles, nitride was observed to be at the oxide-metal interface. N1s peak at 399.9 eV corresponds to NH_3. Two species that may exhibit such a binding energy are NH_3 and NO. According to Pourbaix diagram,[81] the electrochemical formation of NO would be thermodynamically unfavorable. The binding

energy of N1s photoelectron of NH_3 ligands coordinated with Cr^{+3}, as $[Cr(III)(NH_3)_5OH_2]^{+3}$ (399.8 eV in table 4.5), agrees well with the observed binding energy (399.9 eV), lending further support to the probability that this species is a complex of NH_3 rather than NO. Reduced species, NH_3 and NH_4^+, were found regardless of applied potentials, even though they were not thermodynamically predicted in the anodic region. Nitride was formed under conditions (cathodic, active and transpassive) leading to the direct exposure of metal surface to the electrolyte. It was apparently prevented from forming in passive state (0 mV and 950 mV) due to the existence of a barrier film. To confirm the hypothesis that a direct contact of metal surface to NO_3^- ions was the principle mechanism of the nitride formation, another experiment was conducted. After being polarized at 0 mV for 30 min in 0.1M HCl, the Cr sample was further polarized at 0 mV for 30 min in 0.1M HCl + 0.5M $NaNO_3$. In order to temporarily remove the barrier film, sample surface was scratched several times during polarization in a Cl^-/NO_3^- containing solution. XPS analysis which is presented in figure 5.3 reveals the evidence for the formation of a surface nitride. Therefore, it is concluded that NO_3^-

reduction on pure Cr was found regardless of applied potentials and that the surface nitride formation was observed only under conditions leading to the direct contact of metal surface to NO_3^- ions. This is consistent with the conclusion that nitrogen alloyed with stainless does not function by oxidation to NO_3^- or NO_2^-. Furthermore, NO_3^- reduction is a suitable technique by which N-alloying may be simulated for the purpose of our enquiries.

5.1.2 The Effect of Nitrogen on Pure Cr

Figure 5.1 shows a typical polarization curve for pure Cr in 0.1M HCl at room temperature utilizing a potential scan rate of 1 mV/sec. The salient electrochemical characteristics are presented in table 5.1. Polarization for the nitrate-treated Cr sample was started from Open Circuit Potential (OCP) to avoid any loss of surface nitrogen from the metal surface by ammonium formation. It was observed that the active corrosion of Cr was suppressed completely following nitrate-treatment. This observation included a sizable positive shift in OCP. The passive current density for nitrate-treated Cr was, however, slightly increased.

5.1.3 XPS Analysis of NO_3^- Effect on Stainless Steel

Figure 5.4 shows N1s and Mo3p spectra for the stainless steels after nitrate reduction treatment at -700 mV(cathodic region) in 0.1N HCl + 0.5M $NaNO_3$ with ≈750 mC/cm^2. Since the binding energies of Mo3p photoelectrons of various Mo species are very close to those of N1s photoelectrons, Mo3p spectra need to be cross-checked with Mo3d spectra for the accurate identification of nitrogen compounds. In this figure, it is apparently observed that, on the surface of the stainless steels, NO_3^- was reduced to nitride and NH_3 as on pure Cr. According to the polarization curves of 18-8(304) stainless steel (Figure 5.20), this nitride also improved the passivity. The role of surface nitride reduced electrochemically from NO_3^- ions on corrosion is as same as that of segregated nitride from alloying N. This phenomenon will be discussed later in the next chapter.

5.2 The Synergistic Effect of Nitrogen on the Corrosion of Mo Bearing Stainless Steel

5.2.1 Electrochemical Analysis

Potentiodynamic polarization curves obtained for three high Ni stainless steels(Fe20Cr20Ni, Fe20Cr20Ni6Mo, Fe20Cr20Ni6Mo0.2N) in deaerated 0.1M HCl + 0.4M NaCl at room temperature are presented in figure 5.5. Their salient electrochemical characteristics are listed in table 5.2. It was observed that, with the addition of 6 wt%Mo, the critical current density decreased from 80.4 uA/cm^2 to 30.3 uA/cm^2 and that, with further addition of 0.2 wt%N, the active dissolution was completely suppressed. This complete suppression of the active dissolution indicated the presence of some types of Mo-N synergism. Since 6 wt%Mo addition already seems to be sufficient to eliminate pitting completely, the N addition could not further improve pitting resistance. However we have noted that the OCP of Mo alloys were slightly higher than that of the Fe20Cr20Ni alloy, and that this result is consistent with the fact that Mo is more noble than Fe. The passive current densities recorded for all three alloys were about the same.

5.2.2 XPS Analysis

Narrow scan spectra of Cr2p, Mo3d, Fe2p, Ni2p, O1s, N1s and Cl2p were analyzed for three high Ni alloys following passivation treatment at -100mV for 10 min in a deaerated 0.1M HCl + 0.4M NaCl solution at room temperature. By considering the peak area ratios of the species for 20° and 50° photoelectron take-off angles measured with respect to the plane of sample, it is possible to provide an approximate description of the compositional variations throughout the passive film. The 20° take-off angle provides the more surface sensitive spectra. XPS spectra of the Cr, Mo, Fe, Ni and N are presented in figure 5.6-5.10. By comparing XPS spectra of the metallic elements in the passive films of stainless steels, it was concluded that Cr compounds made up the bulk of the passive film (> 60 at%). Figure 5.6 shows the Cr2p XPS spectra for the three high alloys. Five components were commonly found in the spectra-Cr^0, Cr_2O_3, $Cr(OH)_3$, and minor peaks of CrO_4^{-2} and CrO_3. Based upon the peak ratios of photoelectron take-off angles, the inner layer of the passive film was composed primarily of Cr_2O_3 and the outer layer was composed of

$Cr(OH)_3$. Mo3d XPS spectra for Mo bearing alloys are presented in figure 5.7. In this figure, it is observed that MoO_2, Mo^{+5}(possibly an oxide compound) and MoO_3 appeared to reside in the inner Cr_2O_3 layer and that MoO_4^{-2} compounds were incorporated into the outer $Cr(OH)_3$ layer. The N1s and Mo3p XPS spectra of the passive films for the Fe20Cr20Ni6Mo and the Fe20Cr20Ni6Mo0.2N alloys are presented in figure 5.8. For both alloys, two distinct peaks at 397.2 and 399.9 eV were observed, due to alloying N segregation on the surface during the polarization. The N1s binding energy value of 397.2 eV is 0.2 eV higher than that of CrN (397.0 eV), and 0.2 eV lower than NiN (397.4 eV). M. Romand and M. Roubin[82] reported that, while CrN has the binding value of 396.8 eV and VN has the binding value of 397.2 eV, the binding energy of a mixed nitride of Cr and V is 397.0 eV or 397.1 eV. Therefore nitride of this study is a mixed nitride of Cr and Ni. The N1s peak at 399.9 eV is NH_3 as described in section 5.1.2. The binding energy of the NH_3 ligands coordinated with Cr^{+3}, as $[Cr(III)(NH_3)_5OH_2]^{+3}$ (399.8 eV in table 4.5), was agreed well with the observed binding energy (399.9 eV) of the surface nitride on the 18-8 stainless steels lending further support to

the conclusion that this species is a complex of NH_3 rather than NO. The concentrations of these N species differ greatly between the two alloys and depend on the concentration of alloying N. Based upon the peak ratios of the spectra for take-off angles, Nitride and NH_3 were situated near the passive film-substrate interface and in the passive film respectively. In the passive film, Fe^{+2} and Fe^{+3} species were observed (figure 5.9) and only a very little amount of Ni^{+2} species was found (figure 5.10). Also very little amount of chlorine was observed in the passive film. Summarizing the above results, we have constructed the schematics of the passive film for Fe20Cr20Ni6Mo and Fe20Cr20Ni6Mo0.2N alloys which are presented in figure 5.11. We note that the structures of the passive films are consistent with the bipolar model of passivity of austenitic stainless steel.[19,41,50-54] Molybdate (MoO_4^{-2}) anions has been previously reported to serve as a cation-selective species, enhancing the bipolarity and thereby increasing the deprotonation of the passive film.[41,51,53,54] This selectivity is responsible for the densification of the passive film and the resistance of the film to ingressing anionic species. From figure 5.7 and 5.8, the concentration of MoO_4^{-2} for

the Fe20Cr20Ni6M0.2N alloy was observed higher than that for the Fe20Cr20Ni6Mo alloy. The increment of the MoO_4^{-2} concentration is in a good agreement with the results of Mo_2N polarization at 600 mV, which will be presented in the next section 5.3, and shows an additional evidence of Mo-N synergism in the corrosion of stainless steel.

Using the equation 3.10 and 3.11, the thickness of the passive film was calculated based on three assumptions: (1) the passive film is composed of a Cr_2O_3 inner layer and a $Cr(OH)_3$ outer layer, (2) the density and the attenuation length of the $Cr2p_{3/2}$ photoelectrons of $Cr(OH)_3$ are the same as those of Cr_2O_3 and (3) the Fe ions are located in the inner Cr_2O_3 layer. The attenuation lengths used in this calculation are 13 Å for metallic Cr and 16 Å for Cr_2O_3. Relative sensitivities factors are listed in table 5.3. While the oxide layer thickness is almost the same (d_{OX}= 10.65 Å) for all three alloys, the hydroxide layer thickness differed depending on the Mo component (d_{OH}= 4.92 Å for Fe20Cr20Ni alloy and d_{OH}= 2.61 Å for two Mo alloys). This is consistent with deprotonation due to the presence of the cation selective molybdate species in the passive films of two Mo bearing alloys. From O1s spectra, the area ratio of OH^- spectrum

to O^{-2} spectrum for the Fe20Cr20Ni alloy also appears higher than that for the Mo bearing alloys.

The metal composition underneath the passive film of the three alloys studied are presented in figure 5.12. For the Fe20Cr20Ni alloy, the metallic Ni composition changed little only 19.0 to 19.5 at% following passivation, while the metallic Cr was enriched from 20.4 to 29.2 at%. This result is not consistent with the enrichment of Cr and Ni for the 18-8 alloys presented in section 5.4. However, it was observed that the atomic percentage ratio of Ni to Cr were virtually equal (≈0.65). The Fe20Cr20Ni6Mo alloy exhibited the metallic enrichment of 21.6 to 23.9 at% for Cr, 19.4 to 27.4 at% for Ni and 3.5 to 6.1 at% for Mo. With 0.2 wt%N addition to Fe20Cr20Ni6Mo alloy, it was observed that Ni and Mo were more highly enriched (from 19.4 to 30.1 at% for Ni and from 3.6 to 7.0 at% for Mo) and that Cr was less enriched (from 21.9 to 22.0 at%) compared to the results of Fe20Cr20Ni6Mo alloy. The role of Ni on the corrosion behavior of these stainless steel will be discussed in the next chapter using the metallic enrichment data beneath the passive film.

5.3 Passivation Behavior of Mo

5.3.1 Electrochemical Analysis

Figure 5.13 shows potentiodynamic polarization curves for pure Mo, nitrate-treated and nitrided Mo in 0.1M HCl at room temperature utilizing a potential scan rate of 1 mV/sec. The nitrided Mo was identified as Mo_2N using X-ray diffraction.[39] Polarization for the nitrate-treated samples started from OCP to avoid any loss of surface N from the metal surface by ammonium formation. The salient electrochemical characteristics are presented in table 5.1. For OCP and transpassive potentials, a slight increment for the nitrate-treated Mo was observed and a large increment for the Mo_2N were measured. Since Mo is very noble element, a small amount of surface nitride can be formed by nitrate-treatment. The concentration of surface nitrogen by nitrate-treatment is much less than by thermal nitriding. This concentration of the surface N affects the amount of the increment for OCP and transpassive potentials. While no pitting was observed on pure Mo and nitrate-treated Mo, some pitting was observed on the Mo_2N specimen. These pits occurred above 300 mV, which was the transpassive

region for pure Mo and nitrate treated Mo, and corresponded to glitches in the polarization curve in figure 5.13. Therefore, a further increment of the corrosion resistance of Mo is possible, if the weak points for pitting initiation can be eliminated. It can be concluded that the surface N improved the passivity of pure Mo in 0.1M HCl. In order to investigate the influence of N on the passivity of pure Mo, the anodic film was analyzed by XPS after potentiostatic polarization. Polarization conditions were listed in table 4.3. During potentiostatic polarization at 50 mV, the passive current density of pure Mo after 30 min in 0.1M HCl was stabilized around 2.4 $\mu A/cm^2$ and that of nitrate-treated Mo was also stabilized around 0.9 $\mu A/cm^2$. These values agree well with the passive current densities of potentiodynamic polarizations and show that the role of the surface N on pure Mo is different from on pure Cr. This will be discussed in next chapter.

5.3.2 XPS Analysis of Anodic Films

The Cl2p photoelectron signal was found in all cases to be very weak. This indicates that the chloride or chlorine containing complex is not a major surface

species and is therefore not considered further in this research. Figure 5.14-5.16 are a comparison of the XPS spectra obtained from pure Mo and nitrate-treated Mo polarized for 1 hour at 50 mV in 0.1M HCl. The XPS spectra indicate that the passive film is comprised of a mixture of Mo^{+4} and Mo^{+5}. According to a comparison of the spectra for two take-off angles, 5° and 20°, the Mo^{+4} was found much closer to the metal substrate than Mo^{+5}. For the nitrate-treated Mo, a small amount of surface nitride and NH_3 was observed. These N species were electrochemically reduced from NO_3^- ions with the same mechanism as pure Cr. The passive film formed on the nitrate-treated Mo is thicker than that on pure Mo. The XPS data in figure 5.17-5.19 are Mo3d, Mo3p, N1s and O1s spectra obtained from the anodic films formed at 250 mV for 1 hour and at 600 mV for 3 min in a deaerated 0.1M HCl. It shows that the main doublet at 228.1 and 231.3 eV is contributed from the Mo_2N substrate and the passive film is comprised of two surface species corresponding to the binding energy values of 229.1 and 230.8 eV respectively. The peak at 229.1 eV is corresponding to Mo^{+4} and the peak at 230.8 eV is contributed from Mo^{+5}. For the Mo3d spectra of Mo_2N polarized at 600 mV for 3

minutes, the surface is covered with Mo^{+4} and Mo^{+5}. Only a small amount of MoO_4^{-2} is observed on the surface. The chemical species observed on the Mo_2N are much different from that obtained from the pure Mo electrochemically treated at the same condition. According to the previous work,[38] pure molybdenum polarized at 250 mV (transpassive) is covered with thick brown transpassive product which is a mixture of Mo^{+3}, Mo^{+4}, Mo^{+5} and MoO_3 oxides. And the surface species on pure molybdenum polarized at 600 mV is mainly MoO_3. This means that the nitride completely stopped the formation of MoO_3 at 600mV (transpassive potential). Figure 5.18 shows the N species observed on the anodic film formed on Mo_2N at 250 mV and 600 mV. Peak 4 is the N1s spectrum contributed from the nitrogen of Mo_2N. The peak at 400.0 eV corresponds to the NH_3. This peak is stronger in the 5° take-off angle than in 50°. By a comparison of the 5° spectra in figure 5.18, it is clear that there is more NH_3 in the film polarized at 250 mV than at 600 mV. This implies that the NH_3 ligand is located on the surface and increases the local pH at the electrolyte-electrode interface. Increased local pH favors the formation of MoO_4^{-2} instead of MoO_3 which is the main species observed on the surface of pure

Mo. This also, agrees with the Pourbaix diagram,[81] which indicates that, when the pH shifts to high values, the formation of MoO_4^{-2} is preferred.

5.4 The Effect of Nitrogen on the Corrosion of 18-8 Stainless Steel

5.4.1 Electrochemical Analysis

The potentiodynamic polarization behavior of the 18-8 stainless steels in 0.1M HCl at room temperature are presented in figure 5.20. The salient electrochemical characteristics are listed in table 5.5. The 0.04 wt% N alloy has the highest values of critical current density and passivation current density and the lowest values of OCP and pitting potential. These results provide evidence of the beneficial influence of N in the corrosion of 18-8 stainless steel. Even though the critical current density of N-doped 0.04 wt%N alloy was lower than that of 0.24 wt%N steel, the passivation current density was higher and the pitting potential was significantly lower compared to those values of 0.24 wt%N alloy.

Figure 5.21 and 5.22 show the current density curves as a function of passivation time for pure Cr and

18-8 stainless steels during the potentiostatic polarization at -180 mV in 0.1M HCl. The passivation current density of N-doped Cr is greater than that of pure Cr, while the passivation current density of 0.04 wt%N 18-8 alloy is greater than that of 0.24 wt%N 18-8 steel. These results agree well with the data of the potentiodynamic polarization behavior, in which surface N lessens the passivation and critical current density.

From the above electrochemical results, it can be concluded that the surface N affects the OCP, the critical current density, the passivation current density and the pitting potential in the anodic polarization behavior. The surface N on the 18-8 alloy makes the surface more passive, while the surface N on the pure Cr makes the surface more active. This difference will be discussed in the next chapter using XPS data.

5.4.2 XPS Analysis of Passive Film

Narrow scan spectra of Fe2p, Cr2p, Ni2p, O1s, N1s and Cl2p were analyzed for each experiment. Analyzing $Cr2p_{3/2}$ spectra (figure 5.23), five components were commonly found in this study corresponding to (1) metallic Cr from the substrate, (2) Cr^{+3} corresponding

to Cr_2O_3, (3) Cr^{+3} corresponding to $Cr(OH)_3$, (4) Cr^{+6} corresponding to CrO_3, (5) Cr^{+6} corresponding to CrO_4^{-2}. Based upon the peak ratios of 20° and 50° take-off angles, the passive film was composed of the inner Cr_2O_3 layer and the outer $Cr(OH)_3$ layer. CrO_3 and CrO_4^{-2} species were located in outer hydroxide layer. This is the basic structure of the passive film of the austenitic stainless steel and agrees well with the bipolar model of the passive film.[19,41,50-54]

From Fe $2p_{3/2}$ spectra (figure 5.24), three components were found in each case corresponding to (1) metallic Fe from the substrate, (2) Fe^{+2} and (3) Fe^{+3} ions in the passive film. Table 5.6 shows Fe ion peak intensity ratios of the values of 50° take-off angle spectra and 20° take-off angle spectra for various samples. The intensity ratios for the Fe^{+2} peak and the Fe^{+3} peak normalized with the Cr_2O_3 and $Cr(OH)_3$ are virtually same. Therefore, it can be concluded that Fe^{+2} and Fe^{+3} were distributed throughout the passive film. As to the Ni2p spectra (Figure 5.25), only metallic Ni from the substrate was observed. From figure 5.26, two distinct N peaks at 397.2 eV corresponding to nitride and at 399.9 eV corresponding to NH_3 were observed due

to the segregation of the alloying N during polarization in a Cl^- containing solution. Comparing the XPS spectra of 20° and 50° photoelectron take-off angles, it was observed that NH_3 and Cl^- existed in the outer $Cr(OH)_3$ layer, nitride was near the oxide-substrate interface. The passive film structure of 18-8 stainless steel is presented in figure 5.27.

The calculation of the thickness of the passive films were conducted using equations 3.10 and 3.11 based on the same assumptions described in the section 5.2.2. In table 5.6, Thicknesses of the passive films are listed. The thicknesses of the outer hydroxide layers (d_{OH}) are constant 4.11 Å (approximately 1 monolayer) for all samples. This thickness of the hydroxide layer is in good agreement with other's results.[83] The thicknesses of the inner oxide layers are constant 11.17 Å for the 0.04 wt%N alloys and 9.34 Å for the 0.24 wt%N alloys. These results are very close to the values of the passive film of the pure Cr polarized at same potential in 0.1M HCl (d_{OX} = 8 Å and d_{OH} = 3 Å). Therefore, it is concluded that the thicknesses of the passive films are only dependent on the applied potential.

Since NH_3 was distributed in the outer hydroxide

layer and the thickness of this layer was constant (table 5.7), the NH_3 peaks were normalized by $Cr(OH)_3$ peak to calculate their relative concentrations. Figure 5.28 shows the relation between the concentrations of total Fe ions and NH_3. As the NH_3 concentration in the passive film increases, the concentration of total Fe ions decreases. The NH_3 ligands in the passive film enhance the selective dissolution of the Fe ions in the passive film and make more Cr-enriched passive film. This Cr-enriched passive film protects the attack of the aggressive Cl^- ion and reduces the passive current density. However, in the case of Cr, the role of the NH_3 ligands in the passive film appears different. According to figure 5.21, the passivation current density of N-dope Cr is higher than that of non-treated Cr. This means that N on the surface makes the surface of pure Cr more active and enhance the Cr dissolution from the substrate.

From the XPS spectra metallic Cr and Ni enrichment underneath the passive film was observed. The concentrations of metallic Cr and Ni are 21-26 at% (bulk concentration = 20%) and 14-16 at% (bulk concentration = 8.0 at%) respectively. The atomic percentage ratio of Ni and Cr is the same($\approx$0.65) as that of Fe20Cr20Ni alloy

in the section 5.2.2. In the next chapter, the chemistry of the enrichment of Ni by forming intermetallic compound with Cr and Mo in the corrosion of the austenitic stainless steels will be discussed in detail.

5.4.3 Incubation Time Measurement

Figure 5.22 indicates that, when NaCl was added to 0.1M HCl to the final concentration of 0.1M HCl + 0.75M NaCl, following film formation in 0.1M HCl solution for 1 hour, the anodic current noise increased indicating the process of continuous breakdown and repair of the passive film. During the polarization of the 18-8 stainless steel in 0.1M HCl at -180 mV, alloyed N changed to nitride and NH_3. From figure 5.28, the NH_3 in the passive enhanced the selective dissolution of the Fe ions. After the polarization at -180 mV for 1 hour in 0.1M HCl, the NH_3 concentration of the 0.24 wt%N alloy was higher than that of the 0.04 wt%N alloy, i.e the 0.24 wt%N alloy had more Cr-enriched film than 0.04 wt%N alloy. Further polarization at same potential in a 0.1M HCl + 0.75M NaCl solution was conducted. Increased Cl^- concentration could dissolve the Fe ions in the passive film more aggressively and thereby induced pitting of the passive

film. Therefore, for the 0.04 wt%N alloy, the passive film broke down after 42 min, while the 0.24 wt%N alloy still remained passive. This result indicates that the NH_3 ligand appears to modify the passive film, providing an increased resistance to Cl^- induced pitting. Figure 5.29 shows the N1s spectra for the 18-8 alloys polarized at -180 mV for 1 hour in 0.1M HCl following further polarization at same potential for 30 min in 0.1M HCl + 0.75M NaCl. In this figure, NH_3 was observed for both alloys. The NH_3 concentration for 0.24 wt%N alloy is found to be higher than 0.04 wt%N alloy. This result also shows that NH_3 is related to preventing pitting initiation. This pitting mechanism will be discussed based on the interpretation of the XPS results.

6. DISCUSSION

6.1 The Stability of NO_3^- on Metal Surface

6.1.1 The Proposed Model of NO_3^- Reduction on Metal Electrode

Figure 5.2 shows the N1s spectra for pure Cr samples treated as the conditions of table 4.2. Four types of N species were commonly found in these experiments corresponding to (1) nitride, (2) NH_3, (3) NH_4^+ and (4) NO_3^-. Based upon the peak ratios of 20° and 50° take-off angles, nitride was observed to be at the oxide-metal interface. Among the reduction products, NH_3 and NH_4^+ were found regardless of the applied potentials, even though these products were not thermodynamically predicted in the anodic region. However, nitride was formed under the conditions (cathodic, active and transpassive) leading to the direct exposure of a metal surface to the electrolyte, but it was apparently prevented from forming in the passive state (0 mV and 950 mV) due to the existence of a barrier film. To confirm the hypothesis that the direct contact of the metal surface to the NO_3^- ions was the key factor in the

electrochemical formation of the surface nitride, an additional experiment was conducted (condition 6 in the table 4.2). The sample surface was scratched several times in order to temporarily remove the barrier film during polarization in 0.1M HCl + 0.5M $NaNO_3$, following which XPS analysis revealed evidence of a surface nitride (figure 5.3). Therefore, it is concluded that the electrochemical reduction of the NO_3^- on the surface of pure Cr was found regardless of the applied potentials and that the surface nitride was observed only under the conditions leading to the direct contact of the metal surface to the NO_3^- ions. This observation has considerable implications to our understanding of how NO_3^- species improve pitting resistance.

Galvele[84] suggested the Proton Consuming Reaction (PCR) for explaining the role of NO_3^- in increasing the pitting resistance.

$$NO_3^- + 10H^+ + 8e^- = 3H_2O + NH_4^+$$

This is possible reaction for the reduction of NO_3^- on metal surface in the solution. At cathodic potential (figure 6.1(a)), even though NO_3^- ions were repelled from the interface, it was possible that NO_3^- ions could be adsorbed on the metal interface by the direct contact

adsorption.[85] The H^+ ions and the electrons were attracted towards this interface by the electric field. By the PCR model, adsorbed NO_3^- ions were reduced to N^{-3} (in the forms of nitride and NH_3/NH_4^+) in agreement with our observation via the partially reduced form NO_2^-. However, at high anodic potential (figure 6.1(b)), the NO_3^- ions were attracted to the interface, while the H^+ ions were repelled from the interface. Therefore PCR model could not be applied.

We proposed a model for NO_3^- reduction at high anodic potential. As presented in figure 6.2, six electrons which participate in N-O bonds are in the delocalized, extended π-bonds.[86] When a high anodic potential is applied to the metal electrode, the NO_3^- ions are attracted towards to the interface due to the electric field. At close proximity, the O-atom is attracted and the N-atom is repelled, because the electrons in the extended π-bonds are easily shifted by the applied electric field. A repulsive force between the N-atom and the O-atom is developed, which stretches and breaks the surface N-O bond yielding the NO_2^- ion (figure 6.3(a)). The force developed (figure 6.3(b)) due to the electric field increases the bond angle between two N-O

bonds and eventually breaks them. An Intermediate surface nitride is formed (figure 6.3(c)). Further reactions occur and the nitride is protonated to NH_3 as follows:

$$2MN + 3H_2O = M_2O_3 + 2NH_3 \text{ (as a form of ligand)}$$

where M is a metallic element.

6.1.2 Stable Phase of Nitrogen on Metal Surface

According to the Pourbaix diagram, NO_3^- which is a well known corrosion inhibitor is the stable phase of N at high anodic potentials. Therefore, it is considered that N in an alloy is oxidized to NO_3^- at high anodic potential and this NO_3^-, as a corrosion inhibitor, prevents pitting initiation. However, in this study, an apparent formation of surface nitride reduced from NO_3^- was observed only under the conditions leading to the direct contact of metal surface to NO_3^- ions regardless of applied potentials. This result provides important information concerning the stability of N species on metal surfaces. Even though this information is indirect evidence, it can be concluded that surface nitrides are more stable than the NO_3^- ions on the metal surface. Therefore, N alloys do not function by way of forming nitrates or nitrites. Furthermore, the effect of NO_3^- as

a corrosion inhibitor can be simply understood by the formation of the surface nitride in a manner similar to N-alloyed stainless steels. When the metal surface is exposed to the NO_3^- containing electrolyte due to pitting or mechanical damage, surface nitride is formed immediately. Then, this surface nitride acts as a precursor to the passive film and aids in the formation of an oxide passive film. This nitride stabilizes the first formed layer of the passive film by acting as a buffer to local acidity due to the formation of NH_3 or NH_4^+. This behavior is further discussed below.

6.1.3 The Effect of Nitrogen in the Corrosion of Pure Cr

Figure 5.1 shows the typical polarization curves for pure Cr in 0.1M HCl at room temperature. It was observed that the active corrosion of pure Cr was suppressed completely following nitrate-treatment. This observation included a sizable positive shift for the OCP. According to previous studies and Pourbaix diagram, Cr^{+2} is a major dissolving species in the active region. Therefore it can be concluded that the surface nitride aids in corrosion inhibition of pure Cr by inhibiting the Cr^{+2} formation and aids in the formation of the Cr_2O_3

barrier film at OCP. As discussed in the previous section, XPS analysis (figure 5.2 and 5.3) shows that the electrochemical reduction of NO_3^- ions to the surface nitride on pure Cr is possible only under the conditions leading to the direct contact of metal surface to the NO_3^- ions, regardless of the applied potentials. Once pitting was initiated, the surface nitride was formed. This nitride acts as a precursor to the passive film and a buffer to local acidity, thus stabilizing first formed layers of the passive film. This behavior is repeated in N-alloyed stainless steels.

6.2 Synergistic Effect of N and Mo in Corrosion of Stainless Steels

The synergistic effect of N and Mo in corrosion of austenitic stainless steels was evaluated from two perspectives: (1) the influence of N and Mo on the alloy composition beneath the passive film and (2) the influence of N and Mo on the structure and formation of the passive film.

6.2.1 Metallic Enrichment beneath the Passive Film

Since very little Ni was found in the passive layer for all stainless steels, the role of Ni on the passivity of austenitic stainless steels could be overlooked. In recent studies,[9,10,16-19] the enrichment of metallic Ni underneath the passive film has been reported. The metal composition underneath the passive film of the three high Ni alloys investigated in this research are presented in figure 5.12. For the Fe20Cr20Ni alloy, the metallic Ni composition changed little (19.0 to 19.5 at% following passivation), while metallic Cr was enriched from 20.4 to at%. This result is not in good agreement with the results of 18-8 stainless steels, in which Cr and Ni were enriched (from 21 to 24 at% for Cr and from 8.2 to 15 at% for Ni). However the Ni/(Ni+Cr) ratios were almost the same (40.0 at% for Fe20Cr20Ni alloy and 38.5 at% for 304 stainless steels). This composition is close to that of the intermetallic compound Cr_3Ni_2. The 19.0 at% Ni of the Fe20Cr20Ni alloy is already high enough to form the intermetallic phase and therefore the Ni enrichment was not observed. The Fe20Cr20Ni6Mo alloy, exhibited the metallic enrichments of 21.6 to 23.9 at% for the Cr, 19.4 to 27.4 at% for the Ni and 3.5 to 6.1 at% for the Mo

underneath the passive film. The enrichment of Ni and Mo produces a composition ratio of Ni to Mo of ≈4.7. Comparing the results of the Fe20Cr20Ni6Mo alloy with those of the Fe20Cr20Ni alloy, less Cr and more Ni enrichment was observed. It is possible to explain the results for the Fe20Cr20Ni6Mo alloy by considering the formation of a Mo-Ni intermetallic phase of the type $MoNi_4$. According to the Engel-Brewer valence-bond theory of metallic bonding,[87,88] bonding between hypo-hyper d-electronic transition metals can result in intermetallic phases having great stability which is marked by both remarkable electrochemical and mechanical properties. The intermetallic bond between elements suitably separated in the periodic table can result from transfer of electrons from the hyper d-electron metal to the hypo d-electron metal. In consideration of this model it is apparent that $Ni(3d^8 4s^2)$, an hyper d-electron metal may react with $Cr(3d^5 4s^1)$ and $Mo(4d^5 5s^1)$, both hypo d-electron metals. The bonding effectiveness of the d-orbital increases upon going down the periodic table as reduced coulombic forces increase the distance between the nuclei and d-electrons (figure 6.4). The stability of the intermetallic bond between Mo and Ni should be higher

compared to the Cr-Ni bond. We propose that this stronger Mo-Ni intermetallic bond was the driving force for the enrichment of Mo and Ni during polarization. With 0.2 wt%N addition to Fe20Cr20Ni6Mo alloy, we observed that Ni and Mo were more highly enriched (from 19.4 to 30.1 at% for Ni and from 3.6 to 7.0 at% for Mo) and that Cr was less enriched (from 21.9 to 22.0 at%) compared to the results of the Fe20Cr20Ni6Mo alloy. Again we saw that the composition ratio of Ni to Mo was 4.5 and this ratio was very close to the $MoNi_4$ intermetallic compound phase, which is thermodynamically predicted in the Mo-Ni phase diagram.[89] Mo-Ni phase diagram is presented in figure 6.6.

As shown in chapter 5, the N1s binding energy in Mo bearing steel was found to be 397.2 eV, corresponding to N bound to Cr, Mo and Ni as a mixed nitride phase. Jack[48] has recently reported that while single nitrides of Mo and Ni (Mo_2N and Ni_3N) are thermodynamically relatively unstable, a mixed Mo-Ni nitride of the form Ni_2Mo_3N exhibited very high thermal stability (figure 6.5). In this case, according to the Engel-Brewer's model, we could expect strong interaction between Mo and Ni in such a mixed nitride. In the case of a surface

mixed nitride formed by preferential dissolution, a strong Mo-Ni interaction could be formed at the expense of the Cr-Ni interaction. The surface segregation of high N stainless steel during anodic polarization can be explained by the formation of these strong mixed nitrides. For the Fe20Cr20Ni6Mo0.2N alloy, Ni and Mo enrichment underneath the passive film should be expected greater than for the case of the Fe20Cr20Ni6Mo alloy. Strengthened lattice binding by intermetallic bonding with or without N can be expected to cause selective enrichment of Mo, Cr and Ni, in addition to increase selectivity for dissolution.

6.2.2 The Structure of Passive Film

The structure of the passive films of austenitic stainless steels polarized in a deaerated Cl^- solution at anodic potentials consists of inner Cr_2O_3 layer and outer $Cr(OH)_3$ layer. In Mo-bearing steels, MoO_4^{-2} was observed in the outer $Cr(OH)_3$ layer and served as a cation selective species, enhancing the bipolarity of the passive film and thereby decreasing the thickness of hydroxide layer due to the increased deprotonation. The hydroxide layer thickness of two Mo bearing steels (d_{OH}=

2.61 Å for Fe20Cr20Ni6Mo and Fe20Cr20Ni6Mo0.2N) is less than that of Fe20Cr20Ni alloy (d_{ON}= 4.92 Å), while the oxide layer is virtually same for all three alloys (d_{OX}= 10.65 Å). This shows that the deprotonation was enhanced due to the presence of the cation-selective MoO_4^{-2} species in the passive film. When 0.2 wt%N was added to Fe20Cr20Ni6Mo, a further increase of MoO_4^{-2} content in the passive film was observed. Hence, this increment of MoO_4^{-2} species revealed a direct synergistic effect of Mo and N resulting in enhancing the passivity.

6.3 The Effect of Nitrogen in the Corrosion of Pure Mo

In previous section 5.3, it was observed that the NO_3^- ions and surface nitride enhanced the passivity of Mo in a Cl^- solution. The passive film is composed of a mixture of Mo^{+4} and Mo^{+5}. Since this passive film is very thin, it is very hard to identify the Mo compound as oxide or hydroxide. Through a comparison of the XPS spectra shown in figure 5.14-5.16, it can be determined that the passive film formed on nitrate-treated Mo is slightly thicker than for pure Mo in deaerated 0.1M HCl. The formation of Mo oxide is enhanced by increasing the

local pH near the electrolyte-metal interface due to the formation of NH_3 and NH_4^+ and therefore, the passive current density was decreased.

The nitrided Mo remains passive above the transpassive potential for pure Mo (≈150 mV). During anodic polarization at 0.1M HCl at room temperature, pitting is initiated at 360 mV at several points, while the majority of the sample surface remains passive. This pitting corresponded to the glitches in figure 5.13. According to the XPS analysis shown in figure 5.17-5.19, the anodic film polarized at 250 mV (passive region) for 1 hour in 0.1m HCl is comprised of Mo^{+4} and Mo^{+5}. This film is completely different from the film formed on pure Mo at same potential (transpassive region) in the same solution. At 600 mV, Mo^{+4} and Mo^{+5} compounds were also observed, but a small amount of MoO_4^{-2} was detected. From the previous study,[19,39] pure Mo polarized at 250 mV is covered with a mixture of Mo^{+3}, Mo^{+4}, Mo^{+5} and Mo^{+6} oxides and, at 600 mV, the surface species is mainly MoO_3. It seems that nitrided Mo was favorably oxidized to a mixture of Mo^{+4} and Mo^{+5}, completely inhibiting the formation of MoO_3 at anodic potential. If the surface of nitrided Mo is exposed to the electrolyte (due to break

in the passive film), it can be easily and rapidly repassivated. Therefore nitrided Mo remains passive at 600 mV, while pure Mo is in the transpassive region. When the anodic potential becomes high enough to form Mo^{+6}, the nitrided Mo changes directly to MoO_4^{-2} instead of MoO_3 and pitting begins at several weak points. In figure 5.13, the pitting was initiated at 360 mV. The nitrided Mo reacts with H_2O and forms NH_3 ligand (or NH_4^+ in the solution). Due to this reaction, the local pH near the electrolyte-electrode interface becomes higher than that of the bulk solution. From the Pourbaix diagram,[81] when the pH shifts to a high value, MoO_4^{-2}, a soluble product, becomes the stable phase in stead of MoO_3 and the intermediate zone of Mo^{+3} also disappears. This agrees well with our observation that no Mo^{+3} and Mo^{+6} oxide has been observed from the anodic films formed on the nitrided Mo.

6.4 Influence of NH_3 on the Passive Film of 18-8 Steel

The structure of the passive film formed on the surface of 18-8 stainless steel is presented in figure 5.21. Since the NH_3 in ligand form was distributed in

the outer hydroxide layer and the thickness of the hydroxide layer was constant, the NH_3 peak intensity was normalized by the $Cr(OH)_3$ peak to compare different samples. Figure 5.28 shows the relation between the Fe ions and the NH_3 concentrations. As the NH_3 concentration in the passive film increases, the concentration of Fe ions decreases. By making the NH_3 complex with Cr^{+3} ($[Cr(NH_3)_5OH_2]^{+3}$), the NH_3 in the passive film increases the selective dissolution of the Fe ions in passive film and forms a Cr-enriched passive film. This Cr-enriched passive film inhibits attack by Cl^- ions and reduces the passive current density. For the case of pure Cr, the role of the NH_3 in the passive film is different. The NH_3 in the passive film of the N-doped Cr lowered the packing density of the $Cr(OH)_3$ layer by forming a NH_3 complex with Cr^{+3}. The Cl^- ions can easily attack the substrate Cr atoms through the loosened $Cr(OH)_3$ lattice. Therefore, the passivation current density of the N-doped Cr is higher than that of the non-treated Cr (figure 5.21). With the aid of above results, we can explain the incubation experiment. During the polarization of the 18-8 stainless steel in 0.1M HCl at -180 mV, the alloyed nitrogen changed to nitride and NH_3. This NH_3 complex

loosened the lattice of the outer $Cr(OH)_3$ layer and accelerated the selective dissolution of the Fe ions in the passive film. The NH_3 concentration of the 0.24 wt%N steel was higher than that of the 0.04 wt%N steel, i.e the 0.24 wt%N steel formed a more Cr-enriched film than the 0.04 wt%N steel. After 1 hour polarization at -180 mV in 0.1M HCl, by adding 0.1M HCl + 2.25M NaCl to obtain a 0.1M HCl + 0.75M NaCl solution, increased Cl^- ion concentration could more aggressively dissolve the Fe ions in the passive film. This selective dissolution induced the breakdown of the passive film. Therefore, for the 0.04 wt%N steel, the passive film broke down after 42 min, while the 0.24 wt%N steel still remained passive.

Previous work by our laboratory[6,7,10] showed that, during the cathodic nitrate-treatment, the doped N on the surface of the 0.04 wt%N 18-8 steel was almost nitride and that this surface nitride changed to the NH_3 during anodic polarization. Therefore, the potentiodynamic polarization curves presented in figure 5.20 can be explained using the effect of nitrogen species such as nitride and NH_3. At the beginning stage of the anodic polarization, the N-doped 0.04 wt%N alloy had the highest concentration of N on the surface among three samples i.e

the N-doped 0.04 wt%N steel had more surface mixed Cr-Ni nitride than the 0.24 wt%N steel. Because of the stable mixed nitride, the dissolution of Fe atoms increased and the active surface was enriched with Cr and Ni. This Cr and Ni enriched active surface lowered the critical current density by forming passive film. Therefore N-doped 0.24 wt%N alloy had the lowest critical current density. As the anodic polarization proceeded, the concentration of the surface N of the 0.24 wt%N alloy increased due to the surface segregation of alloyed N. Increased surface N due to the anodic segregation on the surface was responsible for the 0.24 wt% N alloy having the lowest value of the passivation current density and the highest value of the pitting potential. These results showed that a mixed surface nitride of the 18-8 stainless steel decreased the critical current densities.

7. CONCLUSION

1. Exposure of Cr surface to NO_3^- ions in the range from -930 mV to 1300 mV results in a surface nitride if the oxide is either; (a) non existence (cathodic condition), (b) perforated (active and transpassive) and (c) mechanically or chemically broken down (passive condition). Hence, the enhanced corrosion resistance of N-bearing stainless steels is not due to N oxidation to NO_2^- or NO_3^- which are very strong corrosion inhibitors.

2. This surface nitride aids in corrosion inhibition of Cr by inhibiting Cr^{+2} formation and aids in the formation of the Cr_2O_3 barrier film at open circuit potential.

3. The role of the surface nitride formed cathodically from NO_3^- ions, is analogous to that formed from anodic segregation of nitrogen in a N alloyed steel. This indicates both how NO_3^- corrosion inhibitors function and how N alloyed to stainless steel improve corrosion resistance.

4. The surface nitride enhances pitting resistance of steels, because the nitride acts as: (a) a precursor to the passive film and (b) a buffer to local acidity, thus stabilizing first formed layers of the passive film.

5. The passive films of pure Mo polarized in a acidic Cl^- solution comprised of Mo^{+4} and Mo^{+5}.

6. The surface N on pure Mo improves the passivity in a acidic Cl^- solution by following reasons: (1) suppressing the transpassive species, MoO_3 and (2) increasing local pH by the formation of NH_3 and NH_4^+.

7. The alloying with Mo improved pitting resistance of Cr-Ni-Fe alloy and lowered the rate of active dissolution of stainless steel in a Cl^- containing solution.

8. The N addition to a Mo-bearing steel was segregated as a surface nitride phase and suppressed active dissolution.

9. For Fe20Cr20Ni steel, only enrichment of metallic Cr underneath the passive film was observed. The Ni/(Ni+Cr) ratio has the same (around 40%) as that of 18-8 stainless steels polarized in 0.1M HCl.

10. For Fe20Cr20Ni6Mo steel, metallic Cr enrichment beneath the passive film decreased, while metallic Ni and Mo enrichment increased by forming what appears to be a stable Mo-Ni intermetallic phase.

11. With 0.2 wt% N addition to the Fe20Cr20Ni6Mo alloy, the metallic Cr enrichment beneath the passive film decreased further, and metallic Ni and Mo enrichment

increased to a greater magnitude compared to the Fe20Cr20Ni6Mo alloy, apparently by forming stable mixed nitride phase with Mo and Ni as the primary metallic constituents.

12. It means that a surface nitride is formed on N-bearing stainless steel which appears to decrease the critical current density and forms a precursor, a surface nitride, to an oxide passive film.

13. The structures of the passive films were agree well with the bipolar model of passivity, which consisted of the inner anion selective layer-oxide phase and the outer cation selective layer-hydroxide phase.

14. In Mo bearing steel, MoO_2, Mo^{+5} and MoO_3 were found in the inner layer of the passive film and MoO_4^{-2} ions were found in the outer layer.

15. The N addition to the Mo bearing steel enhance the bipolarity of the passive film by enhancing the formation of MoO_4^{-2} instead of MoO_3.

16. The NH_3 in the passive film of stainless steel enhances the selective dissolution of Fe ion in the film and leading to Cr-enrichment in the passive film by forming a stable NH_3 complex such as $[Cr(NH_3)_5OH_2]^{+3}$.

17. The NH_3 in the passive film makes passive film more

active for pure Cr, while more passive for the 18-8 stainless steels.

18. The NH_3 plays a major role in improving the pitting resistance and in reducing the passive current density.

8. FUTURE INVESTIGATIONS

8.1 Electrochemical Analysis of Intermetallic Compounds

In this study, metallic Ni enrichment beneath the passive film was observed in detail to determine its important role in enhancing the passivation behavior of austenitic stainless steels by forming an intermetallic compound. For 18-8 and Fe20Cr20Ni alloys, the concentration ratio of Cr to Ni is ≈1.5 and Cr_3Ni_2 intermetallic compound is predicted. For Fe20Cr20Ni6Mo alloy, the ratio of Mo to Ni is ≈4.7 and $MoNi_4$ intermetallic compound is suggested. Therefore, it is probable that electrochemical analysis of Cr_3Ni_2 and $MoNi_4$ intermetallic compounds can lend further proof of the role of Ni. Also, surface nitride, which is formed by electrochemical reduction of NO_3^- on the above intermetallic compounds, will affect metal phase modification during anodic polarization and provide more detailed information on the N-Mo synergism.

8.2 Temperature Effect of N-Mo Synergism

Previous work of our group reported the results of electrochemical analysis for AL6X and AL6XN in acidic solution at high temperature.[90] As electrolytes, two types of solution, 0.1M HCl + 2M NaCl and 0.5M H_2SO_4, were used. Salient electrochemical characteristics vs. temperature trends are presented in figure 8.1 and 8.2. For both alloys and both electrolytes, OCP (open circuit potential) and E_{br}(transpassive potential) are independent of temperature and alloying N concentration. However, big increments of critical and passive current densities were observed, as the temperature increase. For both electrolytes, the passive current density (I_{pass}) of AL6XN was higher than AL6X at all temperatures. The critical current density (I_{crit}) of AL6XN became less than AL6X in Cl^- solution. But, in 0.5M H_2SO_4, AL6XN exhibited little change, while AL6X showed a large increment with increasing temperature. As discussed in chapter 6, the N influence on OCP, E_{br} and I_{pass} at elevated temperature, is similar to that at room temperature except I_{crit} in 0.2M NaCl + 0.1M HCl. As anodic potential increases, alloying N becomes segregated on surface in forms of

nitride, NH_3 and NH_4^+. This segregated N enhances selective dissolution of iron of steel substrate. At elevated temperature, anodic dissolution rate also increases and therefore the concentration of segregated N on AL6XN increases more rapidly than AL6X. If enough N segregates to form surface nitride on the entire surface, extra N changes to NH_3 and NH_4^+. The NH_3 and NH_4^+ enhances the dissolution of metallic elements by reducing local acidity. However, in the passive region, NH_3 and/or NH_4^+ of the passive film, which was discussed in chapter 6, only enhances the selective dissolution of Fe ions in the passive film, aids the formation of more stable Cr-enriched film and lessens I_{pass}. Quantitative XPS analysis of the surface of AL6XN and AL6X in the active and in the passive regions will provide solid information of the role of N on the corrosion of austenitic stainless steels.

According to the research performed by R. Matsuhashi et al.,[91] the corrosion rate of stainless steels in highly concentrated sulfuric acid decreased as Ni content increased in the low temperature below 60°C. Conversely, the corrosion rate increased proportionally to the increase of Ni content in the high temperature

above 60°C. Therefore, through the measurements of the temperature effect on modifying the metallic concentration underneath the passive film, the role of Ni could be also determined.

REFERENCES

1. W. T. Delong, Weld. J., 53, 273-s (1974)
2. J. E. Truman, M. J. Coleman and K. R. Pirt, Br. Corro., J. 12, 236(1977)
3. J. J. Eckenrod and C. W. Kovack, ASTM Prec. Tech. Publ. STP, 679, 17(1977)
4. C. R. Clayton, L. Rosenzweig, M. Oversluizen and Y. C. Lu, in "Inhibition and Passivation", Eds. E. McCafferty and R. J. Brodd, Electrochem. Soc., Pennington N.J., 1986, p.369.
5. J. R. Kearns and H. E. Deverell, Mat. Perf., 26, 18(1987)
6. Y. C. Lu, R. Bandy, C. R. Clayton and R. C. Newman, J. Electrochem. Soc., 130, 1774(1983)
7. R. Bandy, Y. C. Lu, R. C. Newman and C. R. Clayton, Proc. Equilibrium Diagrams and Lcalized Corrosion Symp., Eds. R. Frankenthal and J. Kruger, The Electrochem. Soc., Pennington, 1984, p.471
8. K. Osozawa and N. Okato, in "Passivity and its Breakdown on Iron Base Alloy", Eds. R. Staehle and H. Okada, NACE, Houston, 1976, p.135
9. C. R. Clayton and K. G. Martin, in "High Nitrogen Steels", Eds. J. Foct and A. Hendry, The Inst. of Meatls, 1989, p.256.
10. R. D. Willenbruch, C. R. Clayton, M. Oversluizen, D. Kim and Y. C. Lu, Corro. Sci., 31, 179(1990).
11. A. J. Sedricks, Int. Metal. Rew. 28, 5, 306(1983)
12. M. A. Streicher, J. Electrochem. Soc., 103, 375(1956)
13. R. Bandy and D. Van Rooyen, Corrosion, 39(6), 227

(1983)

14. R. C. Newman, Y. C. Lu, R. Bandy and C. R. Clayton, Proc. Ninth International Congress on Metallic Corrosion, Toronto 3, 1984, p.395
15. O. I. Lukina et al., Zashet. Met. 115(5), 545(1979)
16. C. R. Clayton and J. E. Castle, Corros. Sci., 7, 1(1977)
17. I. Olefjord and B-O. Elfstrom, Proc. 6th Eur. Congress on Metallic Corrosion, T. P. Hoar, ed. Soc. Chem. Indust., London, 1977, p.21
18. I. Olefjord, B. Brox and U. Jelvestam, J. Electrochem. Soc., 132, 2854(1985)
19. Y. C. Lu and C. R. Clayton, J. Electrochem. Soc., 132, 2517(1985)
20. M. Koudelkova and J. Augustynski, J. Electrochem. Soc., 126, 1659(1979)
21. A. M. McKissick Jr., A. A. Adams and R. T. J. Foley, J. Electrochem. Soc., 117, 1459(1970)
22. D. Pletcher and Z. Poorabedi, Electrochemica Acta, 24, 1253(1979)
23. M. Datta, H. J. Mathieu and D. Landolt, in "Passivity of Metals and Semiconductor", Eds. M. Froment, Elsevier Scientific Publishing Co., Amsterdam, 1983, p.113
24. R. C. Newman and T. Shahrabi, Corros. Sci., 27(8), 827(1987)
25. R. C. Newman and A. A. Ajjawi, Corros. Sci., 26, 1057 (1986)
26. M. Oversluizen, M.S. Thesis, 1988, SUNY at Stony Brook

27. R. Willenbruch, M.S. Thesis, 1989, SUNY at Stony Brook
28. H. H. Uhlig, Trans. ASM, 30, 947(1942)
29. V. Chigal, V. M. Knyazheva, Ya. Pitter, S. G. Babich and S. D. Bogolyuskii, Prot. of Met., 22, 164(1986)
30. Ya. M. Kolotyrkin, I. A. Stepanov, V. M. Knyazheva and S. G. Babich, Poc. Ninth International Congress on Metallic Corrosion Toronto 1, 1984, p258
31. K. O. Ozozawa at al., Corros. Eng.(Boshoku Gijuzu), 24, 1(1975)
32. R. C. Newman, Corros. Sci., 25, 331(1985)
33. R. C. Newman, Corros. Sci., 25, 341(1985)
34. I. Olefjord and C. R. Clayton, ISIJ International, 31(2), 134(1991)
35. K. H. Jack, in "High Nitrogen Steels," Eds. J. Foct and A. Hendry, Inst. of Metals, London, 1989, p.117
36. D. E. Williams, C. Westcott and M. Fleishman, J. Electrochem. Soc., 130, 1774(1983)
37. T. Heumann and G. Hauck, Z. Metallk, 56, 75(1965)
38. Y. C. Lu and C. R. Clayton, Corro. Sci., 29(8), 927 (1989)
39. Y. C. Lu and M. B. Ives, Accepted for publication in Corrosion Science.
40. Swanson and Fuyat, NBS Circular 539, Vol III (1953)
41. C. R. Clayton and Y. C. Lu, Corro. Sci., 29(7), 881(1989)
42. L. L. Wilkstrom and K. Nobe, J. Electrochem. Soc., 116, 525(1969)
43. M. N. Hull, J. Electroanal. Chem. Interf. Electrochem., 38, 143(1972)

44. V. B. Kozhevnikov, T. E. Tsenta, V. M. Knyazheva and Ya. M. Kolotyrkin, Prot. Met. 19, 596(1983)
45. B. Brox and I. Olefjord, in "Passivity of Metals and Semiconductors," Eds. M. Froment, Bombannes, France, 1983.
46. B. Brox and I. Olefjord, J. Electrochem. Soc. 132, 2854(1985)
47. R. O. Ansell, T. Dickinson, A. F. Povey and P. M. A. Sherwood, J. Electroanal. Chem., 98, 79(1979)
48. A. A. Pozdeeva, E. I. Antonovskaya and A.M. Sukhotin, Prot. Met. 1, 15(1965)
49. M. König and H. Göhr, Ber. Bunsenges phys. Chem. 67, 837(1963)
50. M. Sakashita and N. Sato, in "Passivity of Metals," Eds. R. P. Frankenthal and J. Kruger, Electrochem. Soc., (1978) p.740
51. M. Sakashita and N. Sato, Corros Sci., 17, 473(1977)
52. C. R. Clayton and Y. C. Lu, J. Electrochem. Soc., 133, 2465(1986)
53. A. R. Brook, C. R. Clayton, K. Doss and Y. C. Lu, J. Electrochem. Soc., 133, 2459(1986)
54. Y. C. Lu, C. R. Clayton and A. R. Brooks, Corro. Sci., 29(7), 863(1989)
55. C. S. Fadley, R. J. Baird, W. Siekhaus, T. Novakov and S. Å. L. Bergström, J. Electron Spec., 4, 93(1974)
56. C. S. Fadley, Faraday Discuss., Chem. Soc., 60, 265 (1975)
57. C. S. Fadley, J. Electron Spec., 5, 725(1974)
58. C. S. Fadley, Prog. Solid State Chem., 11, 265(1976)

59. C. S. Fadley, Prog. Surf. Sci., 16, 275(1984)
60. Y. M. Cross and J. Dewing, Surf. Int. Anal., 1, 26 (1979)
61. L. B. Hazell, I. S. Brown and F. Freisinger, Surf. Int. Anal., 8, 25(1986)
62. C. J. Powell, in "Quantitative Surface Analysis of Materials," Ed. N. S. McIntyre, No. 643, ASTM, Philadelphia(1978), p.5
63. C. Battistoni, G. Mattogono and E. Pararazzo, Surf. Int. Anal., 7, 117(1985)
64. J. C. Ashley, C. J. Tung, Surf. Int. Anal., 4, 52 (1982)
65. J. M. Hill, D. G. Royce, C. S. Fadley, L. F. Wagner and F. J. Grunthaner, Chem Phys. Lett., 44, 225(1976)
66. T. D. Bussing, P. H. holloway, Y. X. Wang, J. F. Moulder and J. S. Hammond, J. Vac. Sci. Technol., B6(5), 1514(1988)
67. T. D. Bussing and P. H. Holloway, J. Vac. Sci. Techno., A3(5), 1973(191985)
68. S. Tanuma, C. J. Powell and D. R. Penn, Surf. Interf. Anal., 11, 577(1988)
69. M. P. Seah and W. A. Dencn, Surf. Interf. Anal., 1(1), 2(1979)
70. C. N. Berglund and W. E. Spicer, Phys. Rew., 136 (1964) A1030, A1044.
71. M. F. Ebel and J. Wernish, Surf. Interf. Anal, 3, 191 (1981)
72. M. P. Seah, Surf. Interf. Anal., 2, 222(1980)
73. D. R. Penn, J. Electron. Spec., 9, 29(1976)
74. C. J. Powell, J. Vac. Sci. Tech., A3, 1338(1985)

75. Y. M. Cross and J. Dewing, Surf. Interf. Anal., 1, 26(1979)
76. ASTM Annual Book of Standards, (1984) Designation G5-82, p 123.
77. "Handbook of X-ray Photoelectron Spectroscopy," Eds. C. D. Wagner, W. M. Riggs, L. E. Davis, J. F. Moulder and G. E. Muilenberg, Perkin-Elmer Corporation,(1979)
78. K. Siegbahn et al., "ESCA, Atomic, Molecular and Solid State Structure Studied by Means of Electroscopy," Almquist and Wikskells, Uppsala(1967)
79. L. C. Feldman and J. W. Mayer, "Fundamentals of Surface and Thin Film Analysis," North-Holland, NY (1986)
80. "Practical Surface Analysis," Eds. D. Briggs and M. P. Seah, J. Wiley and Sons Ltd., (1983)
81. M. Pourbaix, "Atlas of Electrochemical Equilibria," Pergamon Press, Oxford(1966).
82. M. Romand and M. Roubin, Analysis, 4(7), 308(1976)
83. I. Olefjord and L. Wegrelius, Corros. Sci., 31, 89 (1990)
84. J. R. Galvele, in "Passivity of Metals", Eds. R. Frankenthal and J. Kruger, The Electrochem. Soc., Pennington, 1978, p.285
85. D. C. Grahame, Chem. Rev., 41, 441(1947)
86. "The inorganic chemistry of nitrogen," Eds. William L. Jolly, W. A. Benjamin, Inc., (1964).
87. L. Brewer, Science, 161, 115(1968)
88. M. M. Jaksic, Mat. Chem. Phys., 22, 1(1989)
89. M. Hansen, "Constitution of Binary Alloy," McGraw-Hill, NY(1958)

90. K. G. Martin, M.S. Thesis, 1988, SUNY at Stony Brook
91. R. Matsuhashi, E. Sato, S. Abe and H. Abo, Corro. Eng., 39, 89(1990)
92. F. Honda and K. Hirokawa, J. Elect. Spect. Rel. Phenom., 10, 125(1977)
93. F. Honda and K. Hirokawa, J. Elect. Spect. Rel. Phenom., 12, 313(1977)

APPENDIX

XPS Analysis of Molybdenum Pentoxide Formation

1. ABSTRACT

Using the XPS technique, the formation of Mo^{+5} was observed through each of the following different preparations; (1) the oxidation of pure Mo at 400°C in 0.1 torr O_2, (2) thermal reaction of MoO_3 powder with pure Mo at 600°C in 10^{-9} torr, (3) the reduction of MoO_3 powder with Zn in concentrated HCl, (4) the reduction of MoO_4^{-2} ions on an activated platinum electrode following cathodic polarization in deaerated 0.1M $(NH_4)_6Mo_7O_{24}\cdot 4H_2O$ at -470mV, -700mV and -900mV at 22°C. The binding energy of $Mo3d_{5/2}$ photoelectron of Mo^{+5} oxide has been consistent measured at 230.8 eV. These Mo oxyhydroxide compounds and a cathodic reduction product of an ammonium paramolybdate on a platinum electrode have been characterized by XPS and X-ray diffraction. The passive films of pure Mo polarized at 50 mV (vs. S.C.E.) for 1 hour in deaerated 0.1M HCl were found to be comprised of Mo^{+4} and Mo^{+5}.

2. INTRODUCTION

It is well known that Molybdenum has a very strong effect on improving the pitting resistance and lowering the rate of the anodic dissolution of stainless steel.[1,2] In addition, a small amount of nitrogen addition improves the above properties of stainless steels through its apparent synergism with molybdenum.[3-12] XPS has played a major role in determining the influence of Mo in improving passivation.

The Mo(V) species has been indicated from the work of Pozdeeva and co-workers[13], who investigated the electrochemical properties of all known Mo oxides using experimental and thermodynamic methodologies. In that study, thermodynamic calculations of potentials corresponding to the oxidation of Mo and MoO_2 to Mo_2O_5 in an acidic solution were reported. By the electrical measurements, several authors[14-16] have suggested that MoO_2 is the passivation compound of pure Mo. However, the passive films formed on pure Mo in 0.1M HCl have been analyzed, using variable angle XPS, by Lu and Clayton.[17] In that study, the existence of a thin passive film on

pure Mo was observed and the possibility that the passive film was comprised of MoO_2 and Mo_2O_5 was suggested, even though Mo_2O_5 was one of the transpassive products of acidic solution by using XPS technique.

In this study, again using XPS analysis, the existence of Mo^{+5} was confirmed and the binding energy of Mo3d photoelectron of Mo^{+5} was measured via four different types of sample preparations. These were as follows: (1) the oxidation of pure Mo at 400°C in 0.1 torr O_2, (2) thermal reaction of MoO_3 powder with pure Mo at 600°C in 10^{-9} torr, (3)the reduction of MoO_3 powder with Zn in concentrated HCl, (4) the reduction of MoO_4^{-2} ions on an activated platinum electrode following cathodic polarization in deaerated 0.1M ammonium paramolybdate at -470mV, -700mV and -900mV at 22°C. And also the existence of Mo^{+5} in the passive film of pure Mo polarized in a Cl^- solution.

3. XPS ANALYSIS OF Mo^{+5} OXIDE COMPOUNDS

The existence of Mo^{+5} has already been known in chemistry for a long time.[18-21,29] A valence state which has a

binding energy of Mo3d photoelectron between +6 and +4 valent molybdenum was detected by several investigators using XPS.[20-22] Kim et al.[22] used the formula MoO_x(2<x<3) for this state, because they proposed it to be a mixture of valence states between 4 and 6. Olefjord et al.[23-25] investigated the binding energies of Mo3d photoelectron of Mo oxide compounds. Mo oxides were prepared at 700°C in 1 torr O_2 and in 1 torr H_2O and analyzed with XPS. The binding energies of Mo3d photoelectron of Mo oxide compounds reported by them were 232.3 eV corresponding to MoO_3, 229.1 eV corresponding to MoO_2 and 230.7 eV corresponding to Mo^{+4} hydroxide and the satellite peak of MoO_2. Ürgen et al.[26] reported the existence of Mo^{+5} mixed with Mo^{+6}, Mo^{+4} and Mo^{+3} in the films formed on pure molybdenum by anodic oxidation in a acidic chloride solution at different potentials in the passive and transpassive region. In this work, the binding energy of Mo3d photoelectron of Mo^{+5} compound was found to be 230.8 ± 0.2 eV. McIntyre et al.[27] reported using XPS analysis that Mo^{+6} and Mo^{+5} were observed on the pure Mo oxidized at 200°C in 1 atm O_2 for 1 hour and that Mo^{+5} was also observed on Mo oxides film formed during ion beam deposition on Co_3O_4. The binding energy of Mo3d

photoelectron of this Mo^{+5} was found to be at 231.1 ± 0.2 eV($Au4f_{7/2}$ standard is 83,9 eV). Clayton and Lu[28] proved the existence of Mo_2O_5 with XPS analysis by preparing samples in two ways; (1) Reacting MoO_3 powder with pure Mo at 750°C for 1 hour under argon[29] and (2) Reduction of MoO_4^{-2} on an activated Pt electrode by cathodic polarization in 0.1M deaerated ammonium paramolybdate solution.

4. EXPERIMENTAL

It is very difficult to obtain pure Mo_2O_5 or $Mo(OH)_5$, since these compounds are thermodynamically unstable. To prove the existence of Mo^{+5} in the forms of oxide and oxyhydroxide, several types of preparations were performed in this study. All metallic specimens in coupon forms were ground with 600 grit SiC paper disc and polished with 6 μm and 0.25 μm diamond paste followed by ultrasonic cleaning first in acetone and then in ios-propanol.

4.1 Oxidation of Pure Mo

Pure Mo(99.99%) in coupon form was used in this study. After being polished and cleaned, the sample was transferred to the spectrometer. To remove air-formed oxide, the sample was etched with Ar ion plasma for 15 min in UHV(Ultra High Vacuum). Oxidation was carried out at 400°C for 1 hour in 0.1 torr O_2 and then XPS analysis was performed.

4.2 Reaction of MoO_3 Powder with Pure Mo

After pure Mo(99.99%) was polished and cleaned, a little amount of MoO_3 powder was put on the pure Mo. This sample was transferred to the spectrometer. The entire procedure was carried out under argon atmosphere to reduce the possibility of surface modification. XPS analyses of this sample were performed as received. To proceed the reaction between MoO_3 and pure Mo, heat treatment was performed at 600°C for 1 hour in 10^{-9} torr.[29] the final product was also analyzed with XPS technique.

4.3 Formations of Mo Oxyhydroxide Compounds

Mo oxyhydroxides were prepared following Glemser and Lutz[30,31]. The most highly reduced phase, $Mo_5O_5(OH)_{10}$(green compound) was obtained by reducing MoO_3 with Zn in concentrated HCl for 10 hours, whilst $Mo_5O_7(OH)_8$(red compound) was made by oxidizing $Mo_5O_5(OH)_{10}$ in air. To remove any kind of Mo chloride compounds, $Mo_5O_5(OH)_{10}$ compound was rinsed with doubly distilled water after filtration. Further oxidized phase, H_xMoO_3 ($0.34<x<0.93$, blue compound) was made by mixing MoO_3 and $Mo_5O_5(OH)_{10}$ under Ar atmosphere. And then all these compounds were analyzed with XPS and X-ray diffraction techniques.

4.4 Preparation of Reduction Products of MoO_4^{-2} Ions by Cathodic Polarization

A 0.5 mm thick pure Pt(99.99%) coupon of 8 x 12 mm was used as a cathode. After the Pt coupon was polished and cleaned, this coupon was mounted for polarization. Polarization was carried out in a conventional Greene cell containing 0.1M $(NH_4)_6Mo_7O_{24}\cdot 4H_2O$ solution(pH 5.8),

which was first deaerated with argon for at least 2 hours. All polarization were carried out at room temperature (22°C). The specimens were pulsed to a specific potential(-470 mV, -700 mV and -900mV) and maintained there for 1 hour to prepare a surface film of cathodically reduced product for subsequent XPS analysis. Following the potentiostatic polarization treatment, the electrode was removed from the cell, rinsed with deaerated doubly distilled water and transferred to the spectrometer. The entire procedure was conducted in an argon-purged glove box to avoid the possibility of surface modification.

4.5 Formation of the Passive Film on Pure Mo in Cl^- Containing Solution

After pure Mo sample was polished and cleaned, a potentiostatic polarization were performed in a conventional Greene cell at room temperature. In order to remove the air-formed film, cathodic pretreatments were conducted in deaerated 0.1M HCl for 15 min at -700 mV. And then potentiostatic polarizations were performed at 50 mV(passive region) for 1 hour in deaerated 0.1M HCl

at room temperature. After the polarizations, the samples were rinsed immediately with deaerated doubly distilled water, dried with an argon jet and transferred to the spectrometer under argon atmosphere.

4.6 XPS Analysis

All XPS measurements were performed using a V.G. Scientific ESCA 3 MKII spectrometer controlled by a VGX900 data system. An Al $K\alpha_{1,2}$ X-ray(1486.6 eV) source and a 20 eV pass energy were used for all analysis providing a FWHM for the $Au4f_{7/2}$ singlet of 1.25 eV. As a reference, the binding energy of the $Au4f_{7/2}$ electron was found to be 83.8 eV. By taking C1s spectra from the adventitious carbon at 284.6 eV, all binding energies were corrected for charge shifting. A Shirley background subtraction was conducted for each multiplet in the spectral region under analysis.

5. RESULTS AND DISCUSSION

5.1 Oxidation of Pure Mo

Figure 1 showed Mo3d and Mo3p spectra for pure Mo oxidized at 400°C for 1 hour in 0.1 torr O_2. Before oxidation, no oxide was found since sample was ion-etched with Ar^+ plasma. After oxidation, three different types of molybdenum oxides were observed. Their binding energies of $Mo3d_{5/2}$ photoelectron were 229.0 eV, 230.8 eV and 232.5 eV. The peaks at 229.0 eV and at 232.5 eV were agreed well with the standard binding energies of MoO_2 and MoO_3 respectively. Also, the binding energies of Mo3p photoelectron of above two compounds were matched well with MoO_2(395.7 eV) and MoO_3(398.7 eV) standards. Therefore it could be concluded that the oxidation valence of the compound located at 230.8 eV is between +4 and +6. Temporarily this compound can be called $Mo^{+n}(4<n<6)$.

5.2 Reaction of MoO_3 powder with pure Mo

Mo3d and Mo3p XPS spectra before and after reaction of

MoO_3 powder with pure Mo at 600°C for 1 hour in 10^{-9} torr were presented in figure 2. Before reaction, two compounds which corresponded to pure Mo and MoO_3 were observed. After reaction, three types of Mo compounds were observed. The binding energies of $Mo3d_{5/2}$ photoelectron were 227.7 eV, 229.0 eV and 230.8 eV corresponding respectively to metallic Mo, MoO_2 and Mo^{+n}. In this experiment, the peak at 230.8 eV was also found as in the oxidation of pure Mo. Since the condition of the reaction between MoO_3 powder and pure Mo is very similar to the Cotton and Wilkinson's model[29] for the formation of a Mo_2O_5, this reaction can be assumed as following chemical equation;

$$10MoO_3 + 5Mo = 6Mo_2O_5 + 3Mo = 15MoO_2$$

In figure 2, the MoO_3 species is not found after the reaction. It means that all MoO_3 was used for the reaction and that the final products, metallic Mo, Mo_2O_5 and MoO_3, could be observed with XPS. Therefore it is concluded that the peak at 230.8 eV corresponds to Mo_2O_5.

5.3 Analysis of Mo Oxyhydroxide

Following Glemser and Lutz[30,31], three kinds of Mo

oxyhydroxide powders($Mo_5O_5(OH)_{10}$: green, $Mo_5O_7(OH)_8$: red, MoO_3+$Mo_5O_5(OH)_{10}$: blue) were prepared. Mo3d, Mo3p and O1s XPS spectra for these three compounds were presented in figure 3. For all powders, three different types of Mo3d doublet were consistently found at the binding energies of 229.0 eV, 230.8 eV and 232.5 eV. To avoid the possibility of any kinds of Mo chloride formation(the binding energy of $MoCl_5$= 230.5 eV), $Mo_5O_5(OH)_{10}$ was rinsed with deaerated doubly distilled water during filtration. Since Cl2p XPS spectrum was very weak and negligible, the binding energy of 230.8 eV should not correspond to Mo^{+5} chloride. Three values of the binding energies, 229.0 eV, 230.8 eV and 232.5 eV, are identical to the binding energies of MoO_2, Mo_2O_5 and MoO_3 respectively. The peaks area ratios of the OH^- spectrum to the O^{-2} spectrum were found to be 2.00 for green compound and to be 1.25 for the red compound. Compared to the theoretical ratio of OH^- to O^{-2}(2 for $Mo_5O_5(OH)_{10}$ and 1.14 for $Mo_5O_7(OH)_8$), it could be concluded that the green compound was $Mo_5O_5(OH)_{10}$ and that the red compound was very close to $Mo_5O_7(OH)_8$. X-ray diffraction data also supported a strong evidence in identifying these three compounds. Figure 6 shows that the X-ray diffraction data of MoO_2, MoO_3 and $Mo_5O_7(OH)_8$

(Red oxyhydroxide compound) were agreed well with the standards. And it was observed that blue compound was very close to $Mo_2O_5(OH)$ and green compound was a mixture of $Mo_5O_5(OH)_{10}$ and a little amount of $Mo_5O_7(OH)_8$. Because green compound is easily oxidized in air, the surface layer is oxidized a little. Even though the sample was sealed with a thin plastic sheet under Ar atmosphere, there must be a little amount of air leak during X-ray diffraction. In figure 3, the major peak 2(6) at 229.0 eV for green compound should be corresponding to Mo^{+4} oxyhydroxide, since the area ratio of the OH^- spectrum to the O^{-2} spectrum was 2.00. Because average oxidation number of red compound($Mo_5O_7(OH)_8$) is 4.4, two major species corresponding to peaks at 229.0 eV and 230.8 eV should be Mo^{+4} and Mo^{+5} oxyhydroxide. Even though the peak 2(6) for Mo3d XPS spectra for $Mo_5O_5(OH)_{10}$ corresponded to Mo^{+4} oxyhydroxide, the binding energy of $Mo3d_{5/2}$ was identical to that of MoO_2. According to the structure of $H_xMoO_4(0\leq x\leq 2)$ explained by Dickens et al.,[32] the hydrogen insertion reaction,

$$xH(g) + MoO_3(s) = H_xMoO_3(s)$$

leaves the MoO_3 framework unchanged topologically and leads to the formation of $x\text{-}OH_2$. The number of Mo-O

linkages remains unchanged (six per Mo atom) but the mean Mo-O bond strength will vary with the mean oxidation state of Mo. Therefore it can be concluded that the binding energies of Mo3d photoelectron depend on the oxidizing states regardless of Mo oxide or Mo oxyhydroxide compound. As a similar result, it is observed that the binding energy difference for Mo3d photoelectron between H_2MoO_4(232.7 eV) and MoO_3(232.5 eV) is only 0.2 eV. The color of the mixed powder of MoO_3(white) and $Mo_5O_5(OH)_{10}$(green) changed to blue. For this mixed powder, Mo^{+5} and Mo^{+6} species were observed, even though Mo^{+4} and Mo^{+6} compounds were mixed. After being mixed, these two powders reacted with each other and changed to an oxidized compound, $Mo_2O_4(OH)_2$ or $Mo_4O_{10}(OH)_2$, because $Mo_5O_5(OH)_{10}$ was easily oxidized.

5.4 Reduction Products of MoO_4^{-2} by Cathodic Polarization

The cathodic polarization curve of platinum in a deaerated solution of 0.1M ammonium paramolybdate performed by Clayton and Lu[28] is given in figure 4. For the inflexion pcints at potentials, -160, -340 and -540 mV, potentiostatic polarizations were performed at -270, -470, -700 and -900 mV respectively. The formation of

Mo_2O_5 was reported at potentials -470, -700 and -900 mV. The binding energy of $Mo3d_{5/2}$ photoelectron of Mo_2O_5 (231.3 eV) is 0.8 eV higher than that of this work (230.8 eV). To confirm the formation and the binding energy of Mo_2O_5, three potentials, -470mV, -700mV and -900mV were chosen as polarization potentials in this work. Figure 5 is a comparison of XPS spectra obtained from $(NH_4)_6Mo_7O_{24}\cdot 4H_2O$ powder and the surface of the platinum electrode following cathodic polarization at specific potentials in deaerated 0.1M ammonium paramolybdate. After the platinum electrode was cathodically polarized at -470mV for 1 hour, the electrode was covered with a thin brown film. XPS analysis reveals a mixture of $(NH_4)_2MoO_4$ and Mo_2O_5. Following cathodic polarizations at -700 mV and at -900 mV for 1 hour in deaerated 0.1M ammonium paramolybdate, the platinum electrode was covered with a thick, black and very poorly adherent film for both potentials. XPS analysis showed a mixture of Mo^{+5} and a little amount of Mo^{+4}. By exposing to air for 4 days, no change in the XPS spectra was observed. This result indicated the presence of stable Mo_2O_5. On similar experiment performed by A. S. Goncharenko[21], the black cathode deposit was $Mo_2O_5\cdot 2H_2O$. This $Mo_2O_5\cdot 2H_2O$ was very

stable, since they used HNO_3 to oxidize this compound. In figure 6, X-ray diffraction data of this cathodic deposit is different from those of MoO_2 and MoO_3 powders. It means that Mo_2O_5 is not the mixture of MoO_2 and MoO_3. The structural analysis of the Mo_2O_5 compound is assigned to a future study.

5.5 Analysis of the Passive Film on Pure Mo

The possibility that Mo^{+4} and Mo^{+5} are the passivation compounds on the corrosion of pure Mo in 0.1M HCl is suggested through XPS analysis by Lu and Clayton[17]. Figure 7 is the XPS spectra obtained from pure Mo polarized at 50 mV in 0.1M HCl. The XPS data indicates that the passive film is comprised of Mo^{+4} and Mo^{+5}. The values are in good agreement with the binding energies of our standards. This indicates that Mo^{+4} was located close to the metal-passive film interface and that Mo^{+5} was located in the outer region of passive film.

6. CONCLUSION

1. Mo compound, whose binding energy of Mo3d photo-

electron is 230.8 eV in this work, is Mo^{+5} oxide or oxyhydroxide.

2. The binding energies of Mo3d electrons of Mo oxides and oxyhydroxides are consistent, depending on the oxidizing state.
3. In the reduction experiment of MoO_4^{-2} ions on a activated Pt electrode by cathodic polarization, stable Mo_2O_5 compound with a small amount of Mo^{+4} was obtained at potentials of less than -540 mV.
4. The passive films of pure Mo polarized in acidic solutions containing Cl^- ions are comprised of Mo^{+4} and Mo^{+5} species.

7. ACKNOWLEDGEMENT

This work was supported by the Office of Naval Research (Dr. A. J. Sedricks, Contract Officer) under contract No. N0001485k0437.

8. REFERENCE

1. K. Osozawa and N. Okato, in "Passivity and its Breakdown on Iron Base Alloy", Eds. R. Staehle and H. Okada, NACE, Houston, 1976, p.135

2. M. A. Streicher, J. Electrochem. Soc., 103, 375(1956)
3. Y. C. Lu, R. Bandy, C. R. Clayton and R. C. Newman, J. Electrochem. Soc., 130, 1774(1983)
4. R. Bandy, Y. C. Lu, R. C. Newman and C. R. Clayton, Proc. Equilibrium Diagrams and Localized Corrosion Symp., Eds. R. Frankenthal and J. Kruger, Electrochem. Soc., Pennington, 1984, p.471
5. C. R. Clayton, L. Rosenzweig, M. Oversluizen and Y. C. Lu, in "Inhibition and Passivation", Eds. E. McCafferty and R. J. Brodd, Electrochem. Soc., Pennington N.J., 1986, p.369
6. J. E. Truman, M. J. Coleman and K. R. Pirt, Br. Corro., J. 12, 236(1977)
7. R. Bandy and D. Van Rooyen, Corrosion 39, 6, 227 (1983)
8. R. C. Newman, Y. C. Lu, R. Bandy and C. R. Clayton, Proc. Ninth International Congress on Metallic Corrosion, Toronto 3, 1984, p.395
9. O. I. Lukina et al., Zashet. Met. 115, 5, 545(1979)
10. A. J. Sedricks, Int. Metal. Reviews 28, 5, 306(1983)
11. R Bandy, Y. C. Lu, R. C. Newman and C. R. Clayton, in "Equilibrium Diagrams Localized Corrosion", Eds. R. P. Frankenthal and J. Kruger, Electrochem. Soc., Pennington, N.J.(1986) p.369
12. R. D. Willenbruch, C. R. Clayton, M. Oversluizen, D. Kim and Y. Lu, Corros Sci., 31, 179(1990)
13. A. A. Pozdeeva, E. I. Antonovskaya and A.M. Sukhotin, Prot. Met. 1, 15(1965)
14. L. L. Wilkstrom and K. Nobe, J. Electrochem. Soc.,

116, 525(1969)
15. M. König and H. Göhr, Ber. Bunsenges phys. Chem. 67, 837(1963)
16. T. Heumann and G. Hauck, Z. Metallk, 56, 75(1965)
17. Y. C. Lu and C. R. Clayton, Corro. Sci., 29(8), 927(1989)
18 C. L. Rollinson, "The Chemistry of Chromium, Molybdenum and Tungsten, Pergamon Press, Oxford, 1975, p.700
19. R. A. Walton, J. Less-common Metals 54, 71(1977)
20. M. Pourbaix, Atlas of Electrochemical Equilibria, Pergamon Press, Oxford, 1966, ch.10.2
21. A. S. Goncharenko, Z. Prikladno i Khimii., 37(4), 915(1964)
22. K. S. Kim, J. C. Carver, D. E. Leyden and D. M. Hercules, Spectrosc. Lett., 9, 65(1976)
23. B. Brox and I. Olefjord, in "Passivity of Metals and Semiconductors" Eds. M. Froment, Bombannes, France, 1983
24. B. Brox and I. Olefjord, J. Electrochem. Soc. 132, 2854(1985)
25. I. Olefjord, B. Brox and U. Jelvesdam, J. Electrochem. Soc., 132, 2854(1985)
26. M. Ürgen, U. Stolz and R. Kirchheim, Corro. Sci., 30(4), 377(1990)
27. N. S. McIntyre, D. D. Johnston, L. L. Coatsworth, R. D. Davidson and J. R. Brown, Surf. Interf., 15, 265 (1990)
28. C. R. Clayton and Y. C. Lu, Surf. Interf., 14, 66 (1989)

29. F. A. Cotton and G. Wilkins, in Advanced Inorganic Chemistry, Wiley, New York, 1971, p.951
30. O. Glemser, G. Lutz and G. Meyer, Z. Anorg. Allg. Chem., 264, 17(1951)
31. O. Glemser, G. Lutz and G. Meyer, Z. Anorg. Allg. Chem., 285, 173(1956)
32. P. G. Dickens, R. H. Jarman, R. C. T. Slade and C. J. Wright, J. Chem. Phys., 77(1), 575(1982)

Table 1. Binding energies and HWHM's of Mo3d, Mo3p, N1s and O1s unit: eV

	$Mo3d_{5/2}$		$Mo3p_{3/2}$		O1s
	B.E.	HWHM	B.E.	HWHM	
Mo(met)	227.7	0.6	393.9	1.3	
Mo^{+4}	229.0	0.8	395.7	1.5	529.9
Mo^{+5}	230.8	1.0	397.1	1.7	530.0
Nitride			397.2	0.9	
MoO_3	232.5	0.8	398.7	1.5	530.5
NH_3			399.9	1.0	
$FeMoO_4$	232.1	0.8	398.0	1.5	530.2
$NiMoO_4$	234.0		399.9		532.0
$(NH_4)_6Mo_7O_{24}$	232.8	0.8	398.8	1.7	530.5
$(NH_4)_2MoO_4$	232.0	0.8	398.4	1.7	530.5
NH_4^+			401.5	1.0	

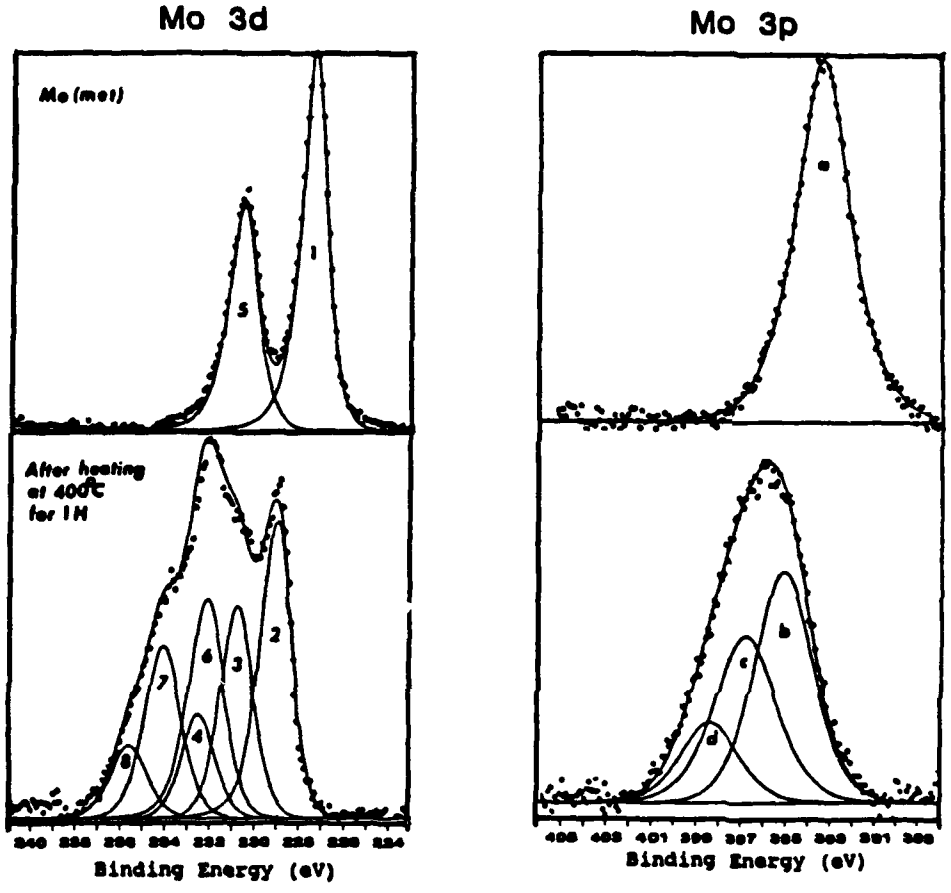

Figure 1. Mo3d and Mo3p spectra for pure Mo oxidized at 400°C for 1 hour in 0.1 torr O_2.

$Mo3p_{3/2}$ a: Mo(met), b: MoO_2, c: Mo^{+5}, d: MoO_3
$Mo3d_{5/2}$ 1: Mo(met), 2: MoO_2, 3: Mo^{+5}, 4: MoO_3
$Mo3d_{3/2}$ 5: Mo(met), 6: MoO_2, 7: Mo^{+5}, 8: MoO_3

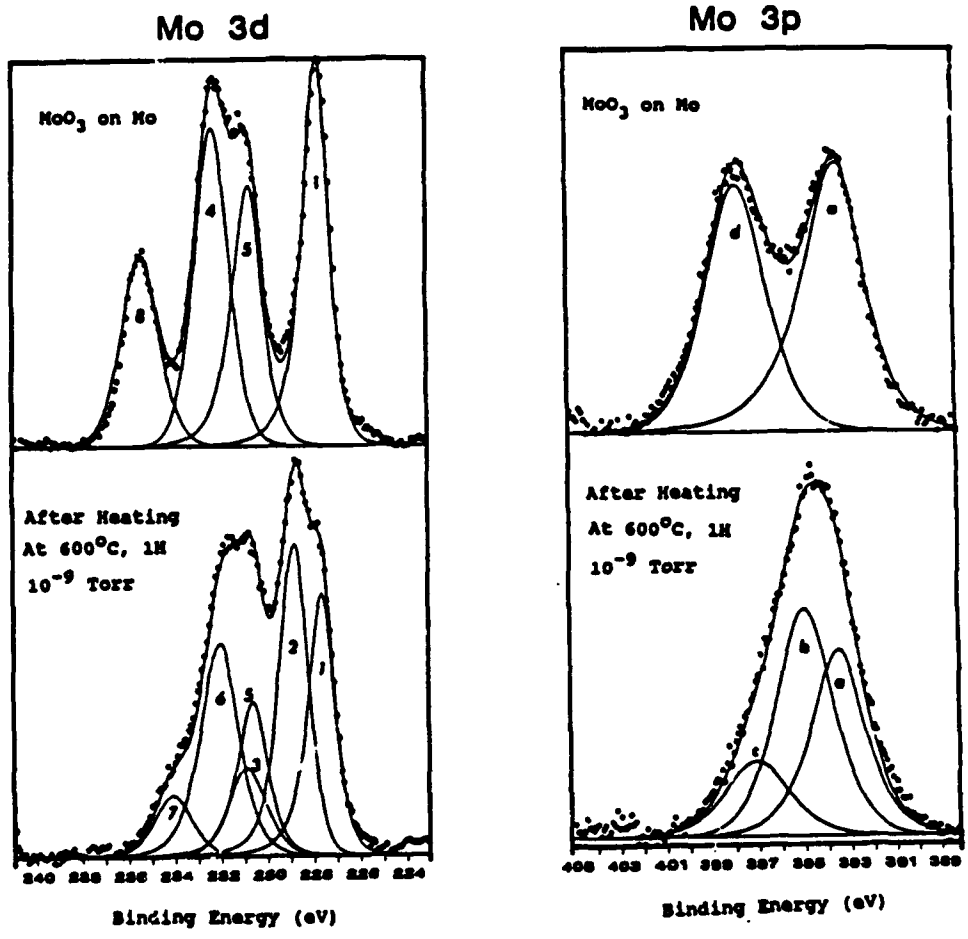

Figure 2. Mo3d and Mo3p spectra for MoO_3 on pure Mo.

$Mo3p_{3/2}$ a: Mo(met), b: MoO_2, c: Mo^{+5}, d: MoO_3
$Mo3d_{5/2}$ 1: Mo(met), 2: MoO_2, 3: Mo^{+5}, 4: MoO_3
$Mo3d_{3/2}$ 5: Mo(met), 6: MoO_2, 7: Mo^{+5}, 8: MoO_3

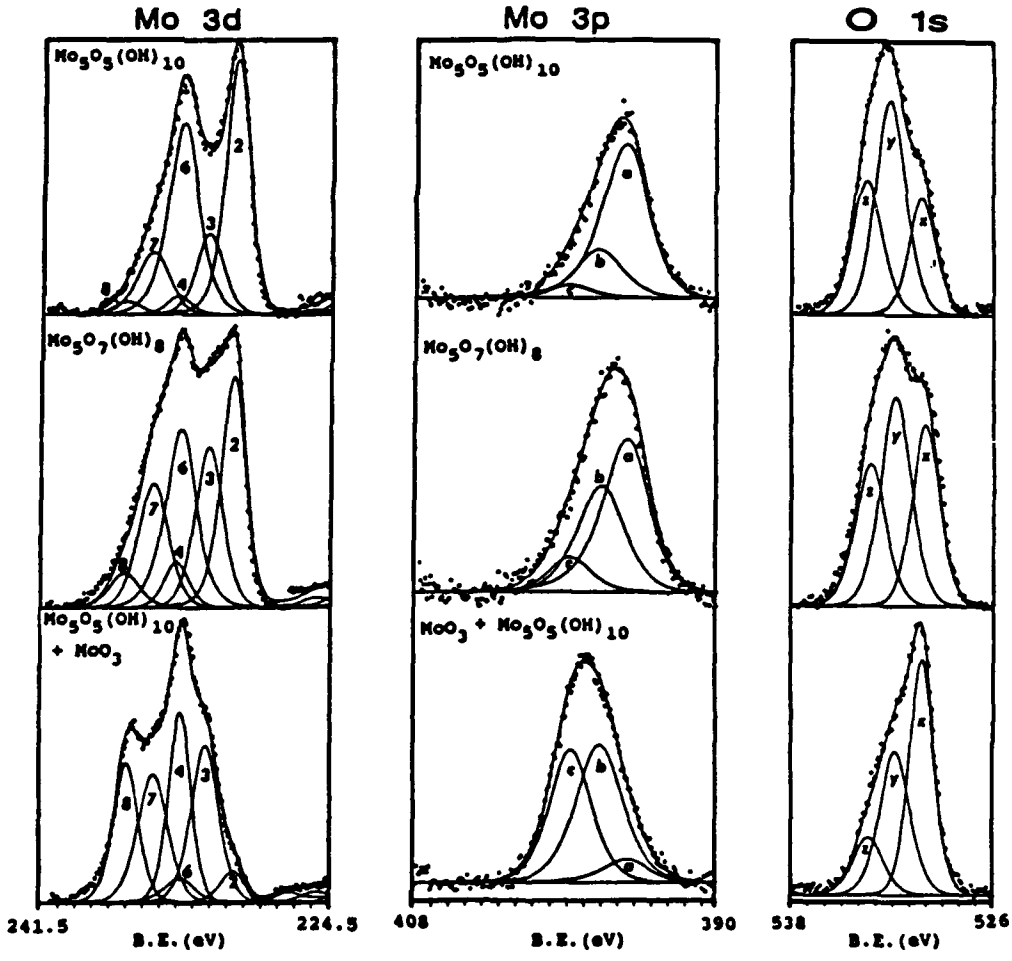

Figure 3. Mo3d, Mo3p and O1s spectra for three types of Mo oxyhydroxide powder.

$Mo3p_{3/2}$ a: Mo^{+4}, b: Mo^{+5}, c: MoO_3
$Mo3d_{5/2}$ 2: Mo^{+4}, 3: Mo^{+5}, 4: MoO_3
$Mo3d_{3/2}$ 6: Mo^{+4}, 7: Mo^{+5}, 8: MoO_3
O1s x: O^{-2}, y: OH^-, z: H_2O

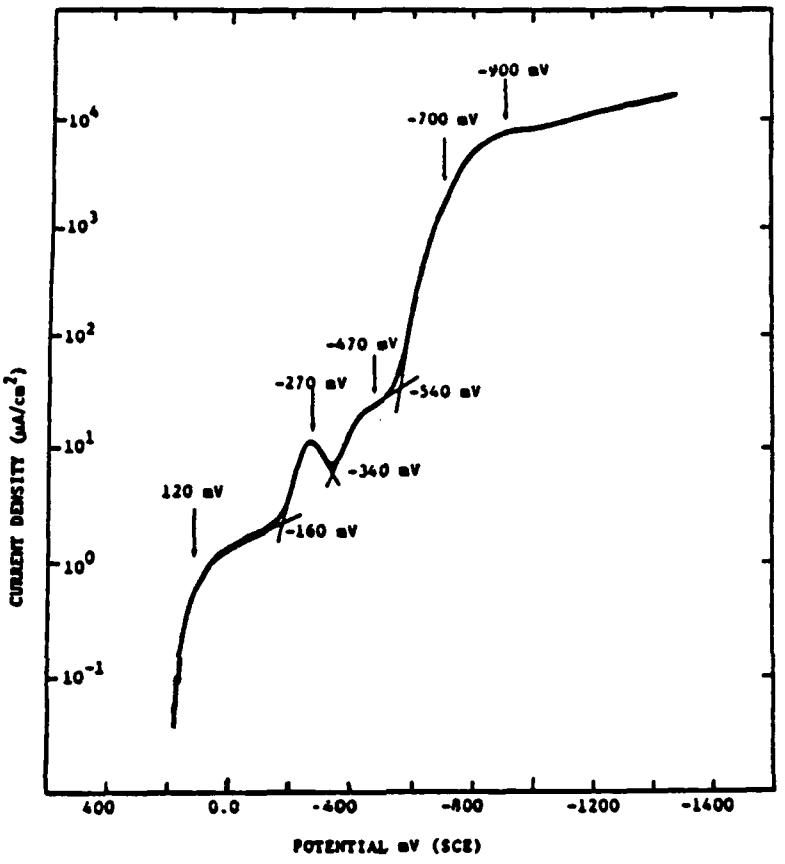

Figure 4. Cathodic polarization curve of platinum in deaerated 0.1M ammonium paramolybdate solution. (Scan Rate: 0.2 mV/sec)[28)]

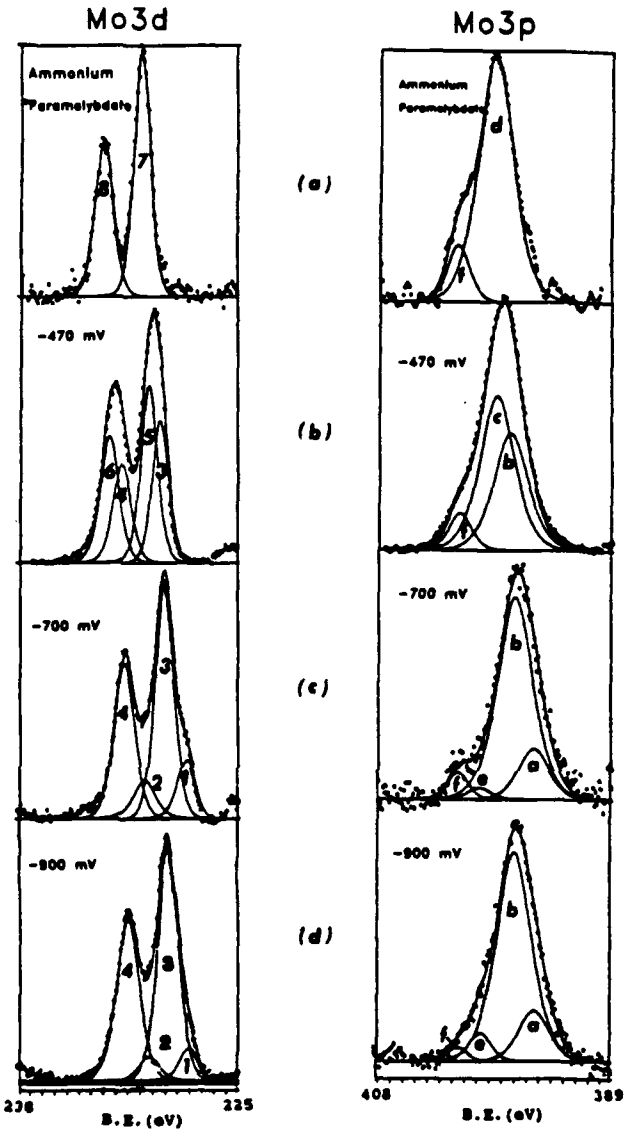

Figure 5. Mo3d and Mo3p spectra obtained from (a) ammonium paramolybdate and from the surface of platinum electrode cathodically polarized in deaerated 0.1M ammonium paramolybdate at (b) -470 mV, (c) -700 mV and (d) -900 mV.

$Mo3d_{5/2}$ 1:MoO_2, 3:Mo^{+5}, 5:$(NH_4)_2MoO_4$, 7:$(NH_4)_6Mo_7O_{24}\cdot 4H_2O$
$Mo3d_{3/2}$ 2:MoO_2, 4:Mo^{+5}, 6:$(NH_4)_2MoO_4$, 8:$(NH_4)_6Mo_7O_{24}\cdot 4H_2O$
$Mo3p_{3/2}$ a:MoO_2, b:Mo^{+5}, c:$(NH_4)_2MoO_4$, d:$(NH_4)_6Mo_7O_{24}\cdot 4H_2O$
N1s e:NH_3, f:NH_4^+

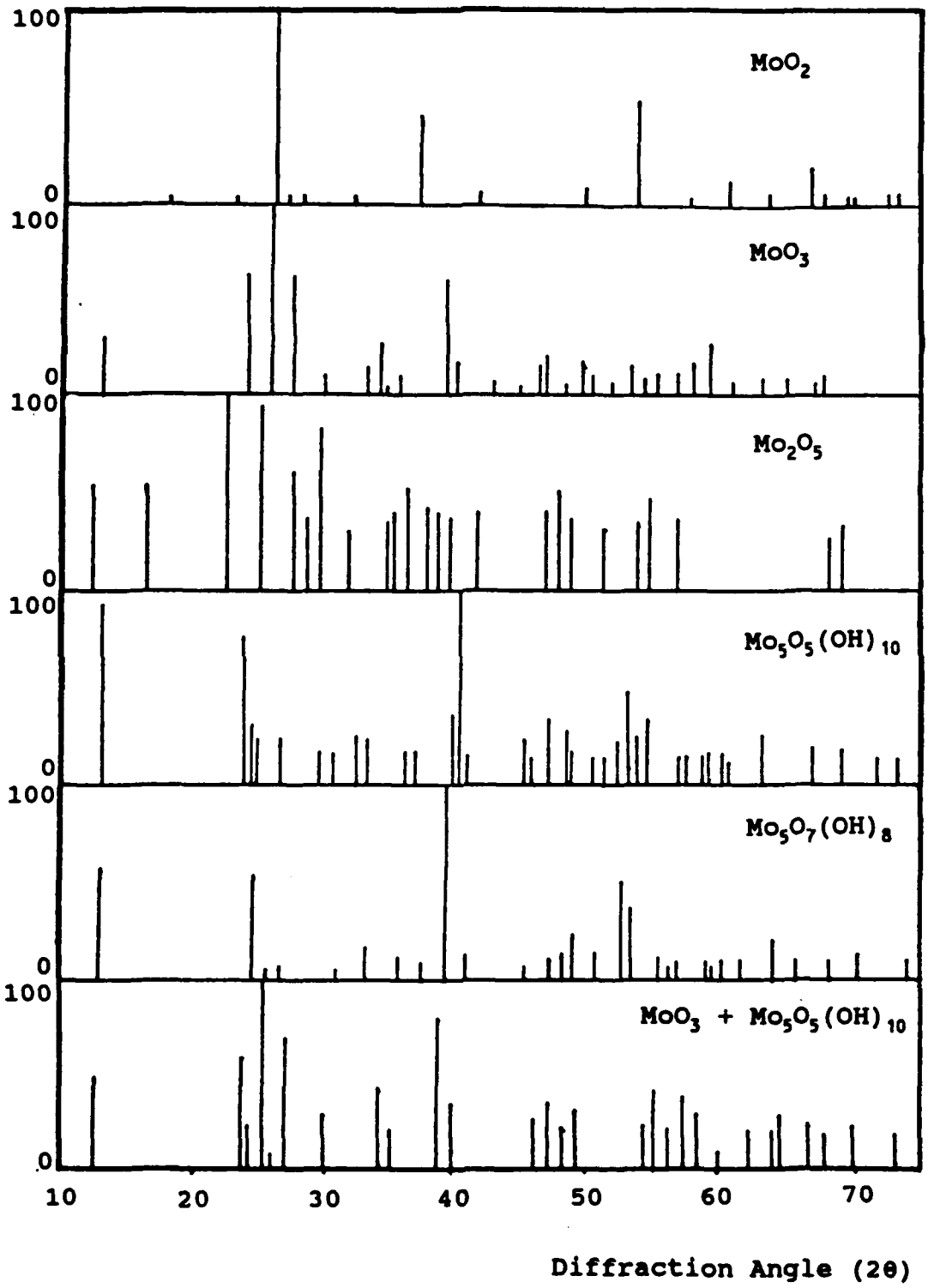

Figure 6. X-ray diffraction spectra for various Mo compounds.

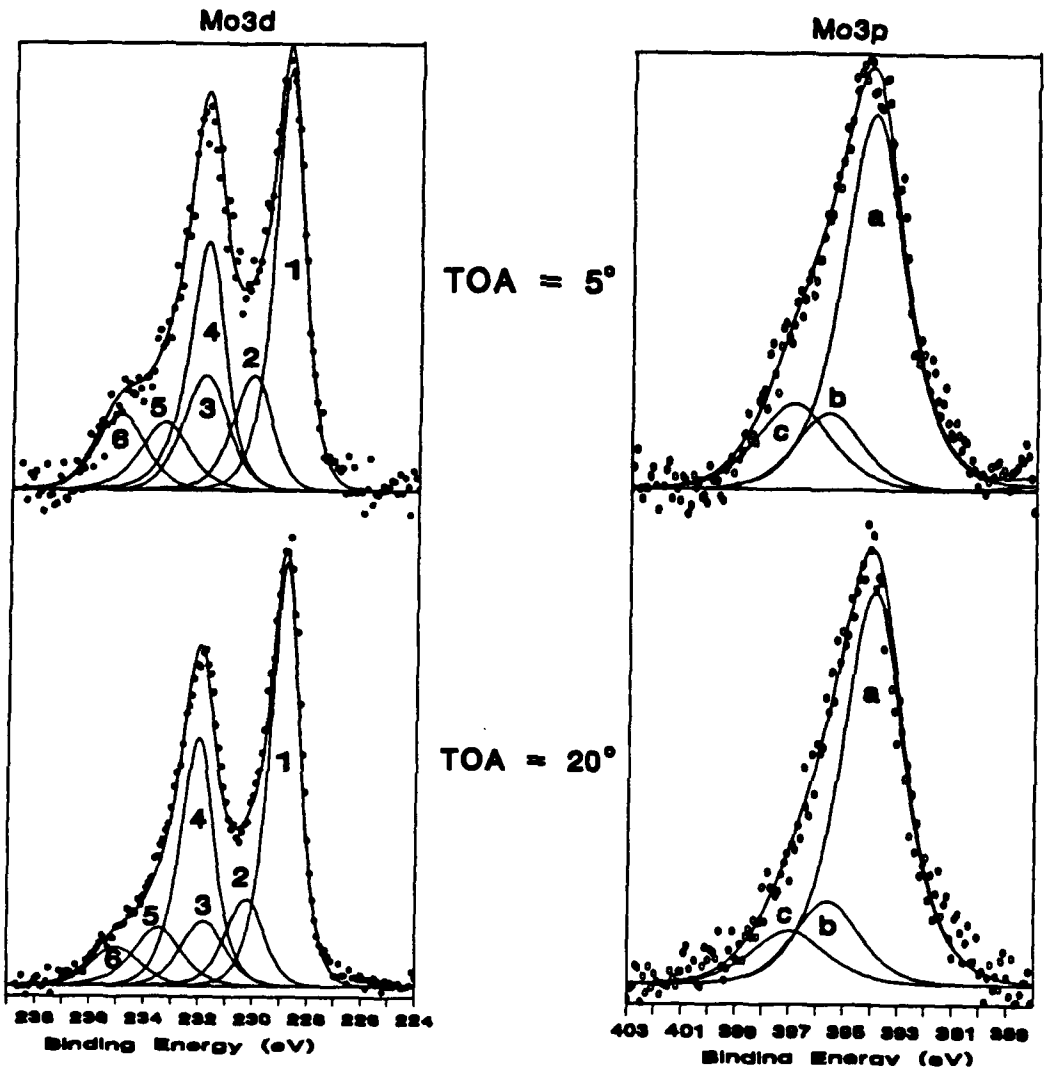

Figure 7. Mo3d and Mo3p XPS spectra for pure Mo polarized at 50 mV for 1 hour in deaerated 0.1M HCl.

$Mo3p_{3/2}$ a: Mo(met), b: Mo^{+4}, c: Mo^{+5}
$Mo3d_{5/2}$ 1: Mo(met), 2: Mo^{+4}, 3: Mo^{+5}
$Mo3d_{3/2}$ 4: Mo(met), 5: Mo^{+4}, 6: Mo^{+5}

Table 4.1 Chemical Compositions of the Stainless Steels(wt%)

Alloy	C	Mn	P	S	Si	Cr	Ni	Mo	Cu	N
304	0.053	1.77	0.031	0.008	0.41	19.27	8.49	0.16	0.16	0.04
304N	0.090	1.74	0.030	0.007	0.39	18.8	8.59	0.36	0.16	0.24
317LX	0.022	1.52	0.018	0.015	0.41	18.43	13.13	3.34	<0.01	0.055
317LXN	0.026	1.59	0.026	0.016	0.43	18.36	13.31	3.36	<0.01	0.192
904L	0.019	1.50	0.023	0.002	0.44	20.46	24.40	4.51	1.48	0.053
904LN	0.024	1.50	0.024	0.002	0.52	20.33	24.58	4.50	1.50	0.200
AL6X	0.028	1.60	0.023	0.004	0.33	20.65	23.86	6.27	<0.01	0.055
AL6XN	0.027	1.59	0.022	0.004	0.31	20.68	23.91	6.25	<0.01	0.103

	C	Mn	P	S	Si	Cr	Ni	Mo	W	N
Fe20Cr20Ni	0.004	0.18	<0.003	22ppm	0.08	20.12	20.18	0.01	0.02	0.011
Fe20Cr20Ni 6Mo	0.006	0.20	0.01	21ppm	0.08	19.86	19.98	5.99	0.03	0.011
Fe20Cr20Ni 6Mo0.2N	0.005	0.14	0.009	22ppm	0.09	19.74	19.74	5.96	0.03	0.19

Table 4.2 Potentiostatic Polarization Conditions of pure Cr

Potential	Polarizing Condition
1. - 930 mV	For 15 min in 0.1M HCl + 0.5M $NaNO_3$
2. - 700 mV	For 15 min in 0.1M HCl + 0.5M $NaNO_3$
3. 0 mV	For 5 min in 0.1M HCl and then for 55 min in 0.1M HCl + 0.5M $NaNO_3$
4. 950 mV	For 5 min in 0.1M HCl and then for 55 min in 0.1M HCl + 0.5M $NaNO_3$
5. 1300 mV	For 1 min in 0.1M HCl and then for 10 min in 0.1M HCl + 0.5M $NaNO_3$
6. 0 mV	For 30 min in 0.1M HCl and then for 30 min in 0.1M HCl + 0.5M $NaNO_3$ (scratch sample surface during polarization)
7. 1300 mV	For 10 min in 0.1M HCl + 0.5M $NaNO_2$

Table 4.3 Potentiostatic Polarization Conditions of Pure Mo

Specimen	Potential(mV)	Time	Solution	NO_3^- Treat
Mo	-50	1 H	0.1M HCl	X
	-50	1 H	0.1M HCl	O
Mo_2N	250	1 H	0.1M HCl	X
	600	3 min	0.1M HCl	X

Table 4.4 Potentiostatic Polarization Conditions of Stainless Steels at Room Temperature.

(a) 18-8 Stainless Steels at -180 mV

	NO_3^- Treatment	Polarization Time	
		0.1M HCl	0.1M HCl+0.75M NaCl
0.04 wt%N	O	1 H	-
Alloy	O	3 H	-
	O	6 H	-
	X	6 H	-
	X	1 H	30 min
0.24 wt%N	X	6 H	-
Alloy	X	1 H	30 min

(b) High Ni Stainless Steels

at -100mV for 1 hour in 0.1M HCl + 0.4M NaCl

Table 4.5 Binding energies and Fitting Parameters Used in This Study

(a) Chromium(Cr)

Species	B.E.(eV)	HWHM(eV)	G/L	TH	ETS	TM
Cr2p$_{3/2}$						
Cr(met)	574.1	0.8	0.65	0.001	0.05	0.5
Cr_2O_3	576.3	1.1	0.5	0.001	20	0.5
$Cr(OH)_3$	577.0	1.1	0.5	0.001	20	0.5
CrO_3	578.3	0.7	0.5	0.001	20	0.5
CrO_4^{-2}	579.3	0.7	0.5	0.001	20	0.5
Cr2p$_{1/2}$						
Cr(met)	583.3	1.1	0.65	0.001	0.05	0.5
Cr_2O_3	586.0	1.2	0.5	0.001	20	0.5
$Cr(OH)_3$	586.7	1.2	0.5	0.001	20	0.5
CrO_3	587.5	0.9	0.5	0.001	20	0.5
CrO_4^{-2}	588.5	0.9	0.5	0.001	20	0.5

(Continue)

(b) Molybdenum(Mo)

Species	B.E.(eV)	HWHM(eV)	G/L	TH	ETS	TM
$\underline{Mo3d_{5/2}}$						
Mo(met)	227.7	0.6	0.75	0.001	0.15	0.5
Mo_2N	228.1	0.7	0.75	0.001	0.15	0.5
MoO_2	229.0	0.8	0.5	0.001	0.11	0.5
Mo^{+5}	230.8	1.0	0.5	0.001	20	0.5
MoO_4^{-2}(in Alloy)	231.9	1.0	0.5	0.001	20	0.5
MoO_3	232.5	0.8	0.5	0.001	20	0.5
$FeMoO_4$	232.1	0.8	0.5	0.001	20	0.5
$NiMoO_4$	234.0	1.2	0.5	0.001	20	0.5
$(NH_4)_6Mo_7O_{24}$	232.8	0.8	0.5	0.001	20	0.5
$(NH_4)_2MoO_4$	232.0	0.8	0.5	0.001	20	0.5
$MoCl_5$	230.6					
$\underline{Mo3d_{3/2}}$						
Mo(met)	230.8	0.7	0.75	0.001	0.11	0.5
Mo_2N	231.2	0.8	0.75	0.001	0.11	0.5
MoO_2	232.2	0.9	0.70	0.001	0.11	0.5
Mo^{+5}	233.9	1.1	0.5	0.001	20	0.5
MoO_4^{-2}(in Alloy)	235.1	1.1	0.5	0.001	20	0.5

(Continue)

Species	B.E.(eV)	HWHM(eV)	G/L	TH	ETS	TM
MoO_3	235.7	0.9	0.5	0.001	20	0.5
$FeMoO_4$	235.3	0.9	0.5	0.001	20	0.5
$NiMoO_4$	237.2	1.3	0.5	0.001	20	0.5
$(NH_4)_6Mo_7O_{24}$	236.0	0.9	0.5	0.001	20	0.5
$(NH_4)_2MoO_4$	235.4	0.9	0.5	0.001	20	0.5
$MoCl_5$	233.8					
$\underline{Mo3p_{3/2}}$						
Mo(met)	394.0	1.3	0.8	0.001	0.10	0.5
MoO_2	395.7	1.5	0.6	0.001	20	0.5
Mo^{+5}	397.1	1.7	0.6	0.001	20	0.5
MoO_4^{-2}(in Steel)	398.2	1.6	0.6	0.001	20	0.5
MoO_3	398.7	1.5	0.6	0.001	20	0.5
$FeMoO_4$	398.0	1.5	0.6	0.001	20	0.5
$NiMoO_4$	399.9	1.8	0.6	0.001	20	0.5
$(NH_4)_6Mo_7O_{24}$	398.8	1.7	0.6	0.001	20	0.5
$(NH_4)_2MoO_4$	398.4	1.7	0.6	0.001	20	0.5

(Continue)

(c) Iron(Fe) and Nickel(Ni)

Species	B.E.(eV)	HWHM(eV)	G/L	TH	ETS	TM
$\underline{Fe2p_{3/2}}$						
Fe(met)	706.8	0.9	0.5	0.001	0.075	0.5
Fe^{+2}	709.0	1.1	0.5	0.001	20	0.5
Fe^{+3}	710.9	1.2	0.5	0.001	20	0.5
$\underline{Ni2p_{3/2}}$						
Ni(met)	852.3	0.8	0.6	0.001	0.07	0.5
NiO	854.5	0.9	0.5	0.001	20	0.5
$Ni(OH)_2$	856.6	1.3	0.5	0.001	20	0.5

(Continue)

(d) Nitrogen(N)

Species	B.E.(eV)	HWHM(eV)	G/L	TH	ETS	TM
N1s						
Nitride(in Steel)	397.2	0.9	0.5	0.001	20	0.5
NH_3(in Steel)	399.9	1.0	0.5	0.001	20	0.5
NH_4	401.5	1.1	0.5	0.001	20	0.5
CrN	397.0 (nitrate-treatment)					
Cr_2N	397.4 reference (80)					
NiN	397.4 (nitrate-treatment)					
	397.7 (nitrided Ni)[90]					
FeN	396.6 (nitrate-treatment)					
	396.8 (N_2 react with Fe at 500°C)[90]					
NH_3	399.4 (Absorbed at 200 torr at 0°C on Fe)[90]					
NO	399.6 (Absorbed at 200 torr on Ni and Fe)[90,91]					
$[Cr(NH_3)_5OH_2](NO_3)_3$	399.8 (powder)					
NH_4^+	401.5 (NH_4Cl)					

(continue)

(d) Nitrogen(N)

Species	B.E.(eV)	HWHM(eV)	G/L	TH	ETS	TM
N1s						
Nitride(in Steel)	397.2	0.9	0.5	0.001	20	0.5
NH_3(in Steel)	399.9	1.0	0.5	0.001	20	0.5
NH_4	401.5	1.1	0.5	0.001	20	0.5
CrN	397.0 (nitrate-treatment)					
Cr_2N	397.4 reference (82)					
NiN	397.4 (nitrate-treatment)					
	397.7 (nitrided Ni)[92]					
FeN	396.6 (nitrate-treatment)					
	396.8 (N_2 react with Fe at 500°C)[92]					
NH_3	399.4 (Absorbed at 200 torr at 0°C on Fe)[92]					
NO	399.6 (Absorbed at 200 torr on Ni and Fe)[92,93]					
$[Cr(NH_3)_5OH_2](NO_3)_3$	399.8 (powder)					
NH_4^+	401.5 (NH_4Cl)					

(continue)

(e) Oxygen(O)

Species	B.E.(eV)	HWHM(eV)	G/L	TH	ETS	TM
O1s						
Oxide(in Steel)	529.9	1.0	0.5	0.001	20	0.5
OH^-(in Steel)	531.4	1.1	0.5	0.001	20	0.5
H_2O	532.7	1.1	0.5	0.001	20	0.5
MoO_2	529.9					
Mo^{+5}	530.0					
MoO_3	530.5					
$FeMoO_4$	530.2					
$NiMoO_4$	532.0					
$(NH_4)_2MoO_4$	530.5					
$(NH_4)_6Mo_7O_{24}$	530.5					

Table 5.1 Salient Electrochemical Characteristics for Pure Metals

Material	Treat	E_{ocp}(mV)	I_{crit}(uA/cm^2)	I_{pass}(uA/cm^2)	E_{tr}(mV)
Pure Cr	-	-790	1821.7	5.5	850
	Nitrate	-445	-	15.0	850
Pure Mo	-	-436	-	2.5	75
	Nitrate	-408	-	1.8	100
Nitrided Mo	-	-197	-	2.0	350

Table 5.2 Salient Electrochemical Characteristics for High Ni Stainless Steels Polarized at -100 mV in 0.1M HCl + 0.4M NaCl

Material	E_{corr}(mV)	I_{crit}(uA/cm^2)	I_{pass}(uA/cm^2)
Fe20Cr20Ni	-356	80.4	4.2
			40.2
Fe20Cr20Ni6Mo	-326	30.0	5.0
Fe20Cr20Ni6Mo0.2N	-314	-	4.5

Table 5.3 Relative Sensitivity Factors

	Cr2p	Ni2p	Fe2p	Mo3d
Sensitivity Factor	1	1.38	1.41	1.29

Table 5.4 Passive Film Thickness(Å) of High Ni Stainless Steels Polarized at -100mV in 0.1M HCl + 0.4M NaCl.

Material	d_{OX}	d_{OH}	d_{TOT}
Fe20Cr20Ni	10.97	4.92	15.89
Fe20Cr20Ni6Mo	10.72	2.73	13.45
Fe20Cr20Ni6Mo0.2N	10.26	2.49	12.75

Table 5.5 Salient Electrochemical Characteristics for 18-8 Alloy Polarized in 0.1M HCl at Room Temperature

Material	Treat	E_{ocp}(mV)	I_{crit}(uA/cm^2)	I_{pass}(uA/cm^2)
0.04 %N 18-8	-	-412	100.6	6.8
	N-dope	-370	35.0	5.7
0.24 %N 18-8	-	-385	73.2	4.5

Table 5.6 Intensity Ratios of Fe Ions for the 50° and 20° Take-off Angle Spectra for 18-8 Alloys Polarized at -180 mV.

Solution	Sample	t	Fe^{+2}/Cr_2O_3		$Fe^{+2}/Cr(OH)_3$		Fe^{+3}/Cr_2O_3		$Fe^{+3}/Cr(OH)_3$	
			50°	20°	50°	20°	50°	20°	50°	20°
0.1M HCl	N-Doped	1H	1.27	1.49	0.46	0.49	1.17	1.28	0.43	0.43
	0.04 %N	3H	0.85	1.01	0.41	0.42	0.78	0.91	0.38	0.38
		6H	0.46	0.56	0.29	0.28	0.25	0.29	0.16	0.15
	0.04 %N	6H	0.55	0.57	0.30	0.27	0.34	0.38	0.18	0.18
	0.24 %N	6H	0.31	0.30	0.21	0.15	0.34	0.34	0.22	0.17
0.1M HCl+ .75M NaCl	0.04 %N*		0.82	0.91	0.55	0.51	0.53	0.57	0.35	0.32
	0.24 %N*		0.50	0.61	0.34	0.36	0.26	0.28	0.17	0.16

* Passivated at -180 mV for 1 hour in 0.1M HCl and for 30 min in 0.1M HCl + 0.5M NaCl

Table 5.7 Thickness(Å) of the Passive Film of 18-8 Alloys Polarized at -180 mV.

Polarization Condition			d_{ox}	d_{oh}	d_{tot}
0.1M HCl	N-Doped 0.04 %N	1H	11.17	4.31	15.48
		3H	11.45	4.15	15.60
		6H	10.71	4.32	15.03
	0.04 %N	6H	11.40	4.66	16.06
	0.24 %N	6H	9.01	3.87	12.88
0.1M HCl+ .75M NaCl	0.04 %N*		11.12	3.54	14.66
	0.24 %N*		9.67	3.96	13.63

* Passivated at -180 mV for 1 hour in 0.1M HCl and for 30 min in 0.1M HCl + 0.75M NaCl

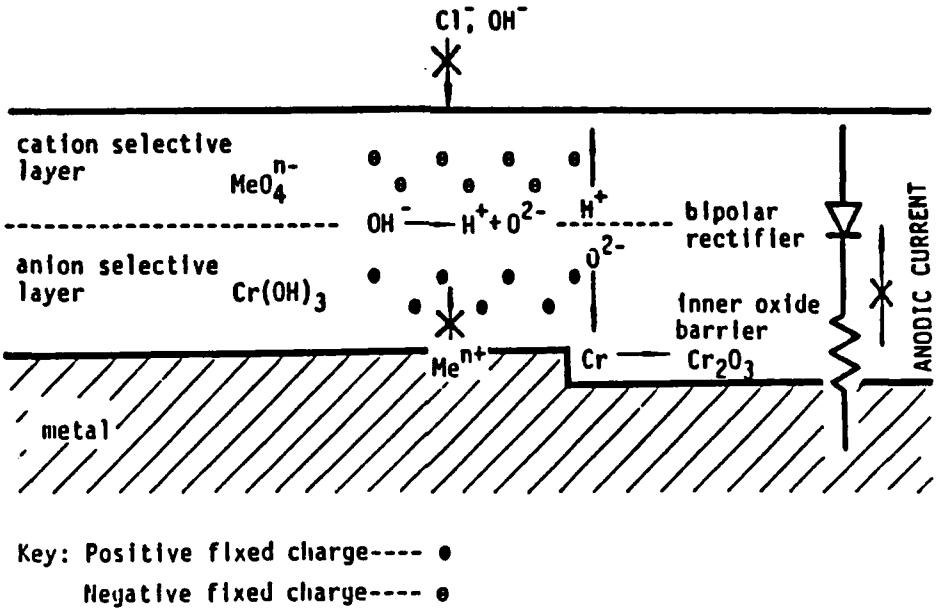

Figure 2.1 Schematic representation of the bipolar behavior of the passive film formed on stainless steel.[53,54]

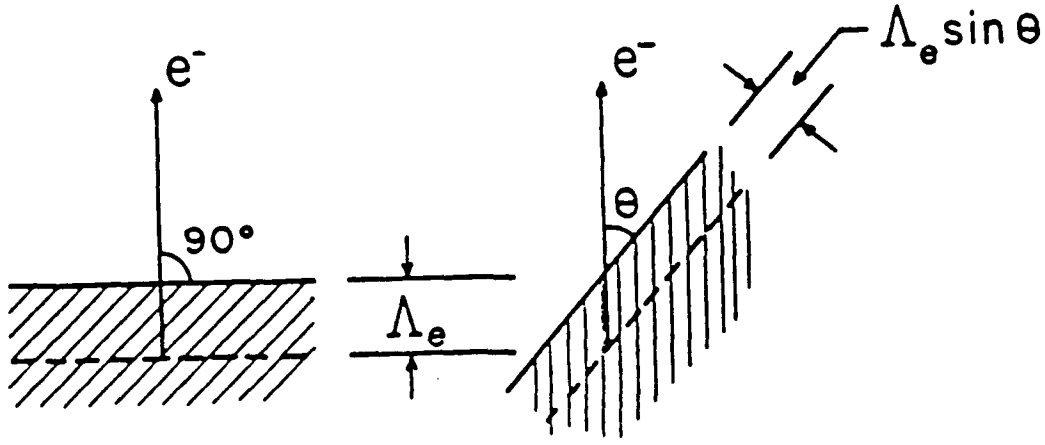

Figure 3.1 The variable angle XPS technique.

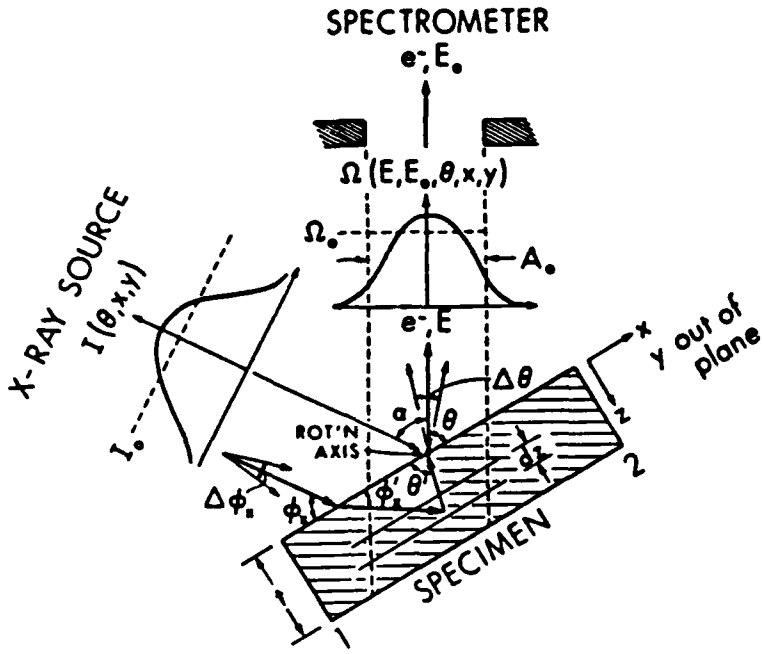

Figure 3.2 Basic features of photoemission experiment.[58]

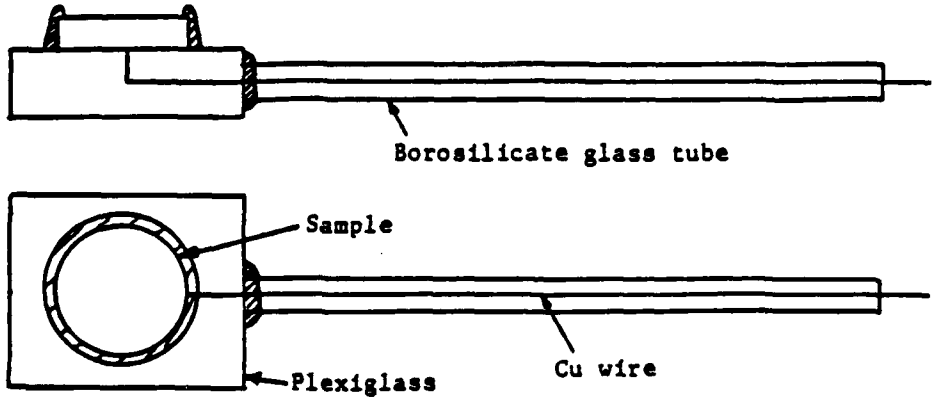

Figure 4.1 Specimen mounting for electrochemical studies.

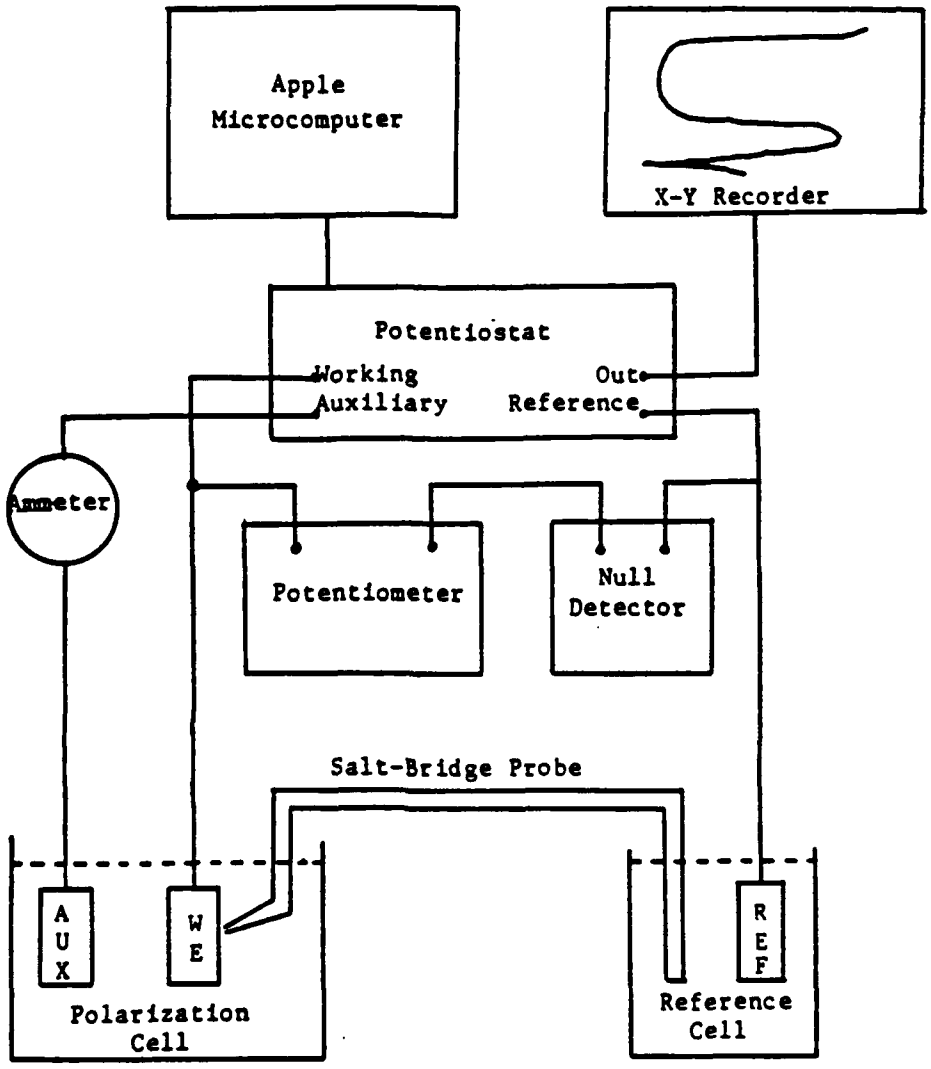

Figure 4.2 Electrochemical instrumentation.

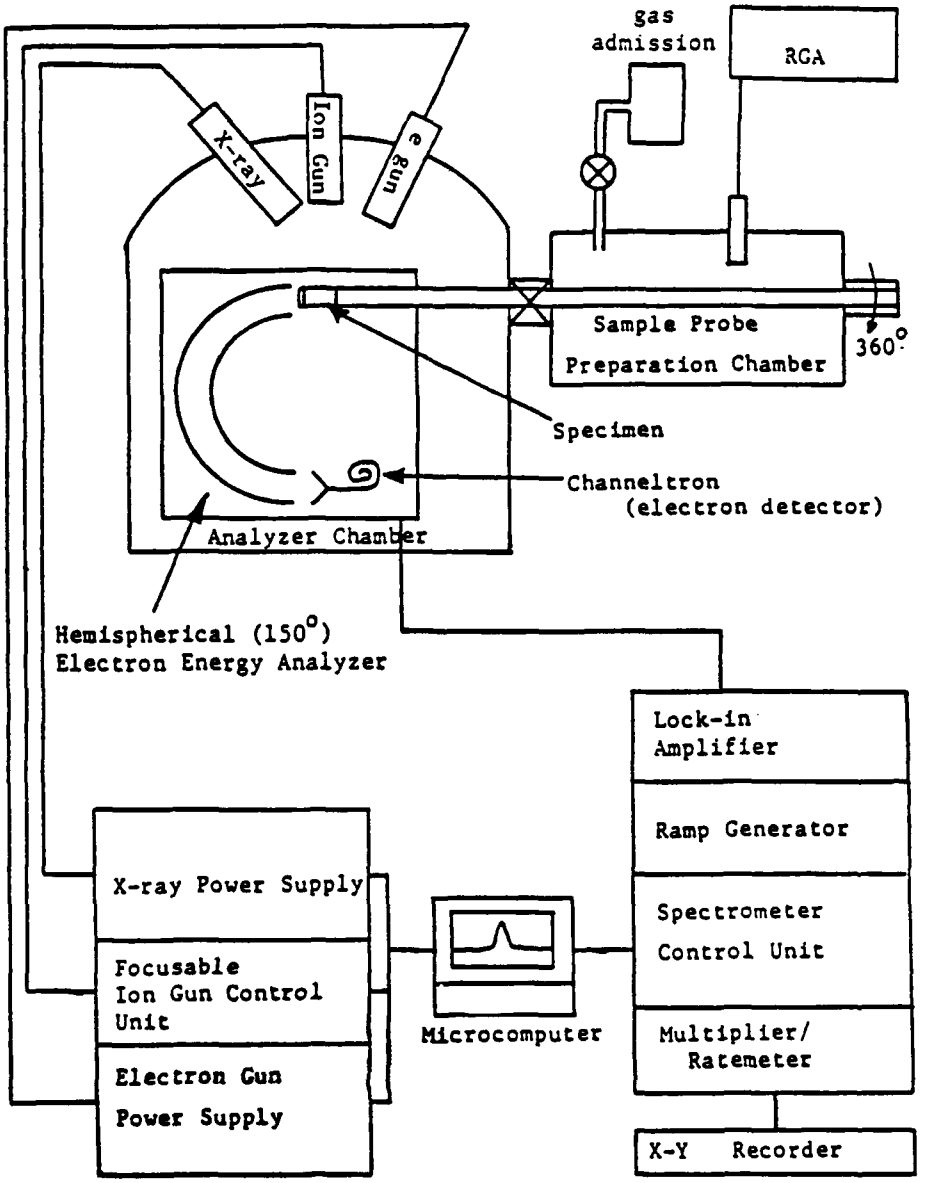

Figure 4.3 A schematic of electron analyzer.

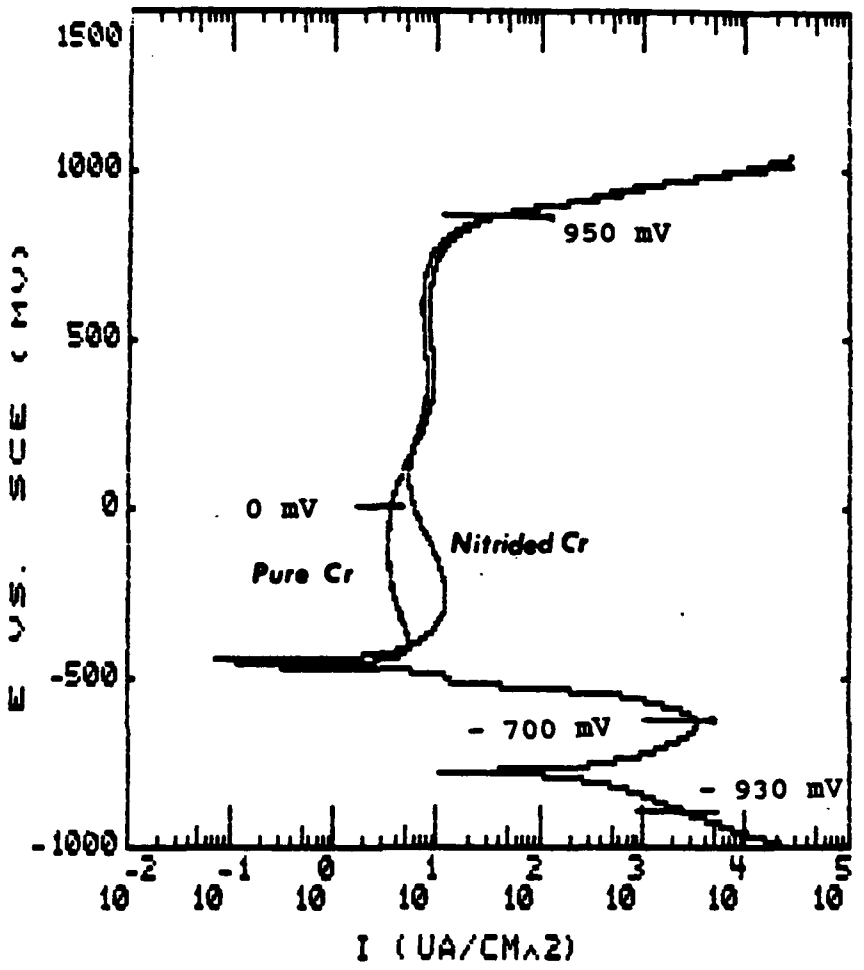

Figure 5.1 Potentiodynamic polarization curve for pure Cr in 0.1M HCl at room temperature(scan rate = 1 mV/sec).

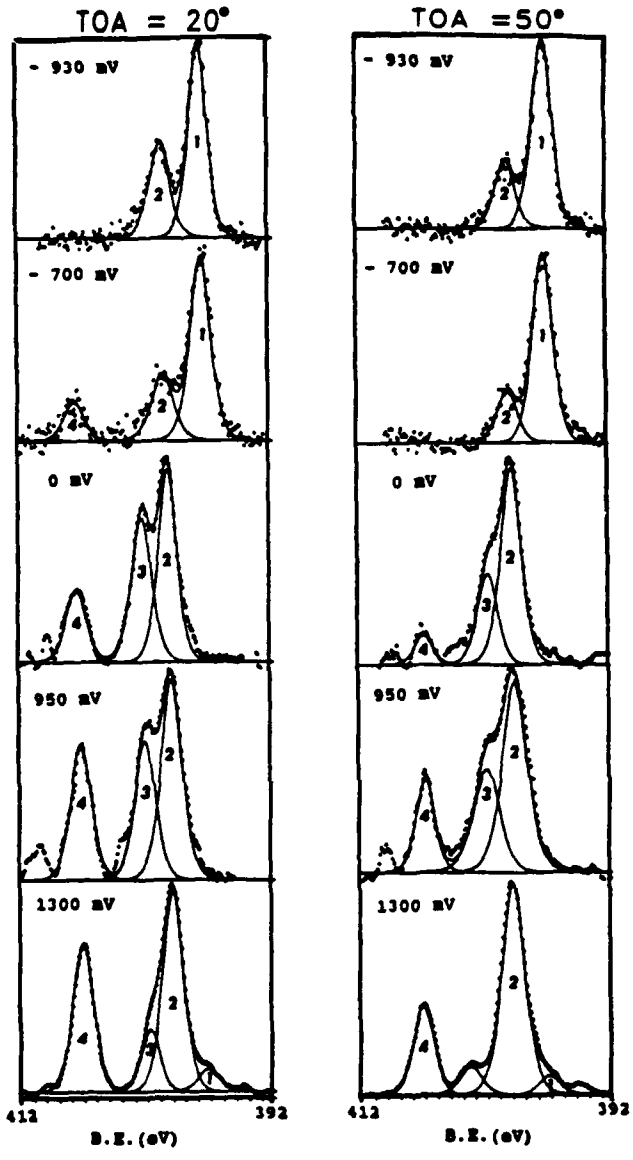

Figure 5.2 N1s XPS spectra for Cr samples treated in 0.1M HCl + 0.5M $NaNO_3$ at various potentials.

1: Nitride, 2: NH_3, 3: NH_4^+, 4: NO_3^-

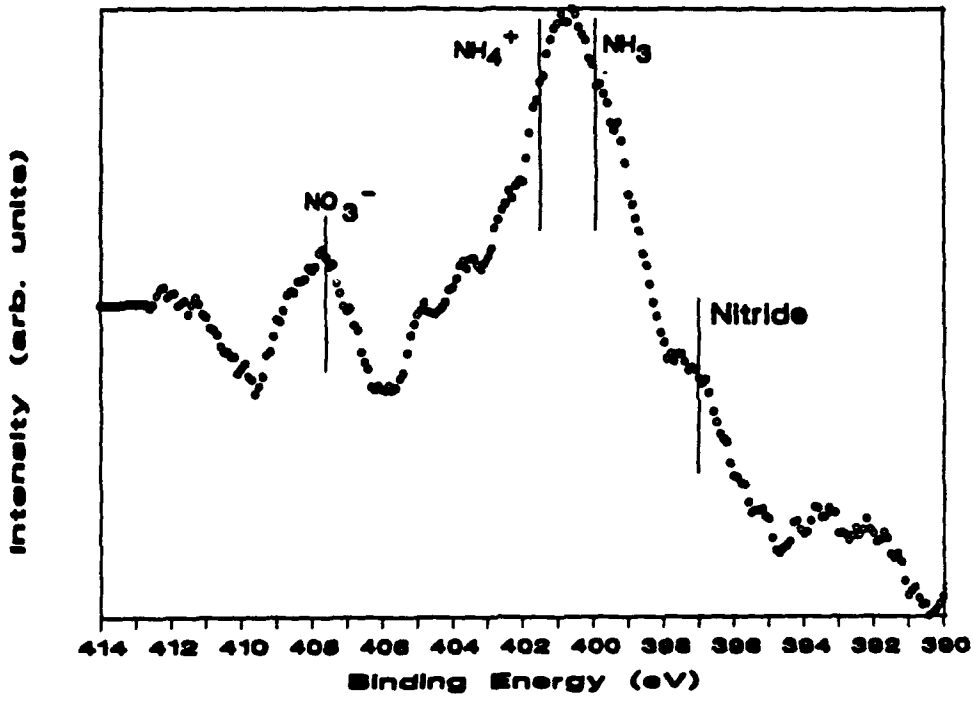

Figure 5.3 N1s XPS spectrum for scratched Cr sample at 0 mV in 0.1M HCl + 0.5M $NaNO_3$ solution.

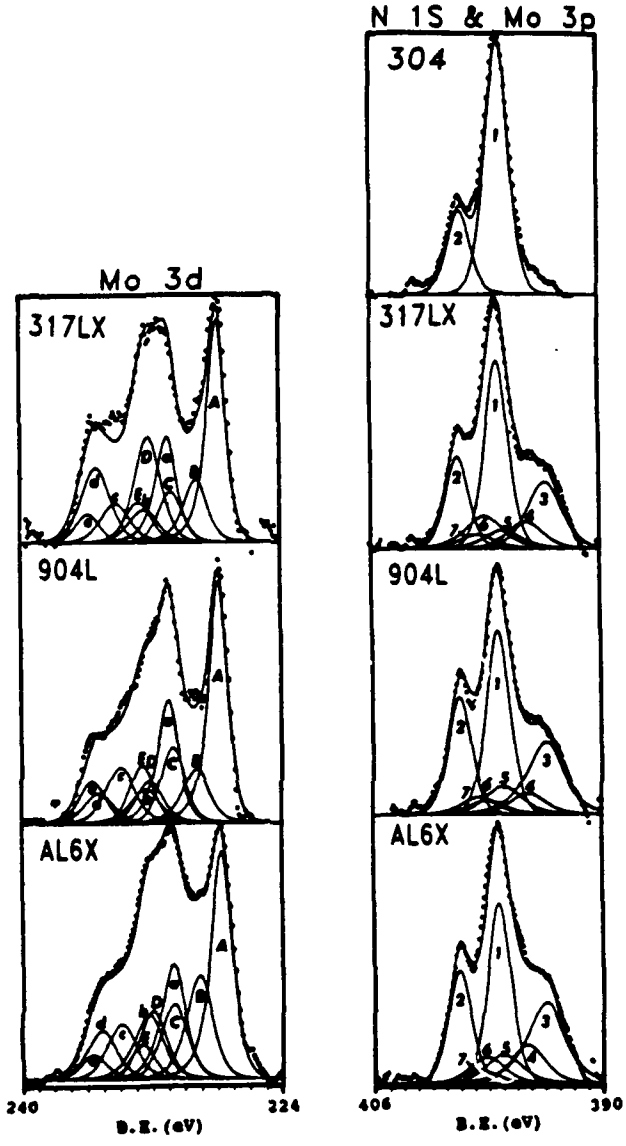

Figure 5.4 N1s and Mo XPS spectra for the stainless steels after nitrate reduction treatment.

N1s	1: Nitride, 2: NH_3
$Mo3p_{3/2}$	3: Mo(met), 4: MoO_2, 5: Mo^{+5}, 6: MoO_4^{-2}, 7: MoO_3
$Mo3d_{5/2}$	A: Mo(met), B: MoO_2, C: Mo^{+5}, D: MoO_4^{-2}, E: MoO_3
$Mo3d_{3/2}$	a: Mo(met), b: MoO_2, c: Mo^{+5}, d: MoO_4^{-2}, e: MoO_3

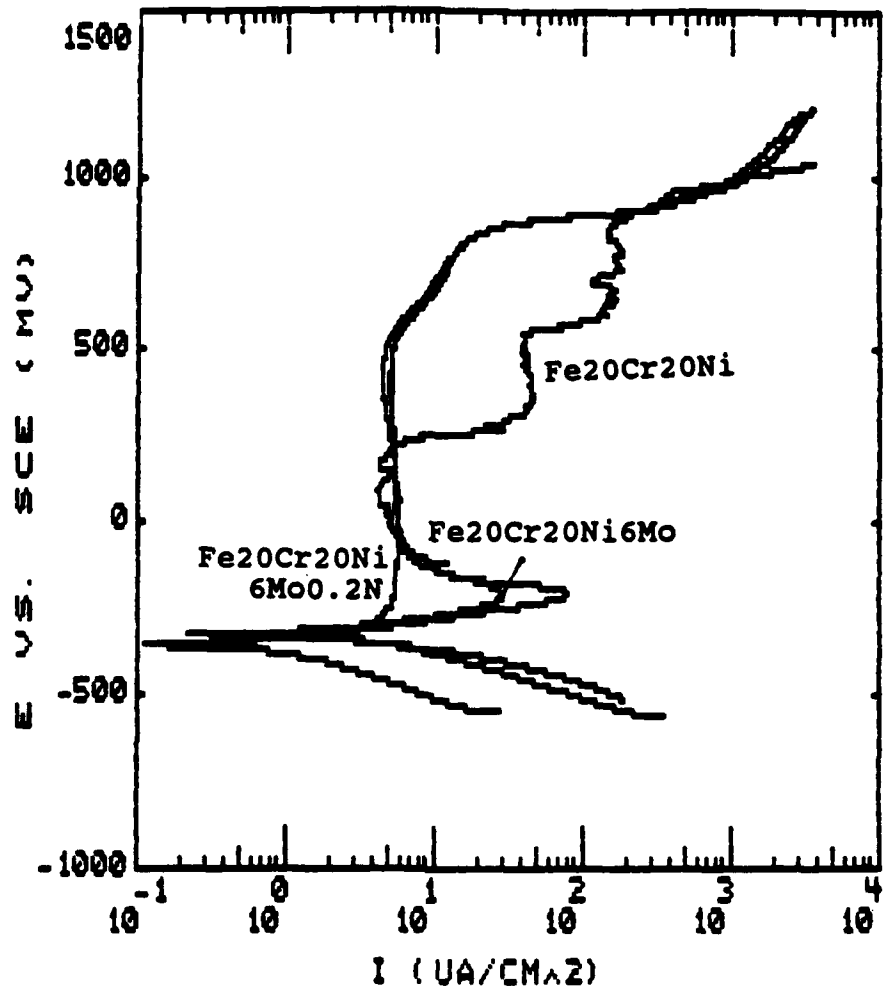

Figure 5.5 Polarization curves for the high Ni stainless steels in 0.1M HCl + 0.4M NaCl at room temperature.

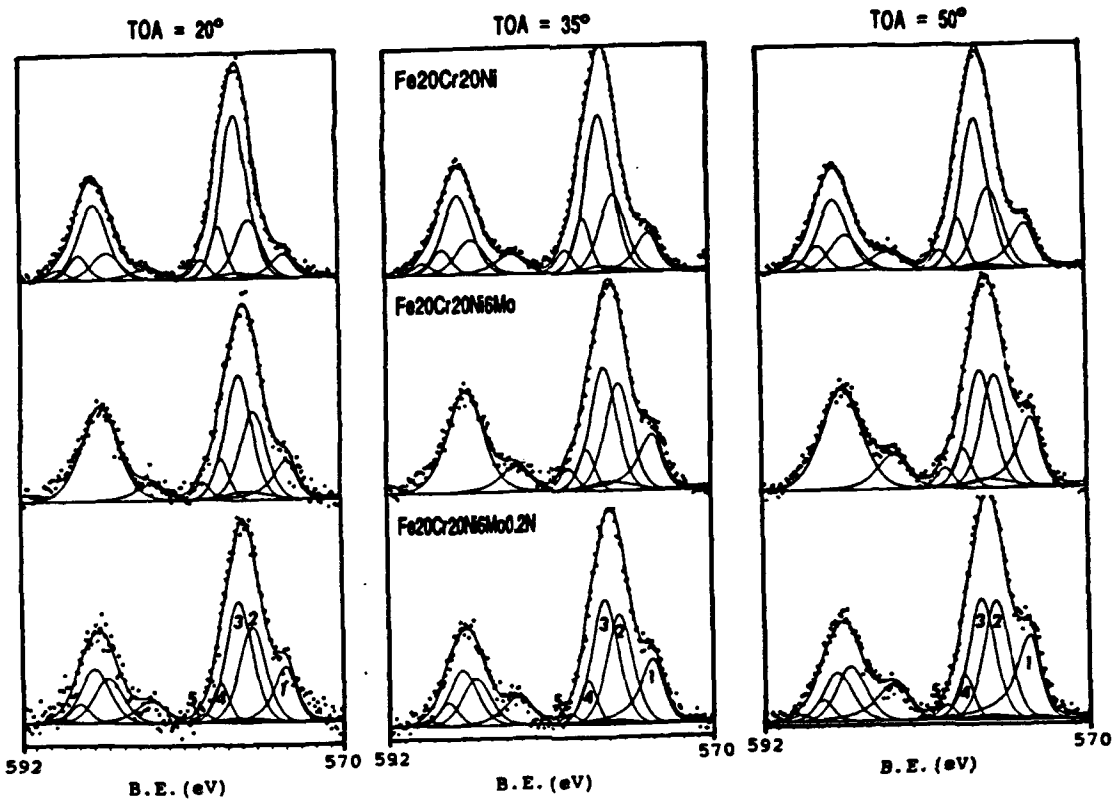

Figure 5.6 Cr2p XPS spectra for the high Ni stainless steels polarized at -100 mV for 10 min in 0.1M HCl + 0.4M NaCl at room temperature.

1: Cr(met), 2: Cr_2O_3, 3: $Cr(OH)_3$, 4: CrO_3, 5: CrO_4^{-2}

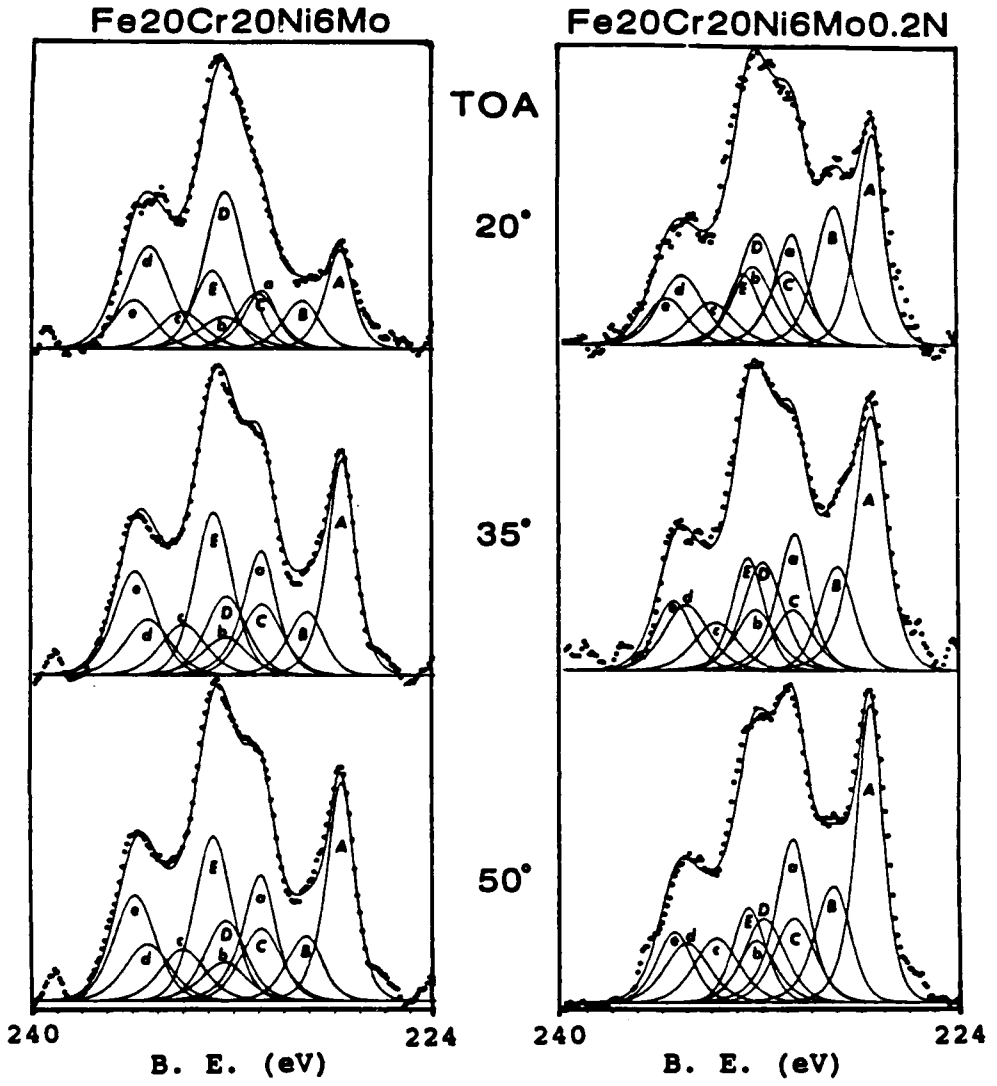

Figure 5.7 Mo3d XPS spectra for high Ni stainless steels polarized at -100 mV for 10 min in 0.1M HCl + 0.4M NaCl at room temperature.

$Mo3d_{5/2}$ A: Mo(met), B: MoO_2, C: Mo^{+5}, D: MoO_4^{-2}, E: MoO_3
$Mo3d_{3/2}$ a: Mo(met), b: MoO_2, c: Mo^{+5}, d: MoO_4^{-2}, e: MoO_3

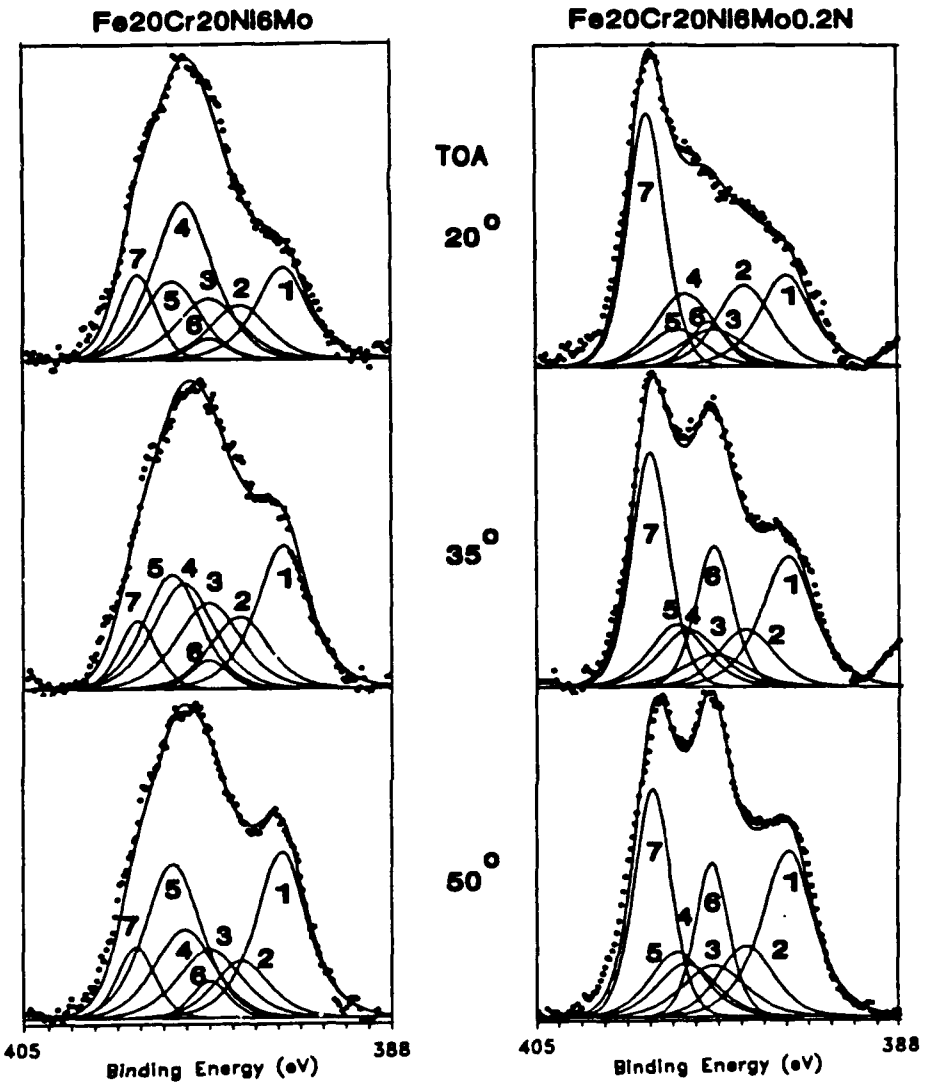

Figure 5.8 N1s and Mo3p XPS spectra for Fe20Cr20Ni6Mo and Fe20Cr20Ni6Mo0.2N alloys polarized at -100 mV for 10 min in 0.1M HCl + 0.4M NaCl at room temperature.

$Mo3p_{3/2}$ 1: Mo(met), 2: MoO_2, 3: Mo^{+5}, 4: MoO_4^{-2}, 5: MoO_3
N1s 6: Nitride, 7: NH_3

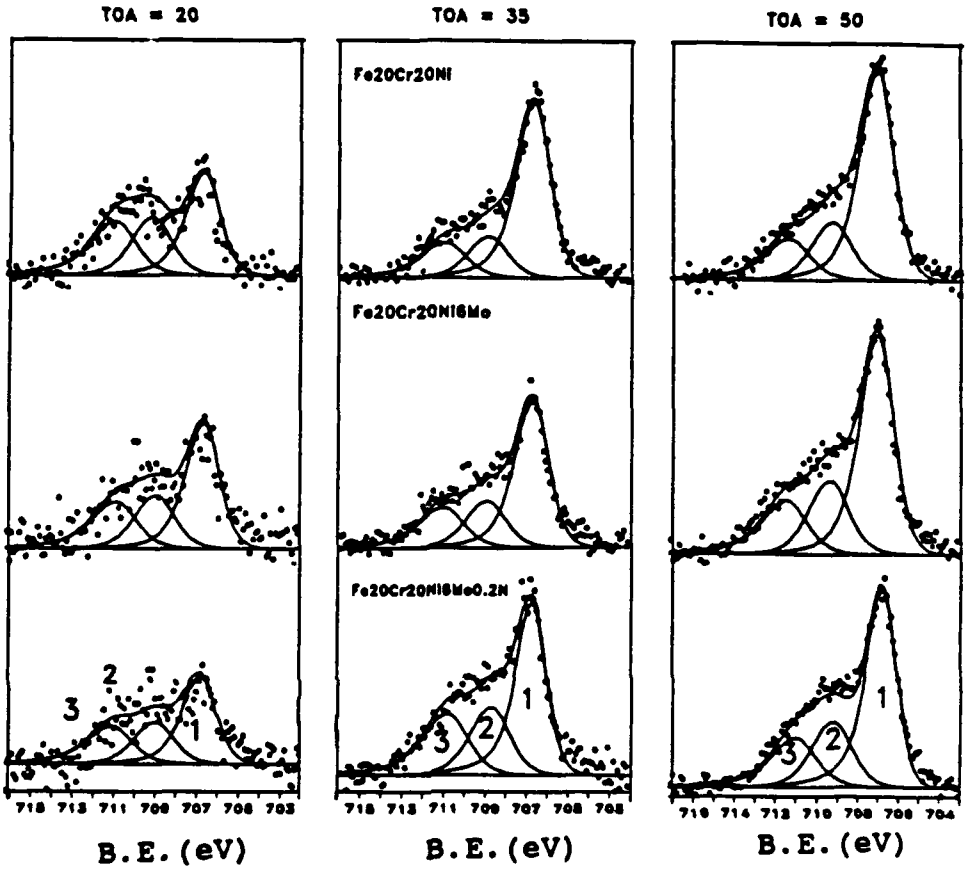

Figure 5.9 Fe2p XPS spectra for high Ni stainless steels polarized at -100 mV for 10 min in 0.1M HCl + 0.4M NaCl at room temperature.

1: Fe(met), 2: Fe^{+2}, 3: Fe^{+3}

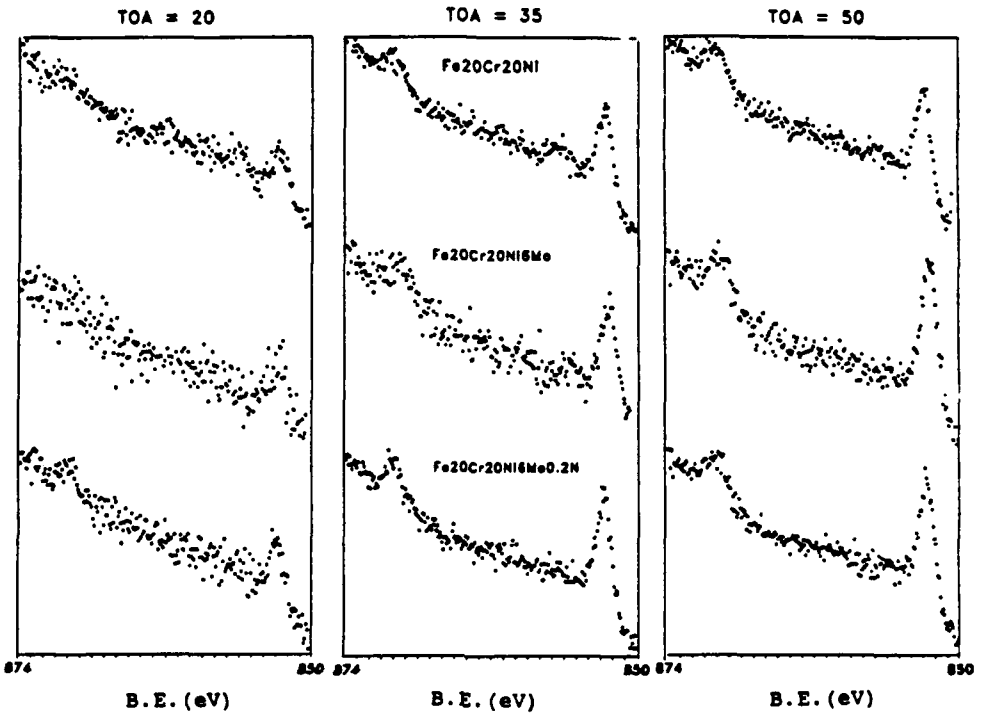

Figure 5.10 Ni2p XPS spectra for high Ni stainless steels polarized at -100 mV for 10 min 0.1M HCl + 0.4M NaCl at room temperature.

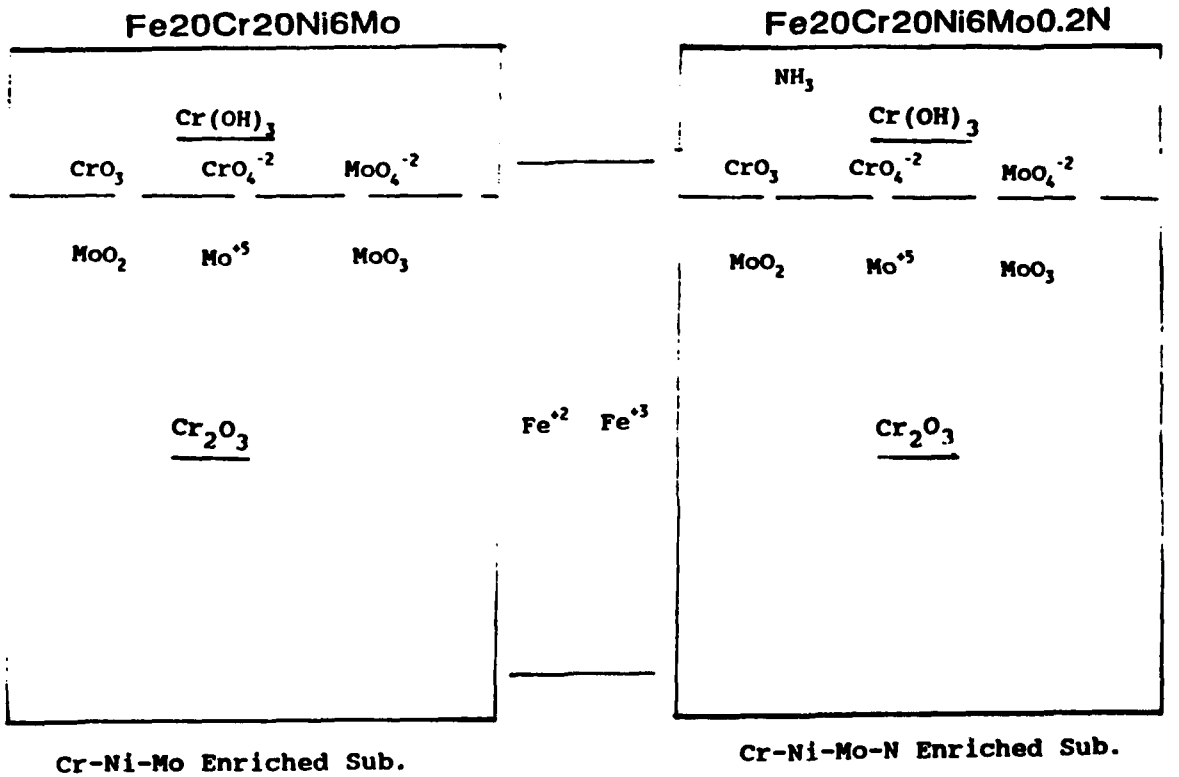

Figure 5.11 Passive film structures of Mo bearing stainless steels polarized at -100 mV for 10 min in 0.1M HCl + 0.4M NaCl at room temperature.

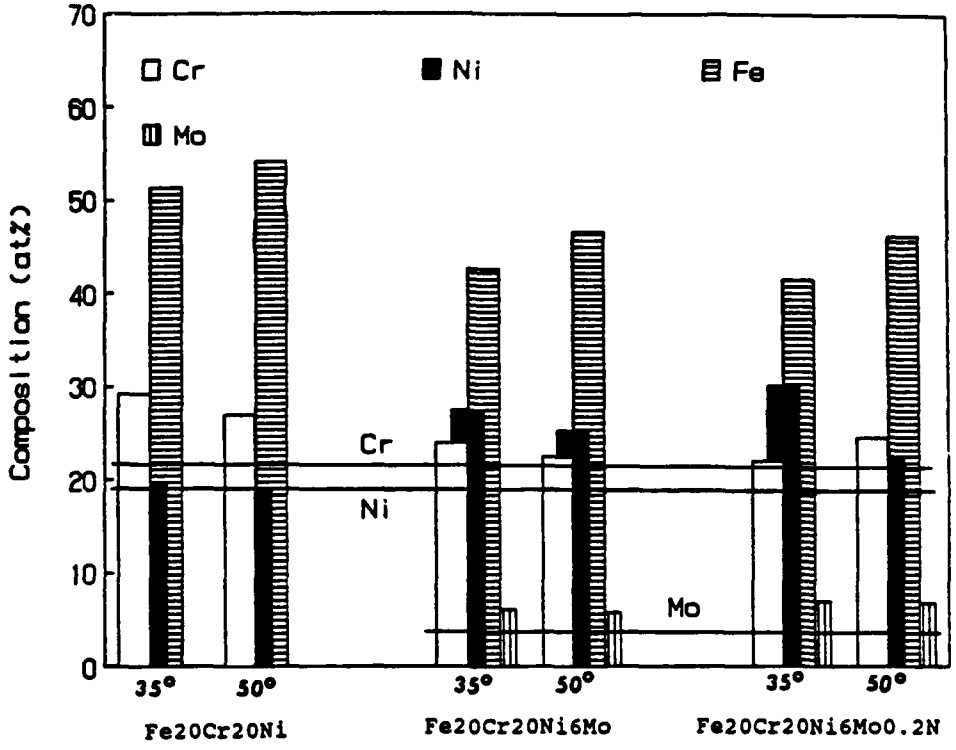

Figure 5.12 Metallic element compositions underneath the passive film for high Ni alloys.

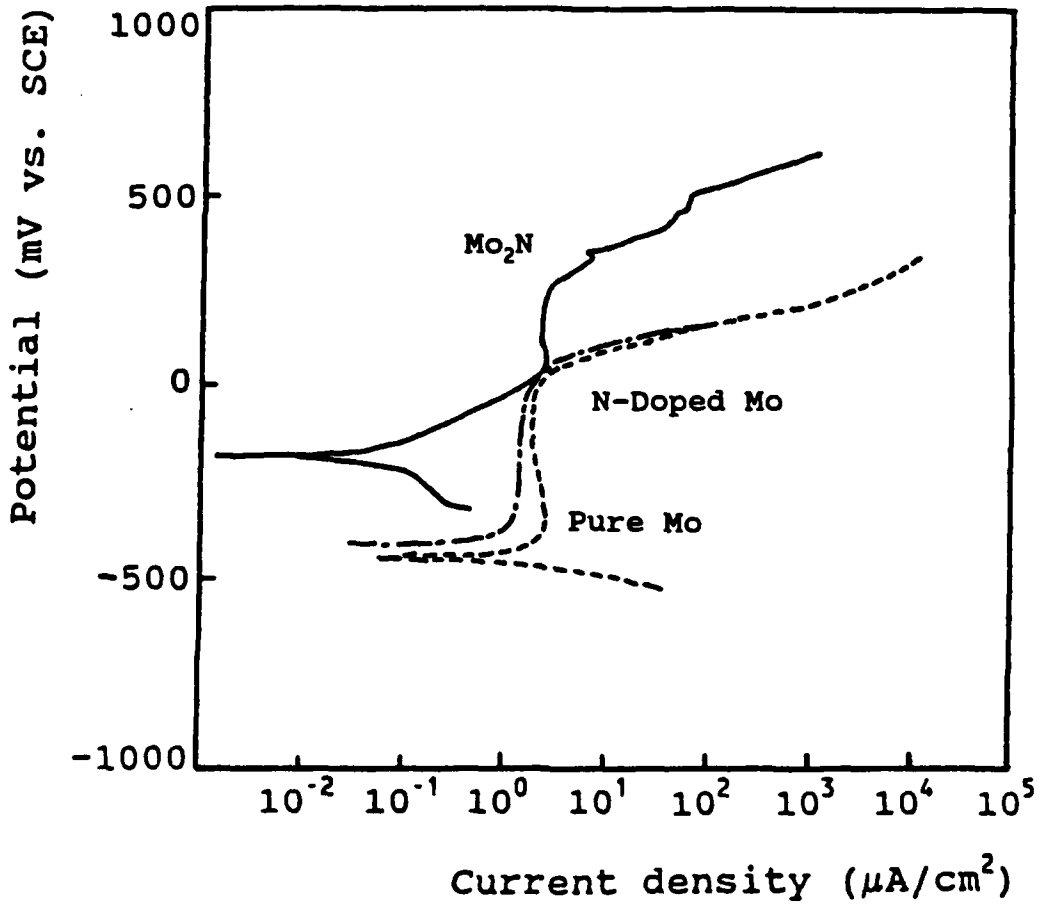

Figure 5.13 Potentiodynamic polarization curves for pure Mo in 0.1M HCl at room temperature.

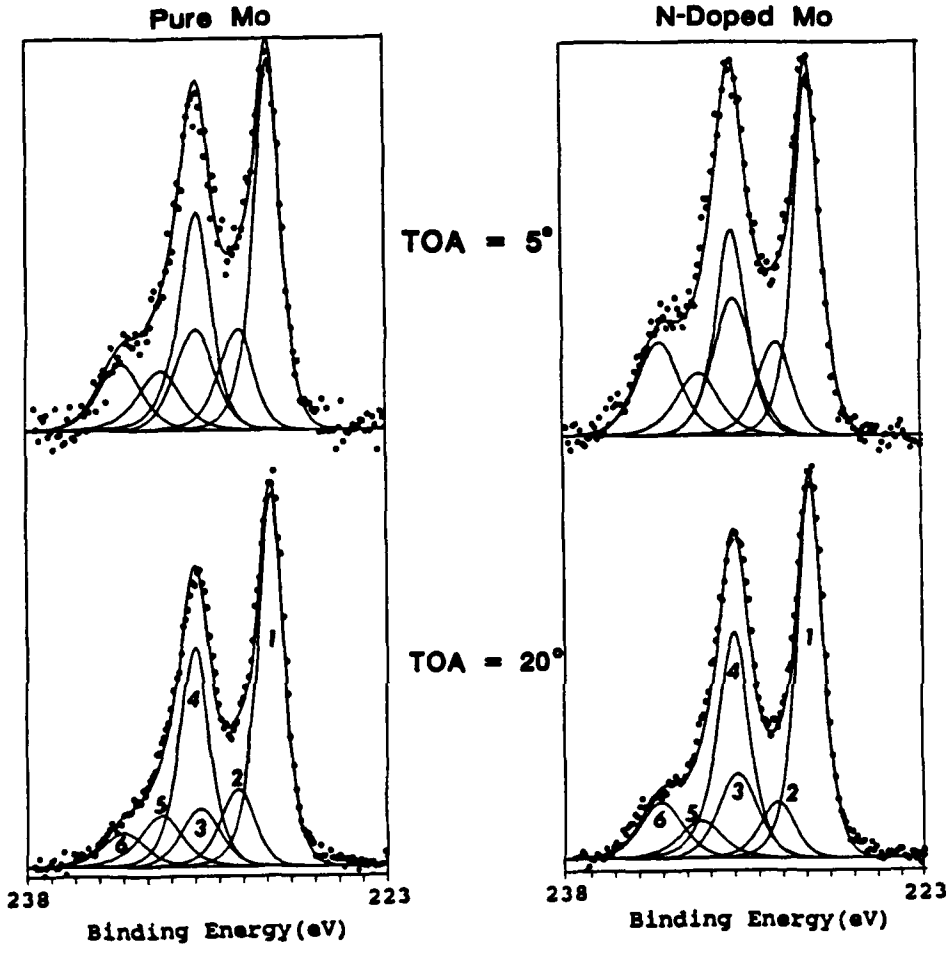

Figure 5.14 Mo3d XPS spectra for pure Mo and nitrate treated Mo polarized at 50 mV for 1 hour in deaerated 0.1M HCl at room temperature.

$Mo3d_{5/2}$ 1: Mo(met), 2: Mo^{+4}, 3: Mo^{+5}
$Mo3d_{3/2}$ 4: Mo(met), 5: Mo^{+4}, 6: Mo^{+5}

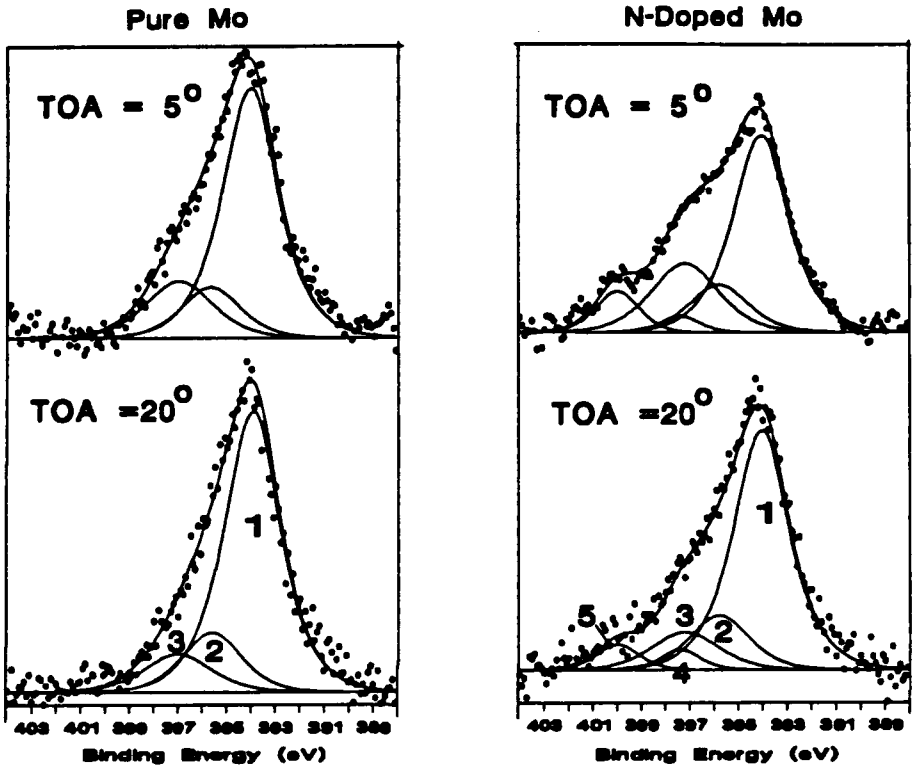

Figure 5.15 N1s and Mo3p XPS spectra for pure Mo and nitrate treated Mo polarized at 50 mV for 1 hour in deaerated 0.1M HCl at room temperature.

$Mo3p_{3/2}$ 1: Mo(met), 2: Mo^{+4}, 3: Mo^{+5}
N1s 4: Nitride, 5: NH_3

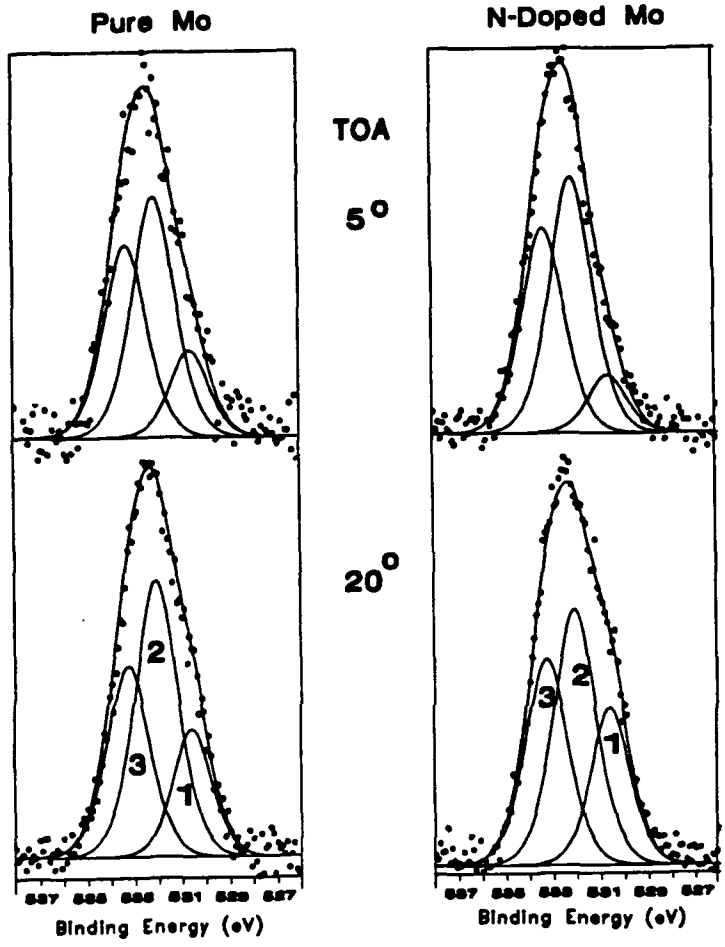

Figure 5.16 O1s XPS spectra for pure Mo and nitrate treated Mo polarized at 50 mV for 1 hour in deaerated 0.1M HCl at room temperature.

1: O^{-2}, 2: OH^-, 3: H_2O

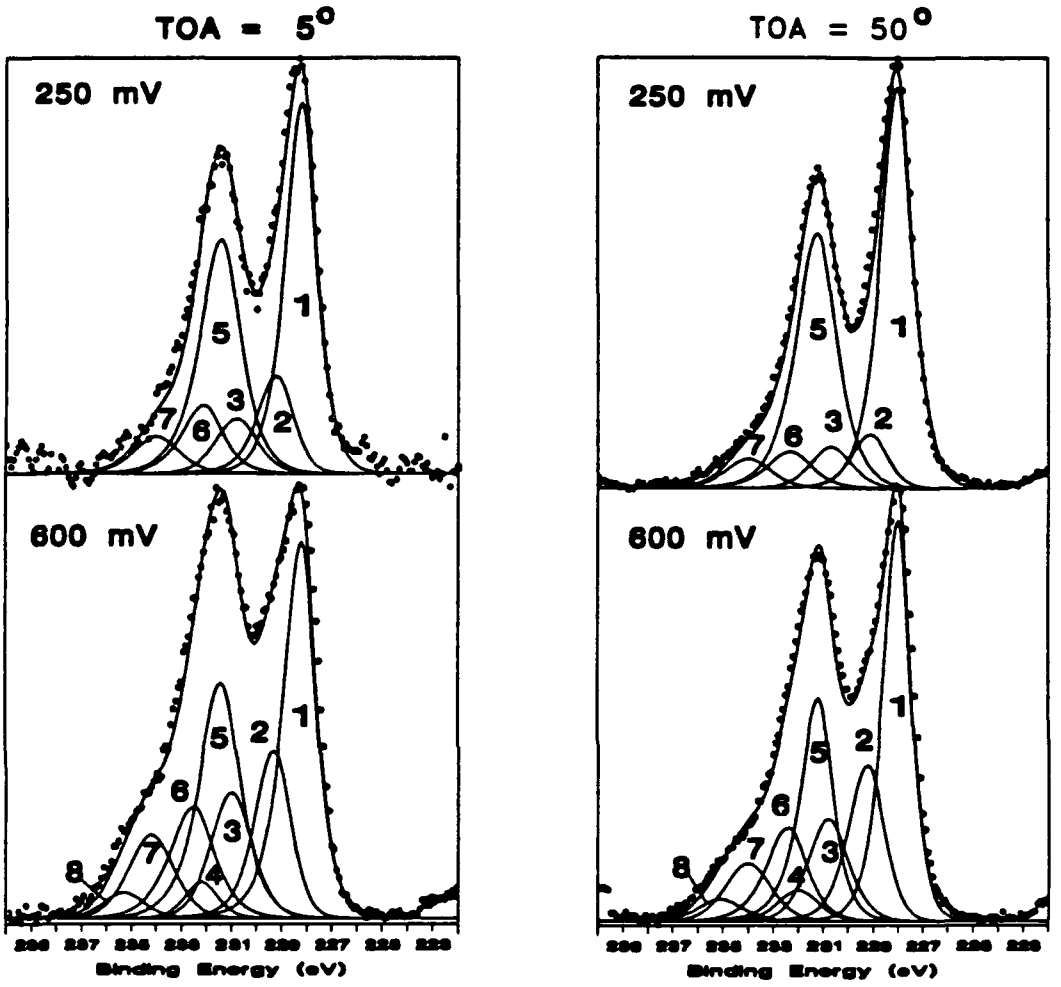

Figure 5.17 Mo3d XPS spectra for nitrided Mo polarized at 250 mV for 1 hour and at 600 mV for 3 min in deaerated 0.1M HCl at room temperature.

$Mo3d_{5/2}$ 1: Mo_2N, 2: Mo^{+4}, 3: Mo^{+5}, 4: MoO_4^{-2}
$Mo3d_{3/2}$ 5: Mo_2N, 6: Mo^{+4}, 7: Mo^{+5}, 8: MoO_4^{-2}

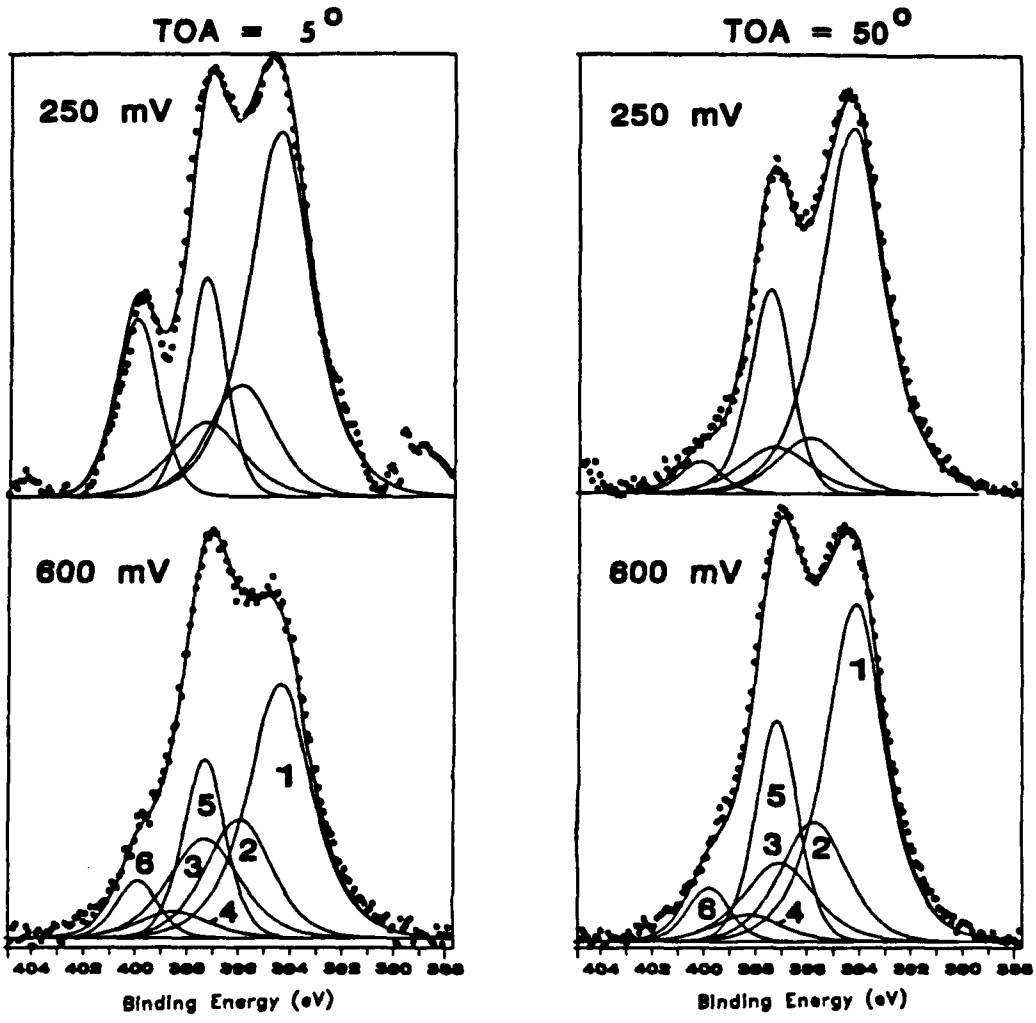

Figure 5.18 N1s and Mo3p XPS spectra for nitrided Mo polarized at 250 mV for 1 hour and at 600 mV for 3 min in deaerated 0.1M HCl at room temperature.

$Mo3p_{3/2}$ 1: Mo_2N, 2: MoO_2, 3: Mo^{+5}, 4: MoO_4^{-2}
N1s 5: Nitride, 6: NH_3

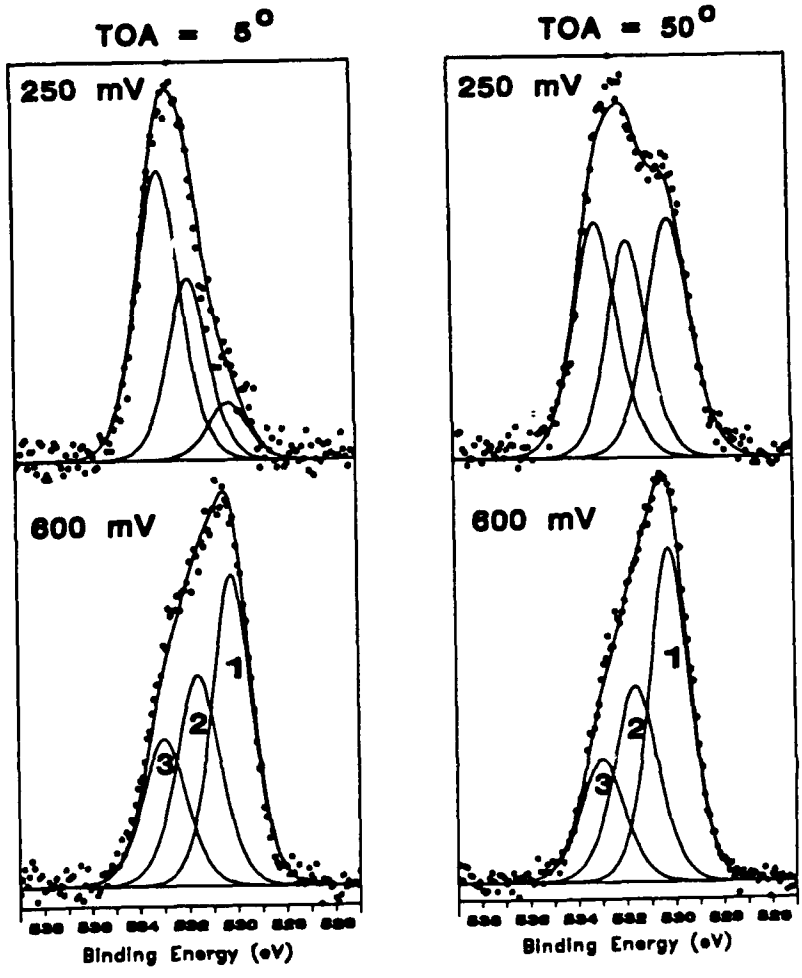

Figure 5.19 O1s XPS spectra for nitrided Mo polarized at 250 mV for 1 hour and at 600 mV for 3 min in deaerated 0.1M HCl at room temperature.

1: O^{-2}, 2: OH^{-}, 3: H_2O

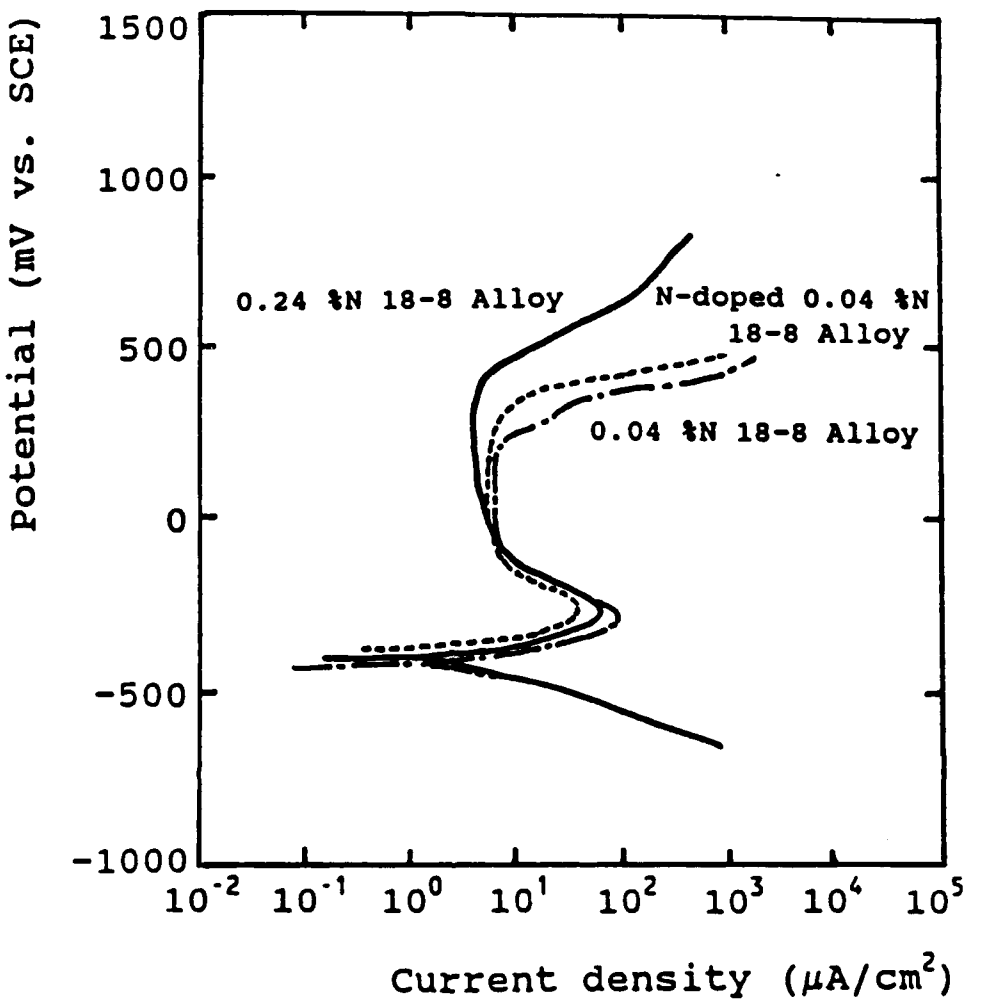

Figure 5.20 Polarization curves for 18-8 (304) stainless steels in deaerated 0.1M HCl at room temperature.

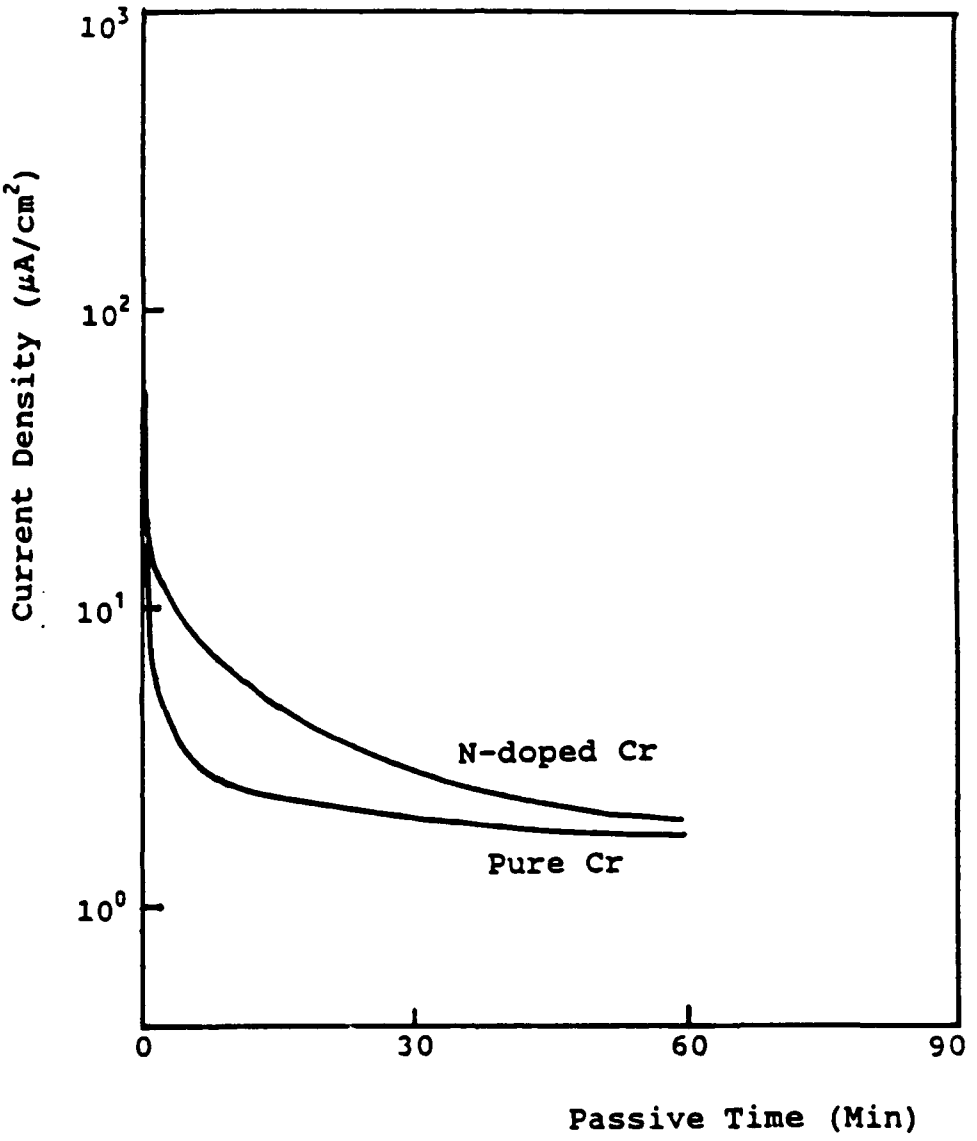

Figure 5.21 Passive current density vs. time curves for pure Cr passivated in 0.1M HCl at -180 mV(SCE).

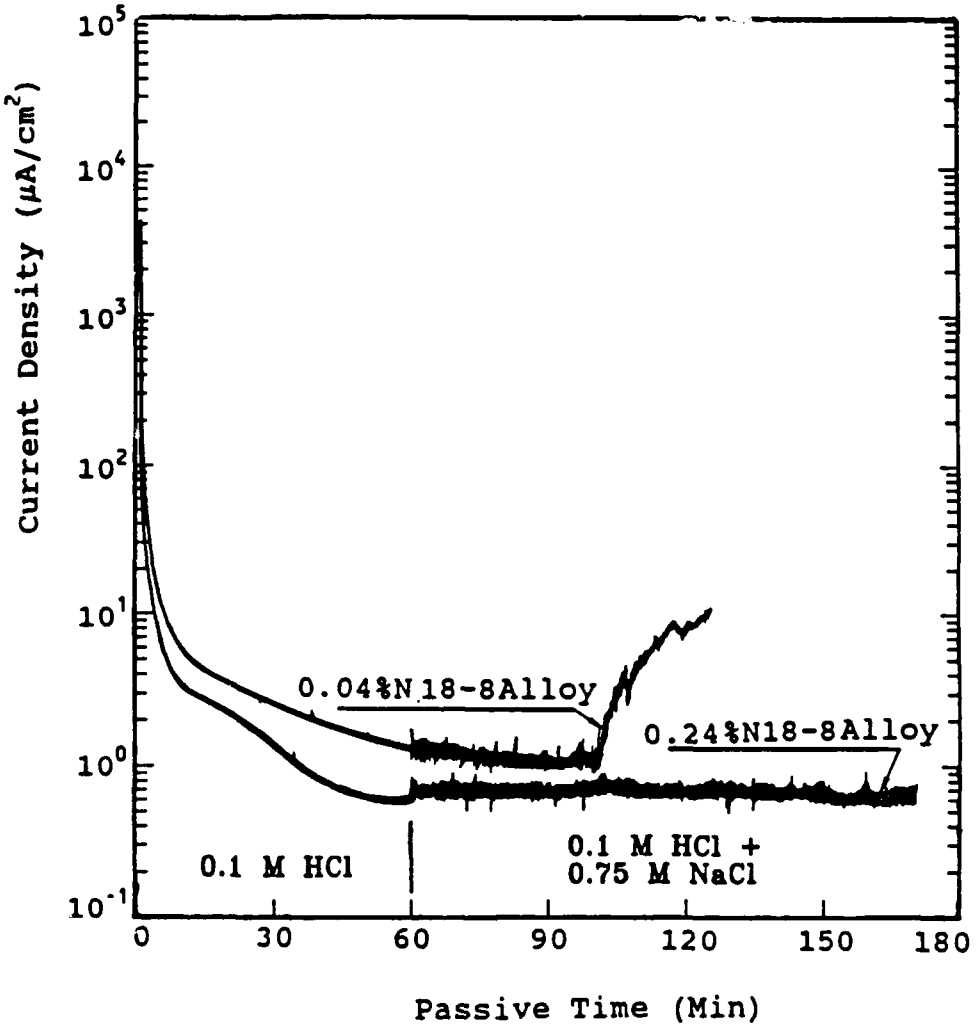

Figure 5.22 Measurements of induction time to pitting of passive films formed on 18-8 stainless steels in 0.1M HCl at -180 mV.

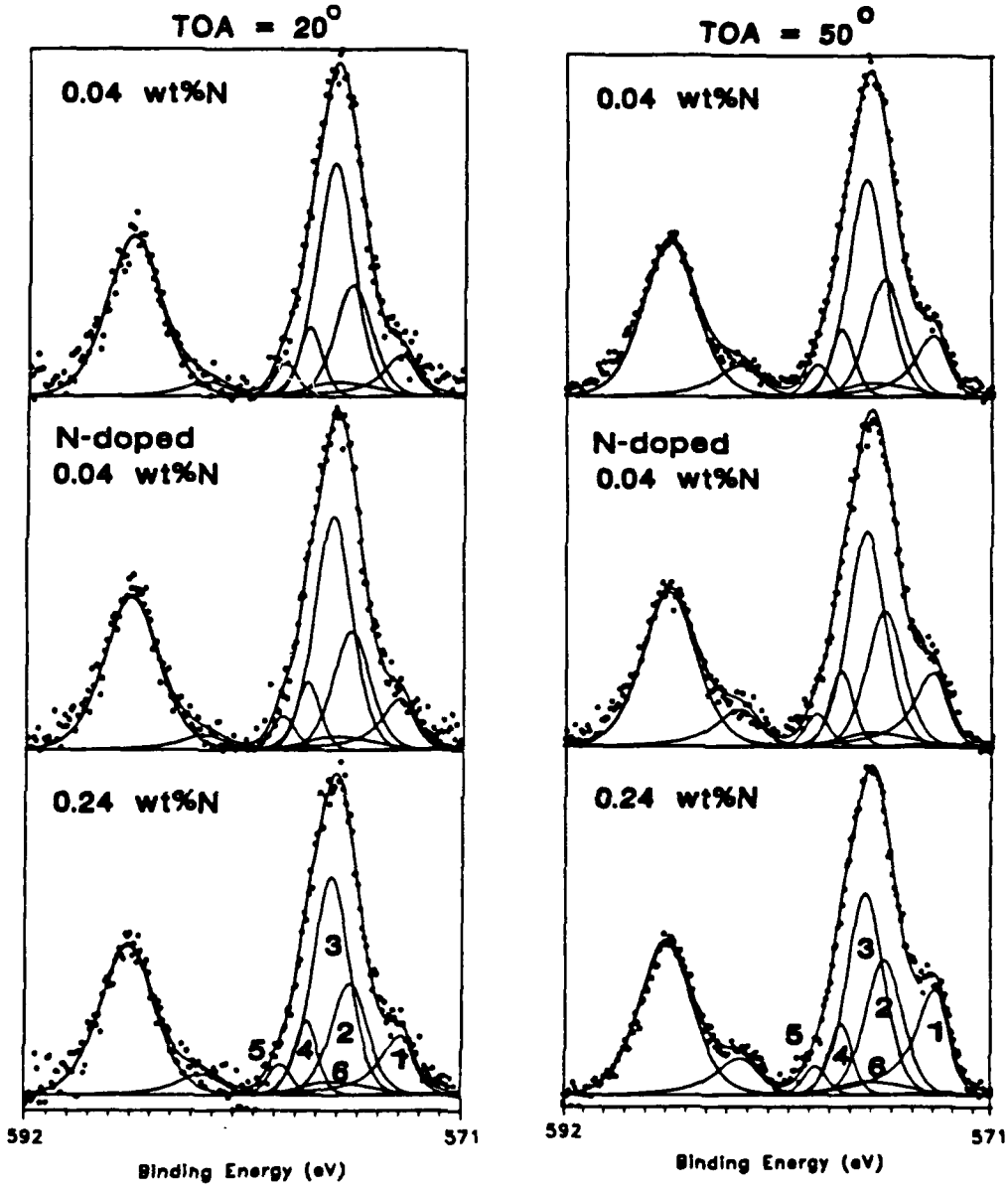

Figure 5.23 Cr2p XPS spectra for the passive films of 18-8 alloys polarized at -180 mV for 6 hours in 0.1M HCl.

1: Cr(met), 2: Cr_2O_3, 3: $Cr(OH)_3$, 4: CrO_3, 5: CrO_4^{-2}
6: Satellite

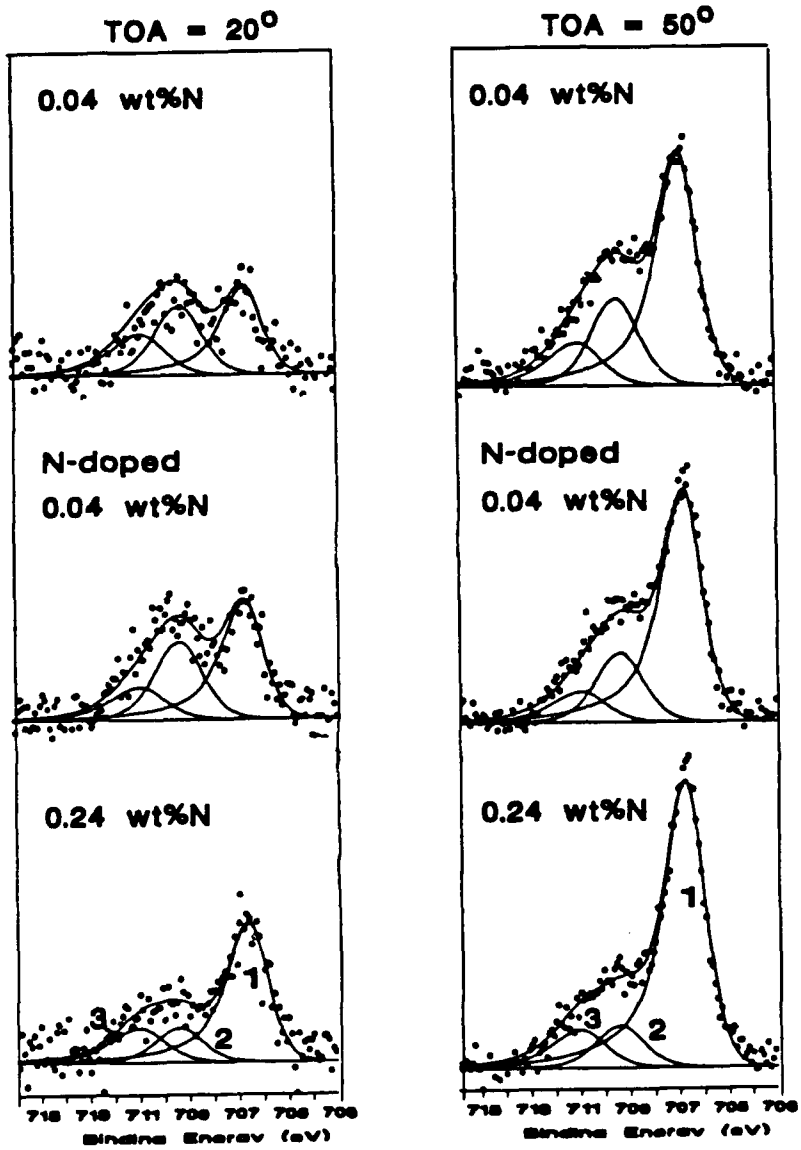

Figure 5.24 Fe2p XPS spectra for the passive films of 18-8 alloys polarized at -180 mV for 6 hours in 0.1M HCl.

1: Fe(met), 2: Fe^{+2}, 3: Fe^{+3}

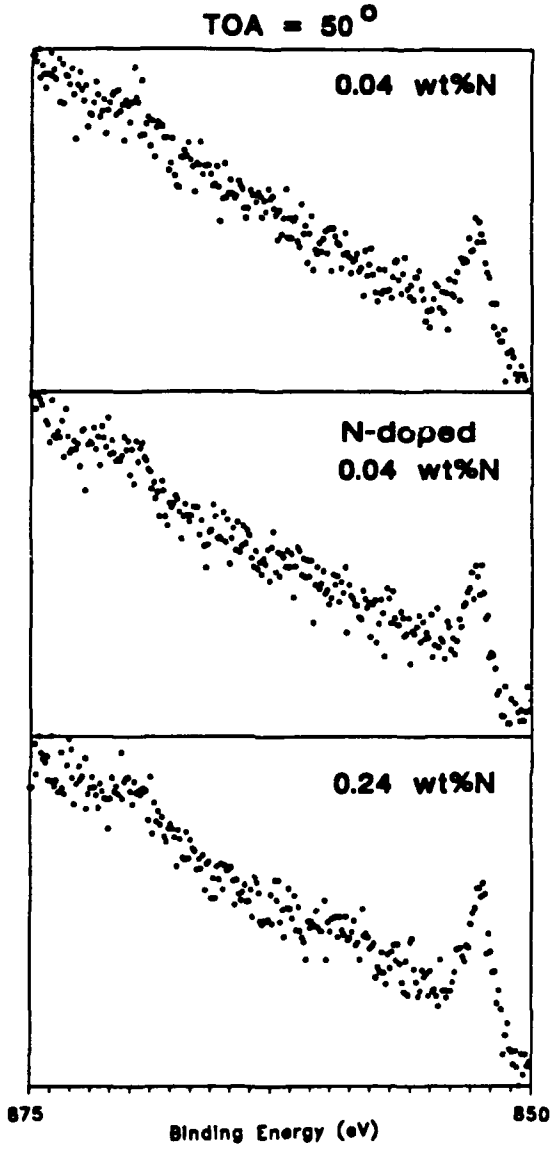

Figure 5.25 Ni2p XPS spectra for the passive films of 18-8 alloys polarized at -180 mV for 6 hours in 0.1M HCl.

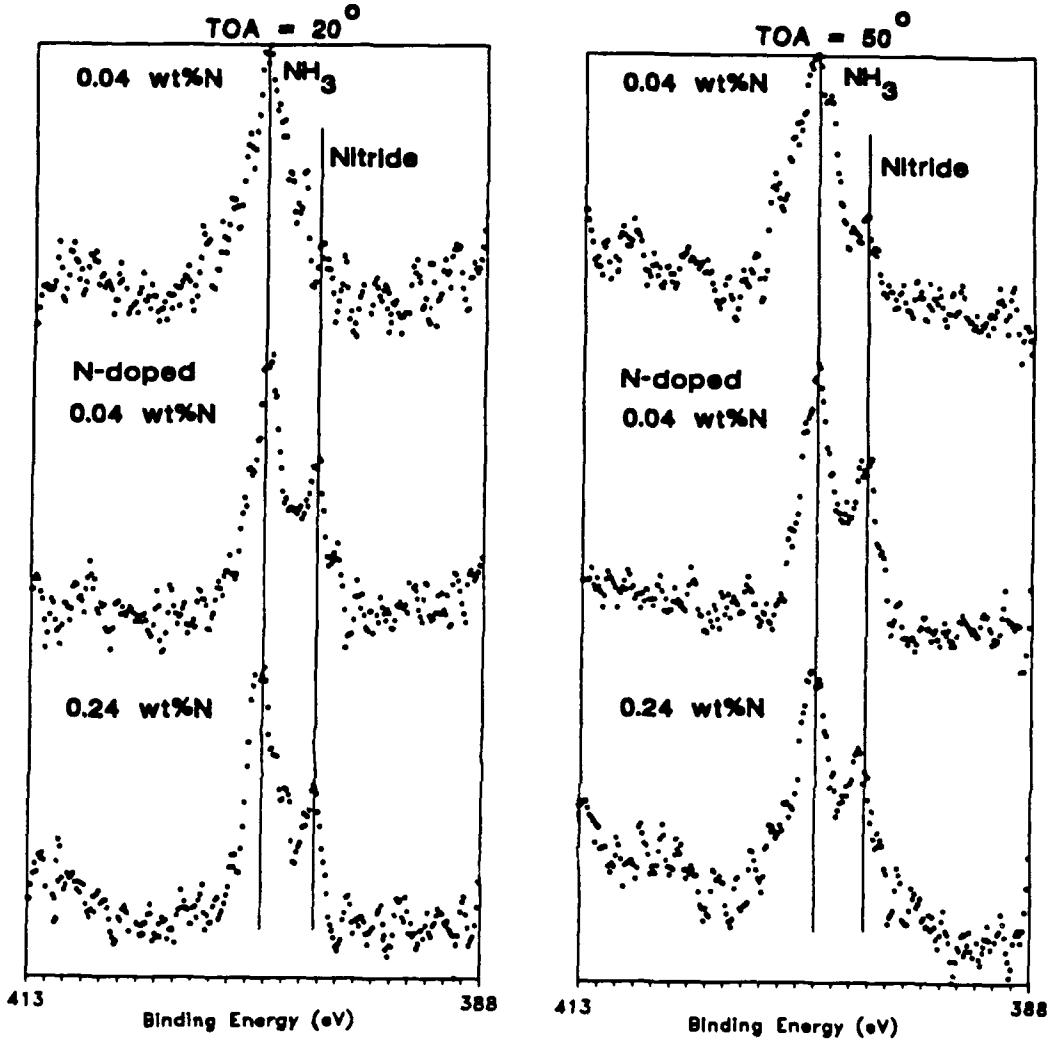

Figure 5.26 N1s XPS spectra for the passive films of 18-8 alloys polarized at -180 mV for 6 hours in 0.1M HCl.

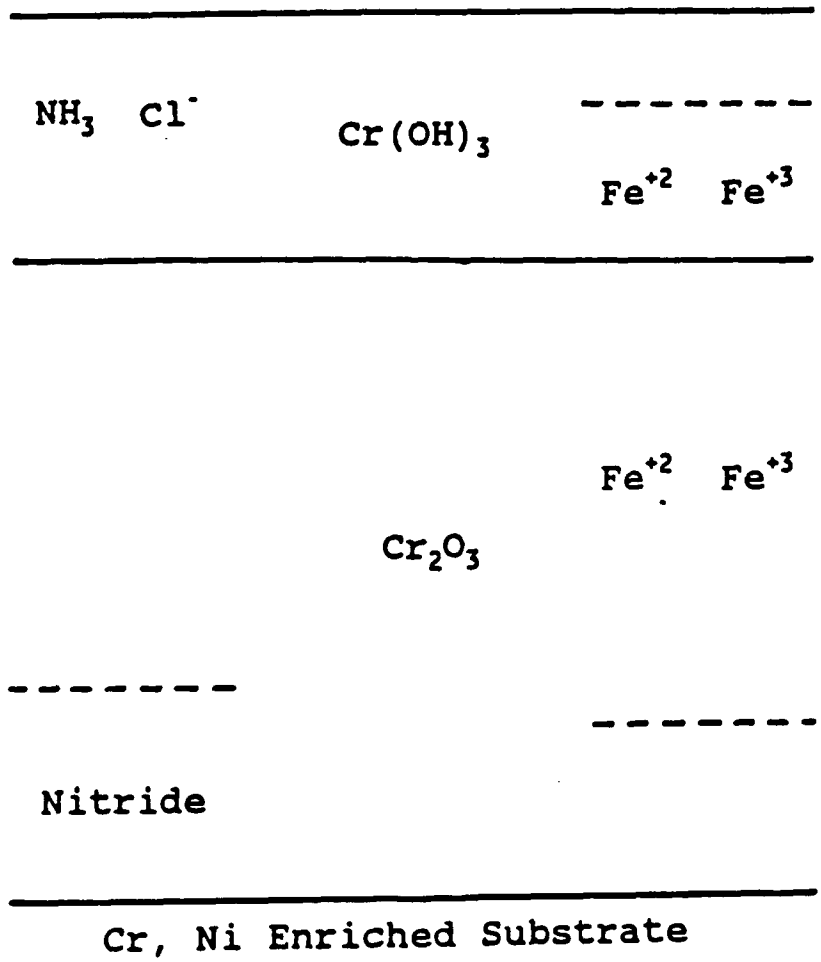

Figure 5.27 Passive film structure of 18-8 stainless steel polarized at -180 mV in Cl^- solution.

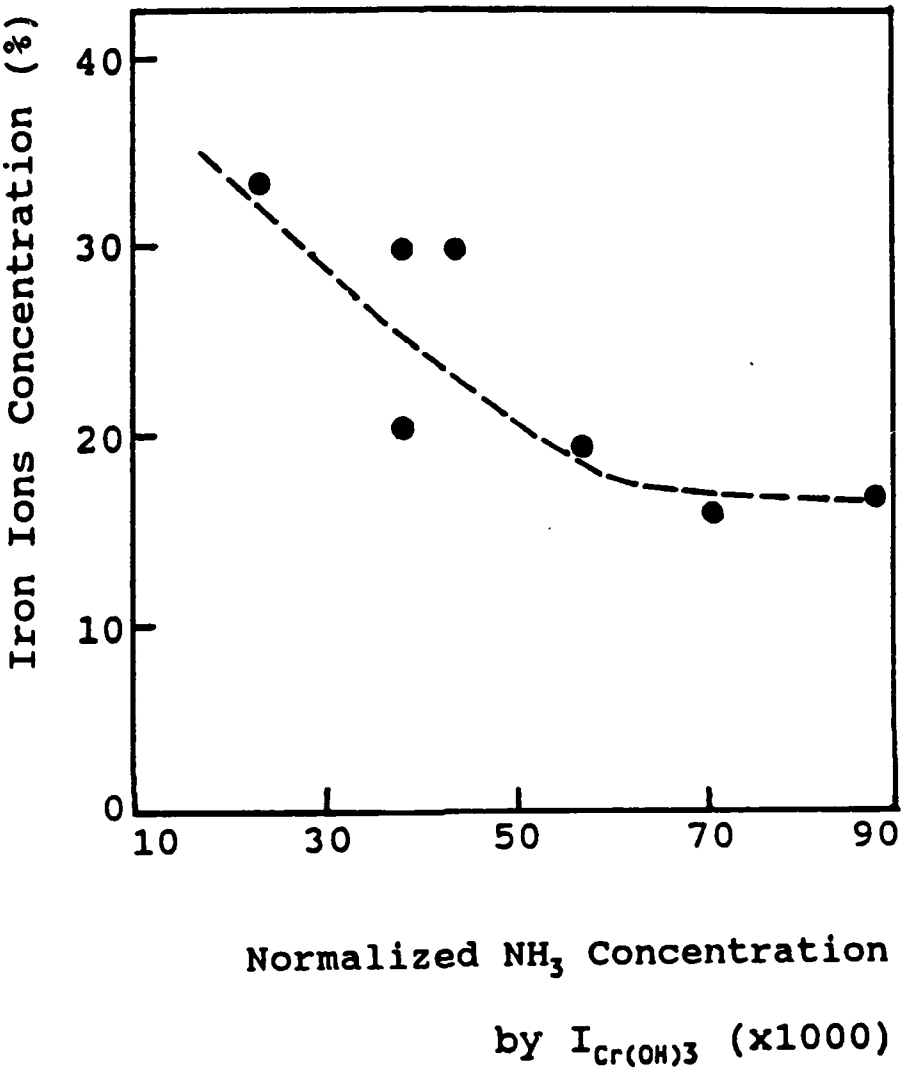

Figure 5.28 Relation between Fe ions and NH_3 concentrations in the passive films formed on 18-8 stainless steels at -180 mV in Cl^- solution.

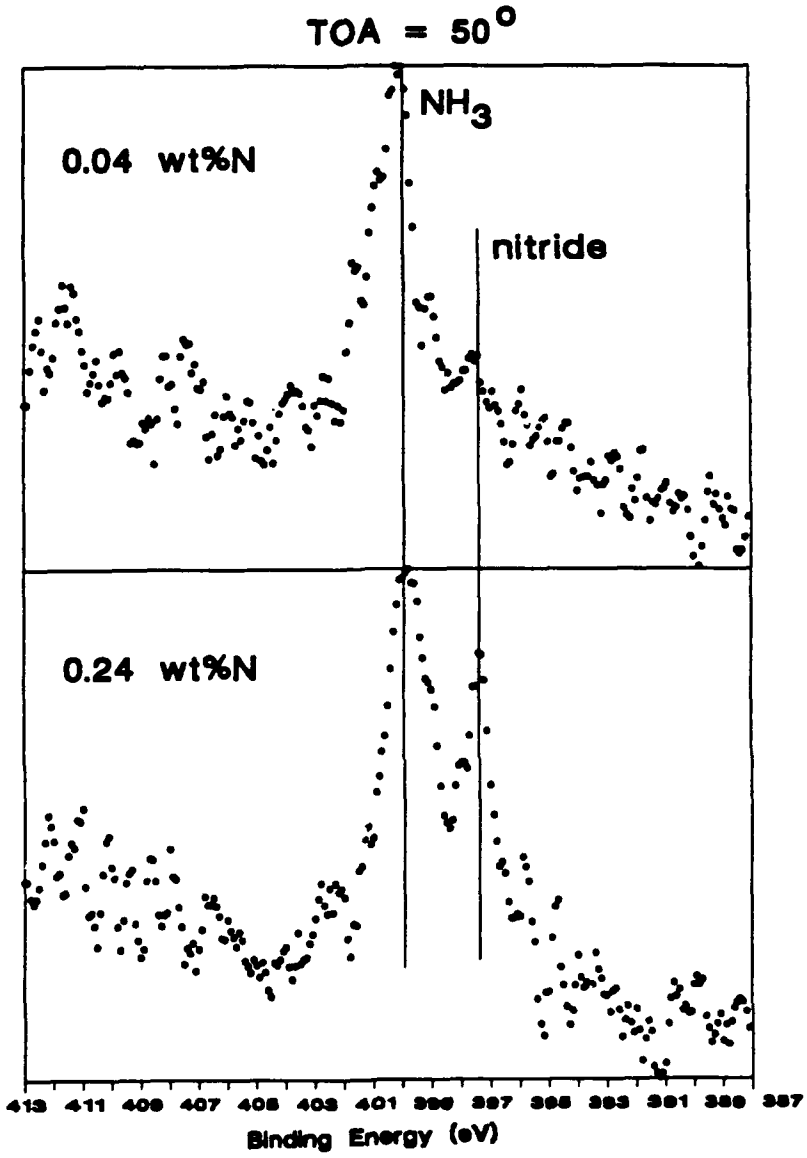

Figure 5.29 N1s XPS spectra for the passive films of 18-8 alloys polarized at -180 mV for 1 hour in 0.1M HCl and further polarized for 30 min in 0.1M HCl + 0.75M NaCl.

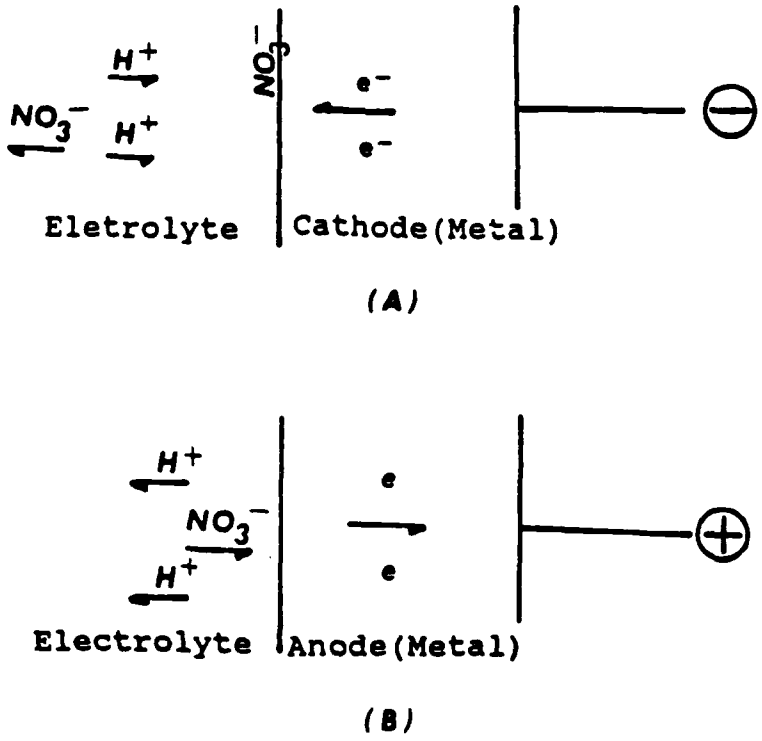

Figure 6.1 Schematic of ion movements, when applied voltage is (a) negative, (b) positive.

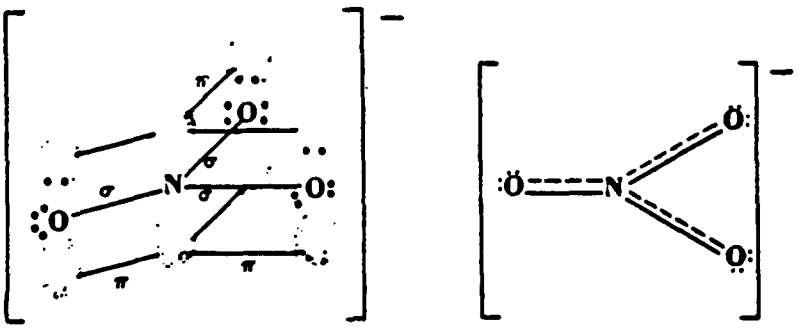

Figure 6.2 Bond structure of NO_3^- ion.

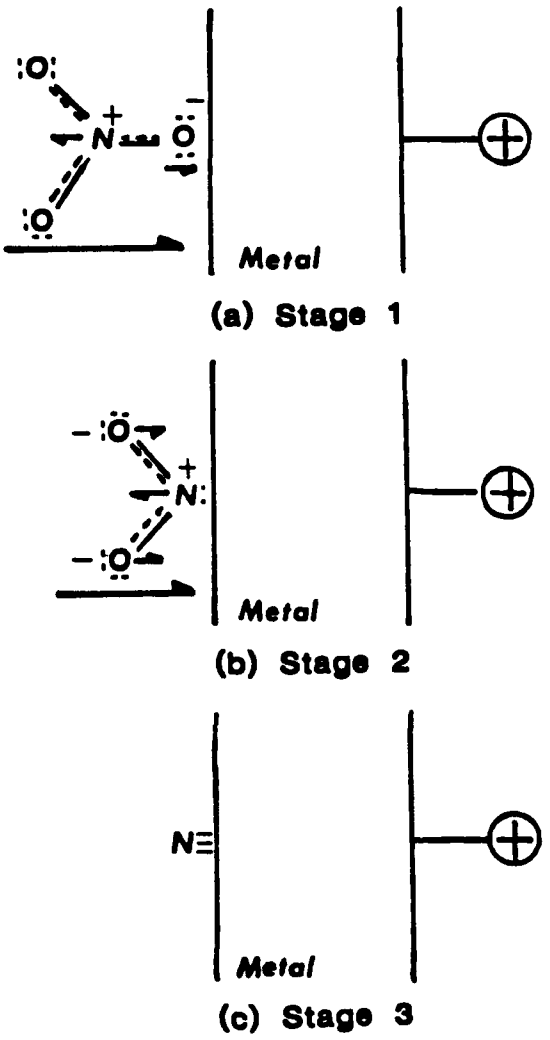

Figure 6.3 Surface effect of NO_3^- reduction at high anodic potential.

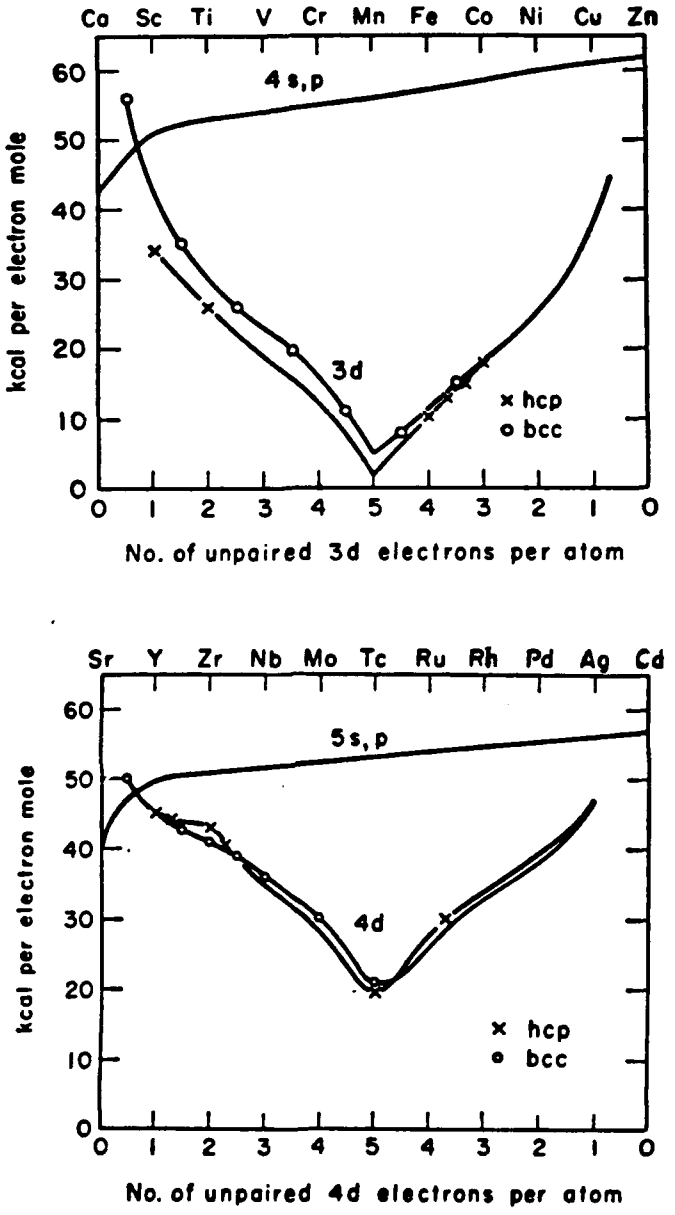

Figure 6.4 Valence-state bonding enthalpy per unpaired 4d and 5d electrons.[87]

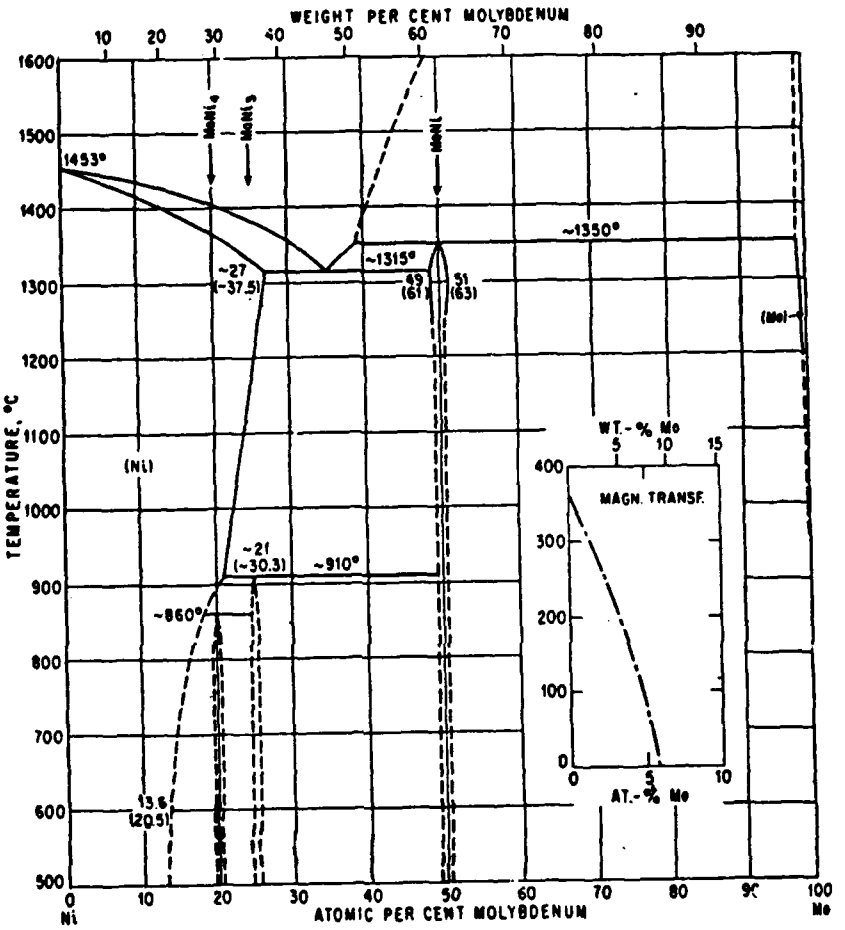

Fig. 537. Mo-Ni

Figure 6.6 Mo-Ni phase diagram [89)]

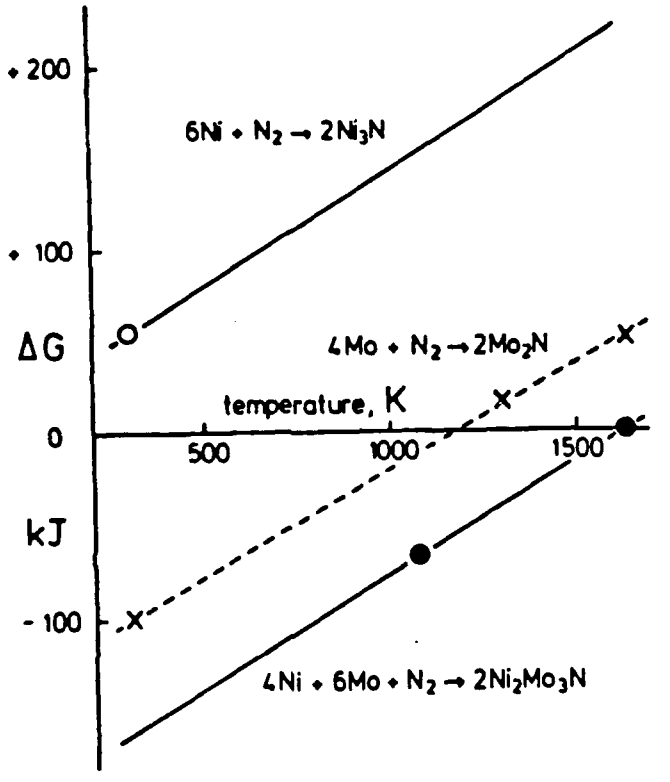

Figure 6.5 Free energies of the reactions to form Ni_3N, Mo_2N and β^m-Ni_2Mo_3N.[35]

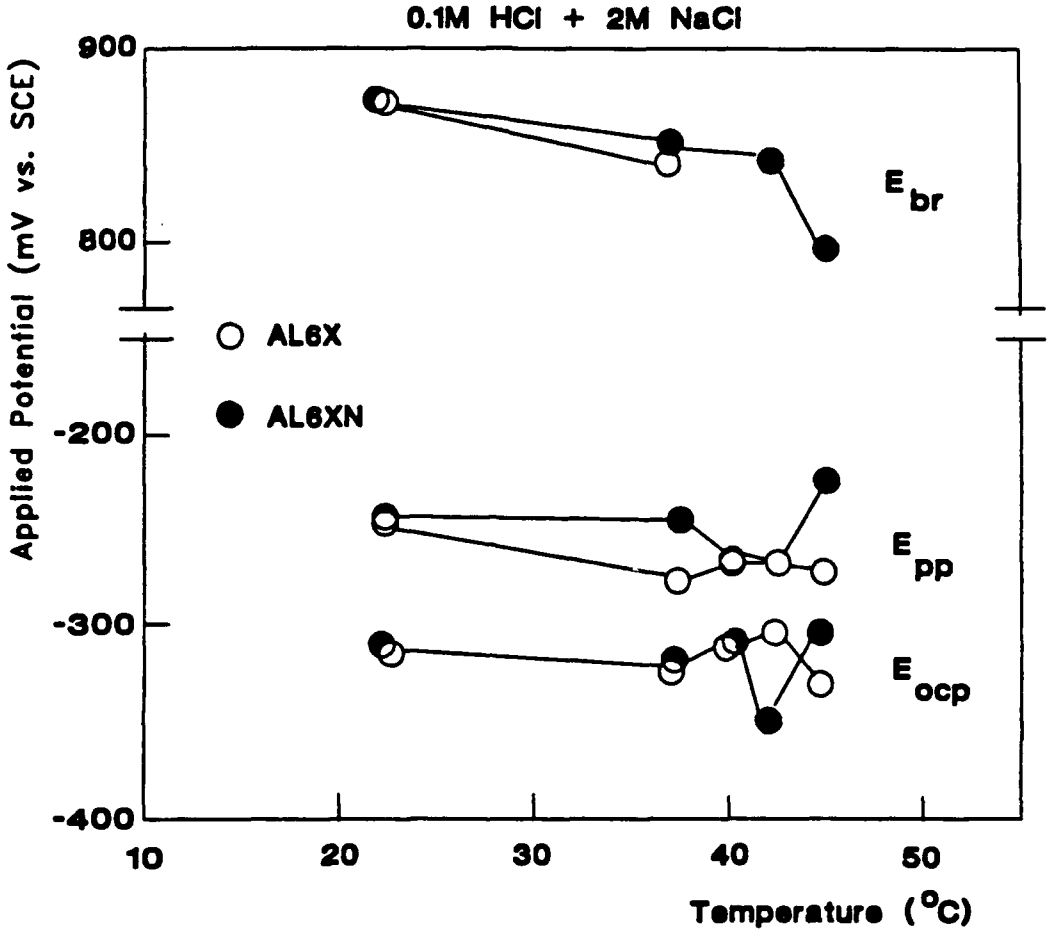
0.1M HCl + 2M NaCl
900
800
-200
-300
-400
Applied Potential (mV vs. SCE)
AL6X
AL6XN
E br
E pp
E ocp
10
20
30
40
50
Temperature (°C)

Figure 8.1 (a)

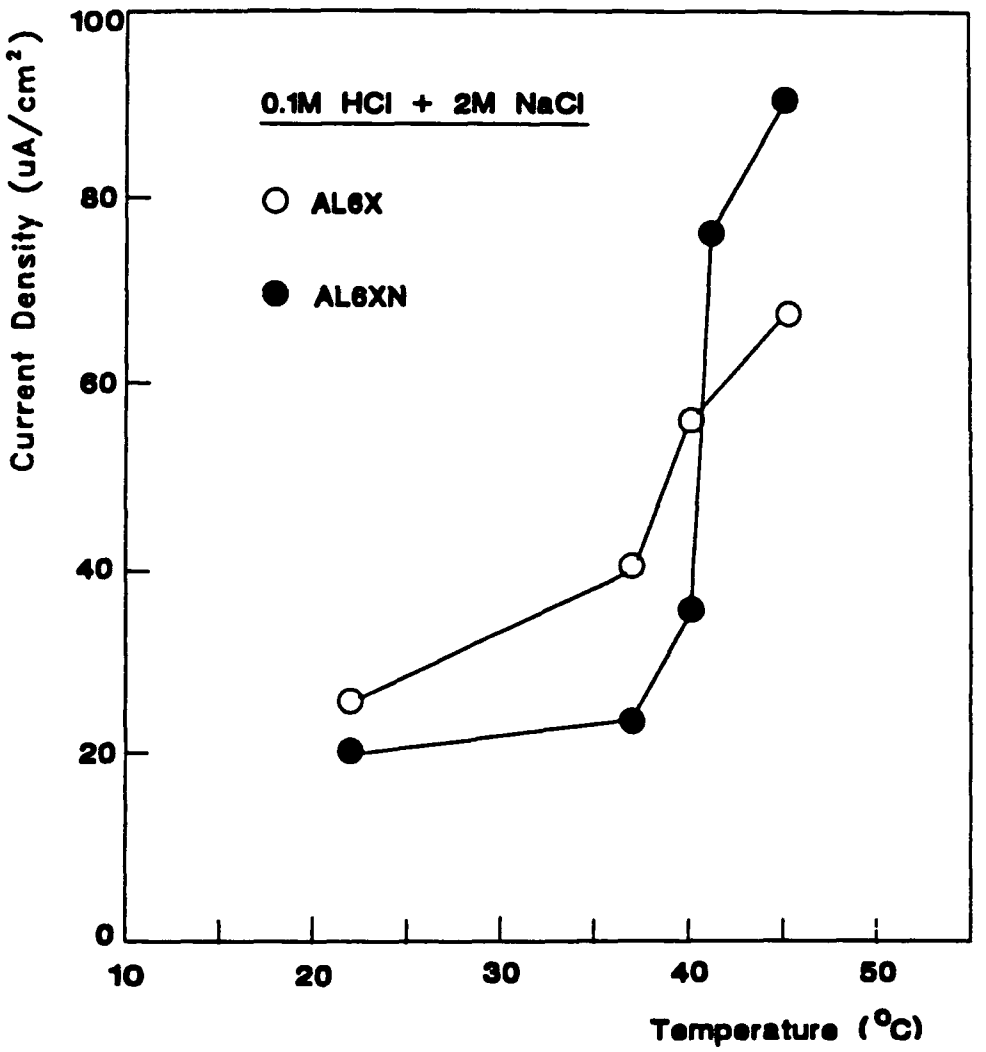
0.1M HCl + 2M NaCl
AL6X
AL6XN
Current Density (uA/cm²)
100
80
60
40
20
0
10
20
30
40
50
Temperature (°C)

Figure 8.1 (b)

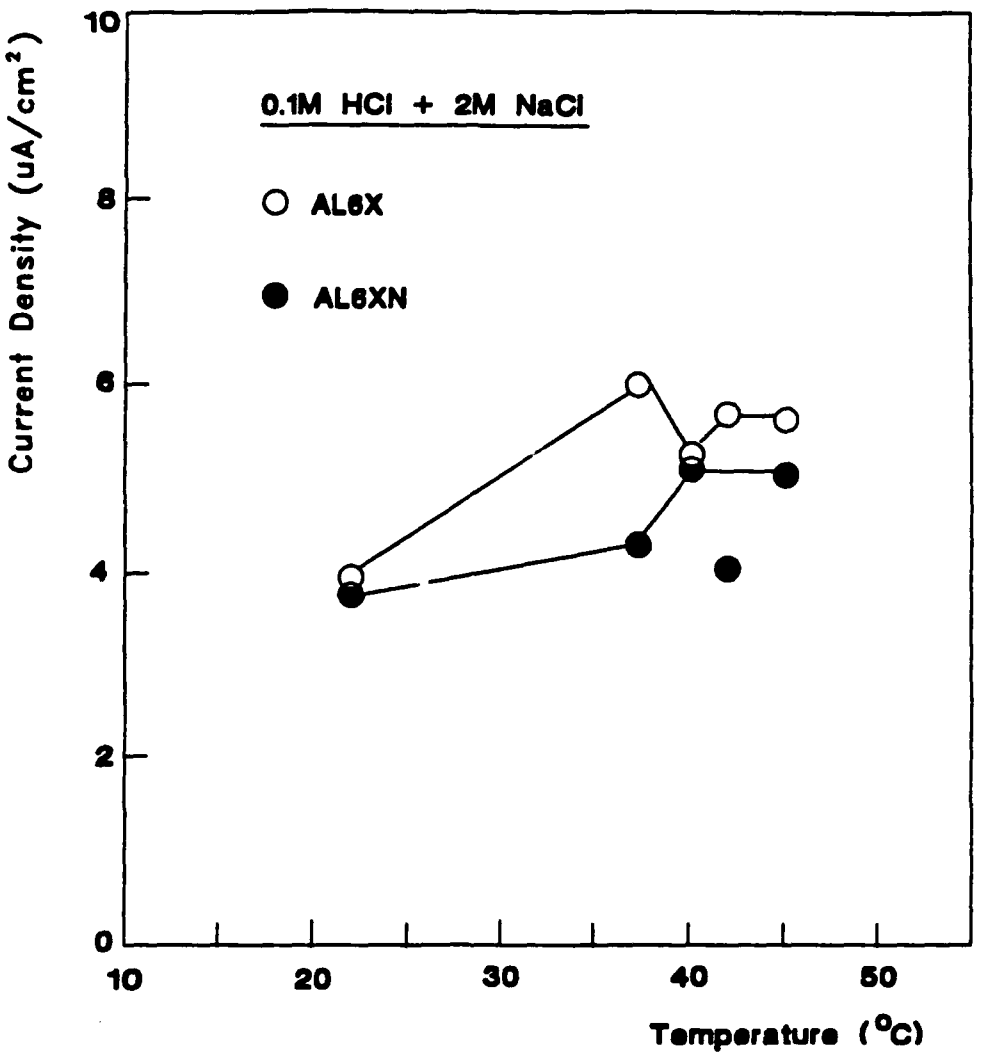

(c)

Figure 8.1 Salient electrochemical characteristics vs. temperature for AL6X and AL6XN alloys polarized in 0.1M + 2M NaCl. (a) Potentials(E_{br}, E_{pp} and E_{ocp}), (b) Critical current density(I_{crit}) and (c) Passivation current density(I_{pass})

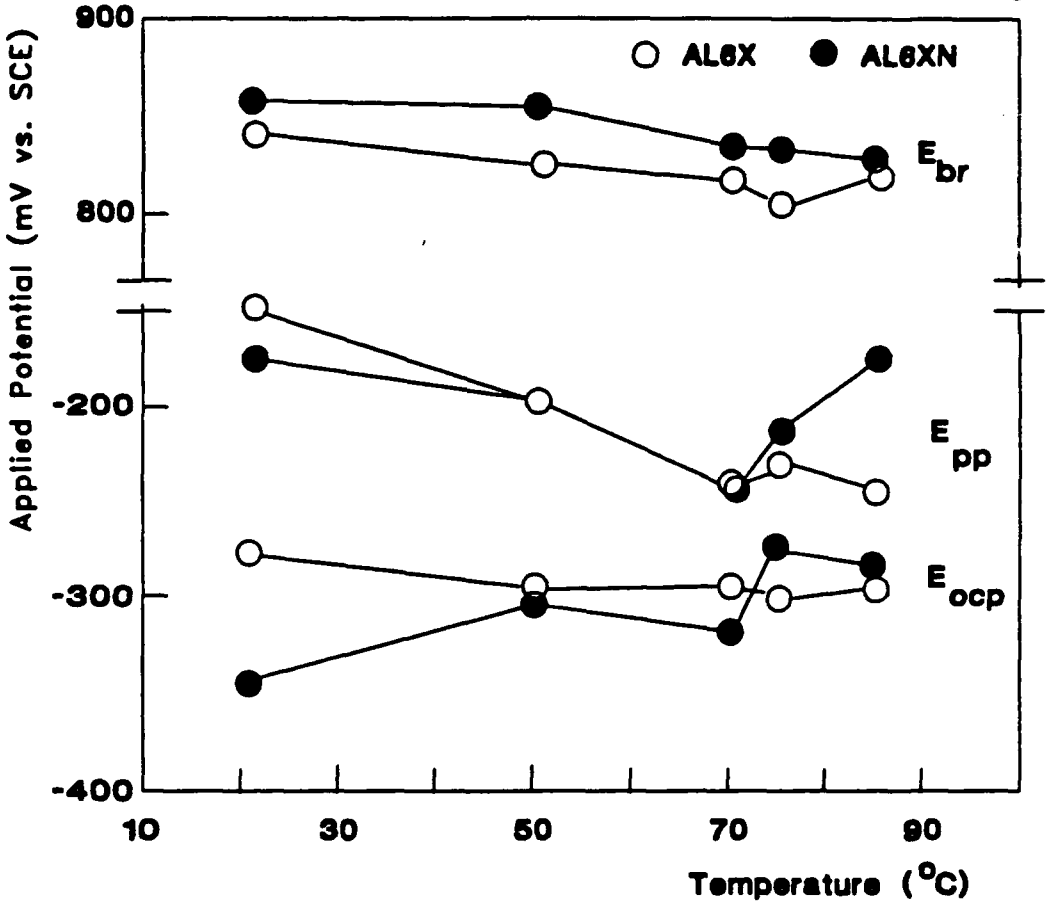
900
800
-200
-300
-400
10
30
50
70
90
Applied Potential (mV vs. SCE)
Temperature (°C)
AL6X
AL6XN
E br
E pp
E ocp

Figure 8.2 (a)

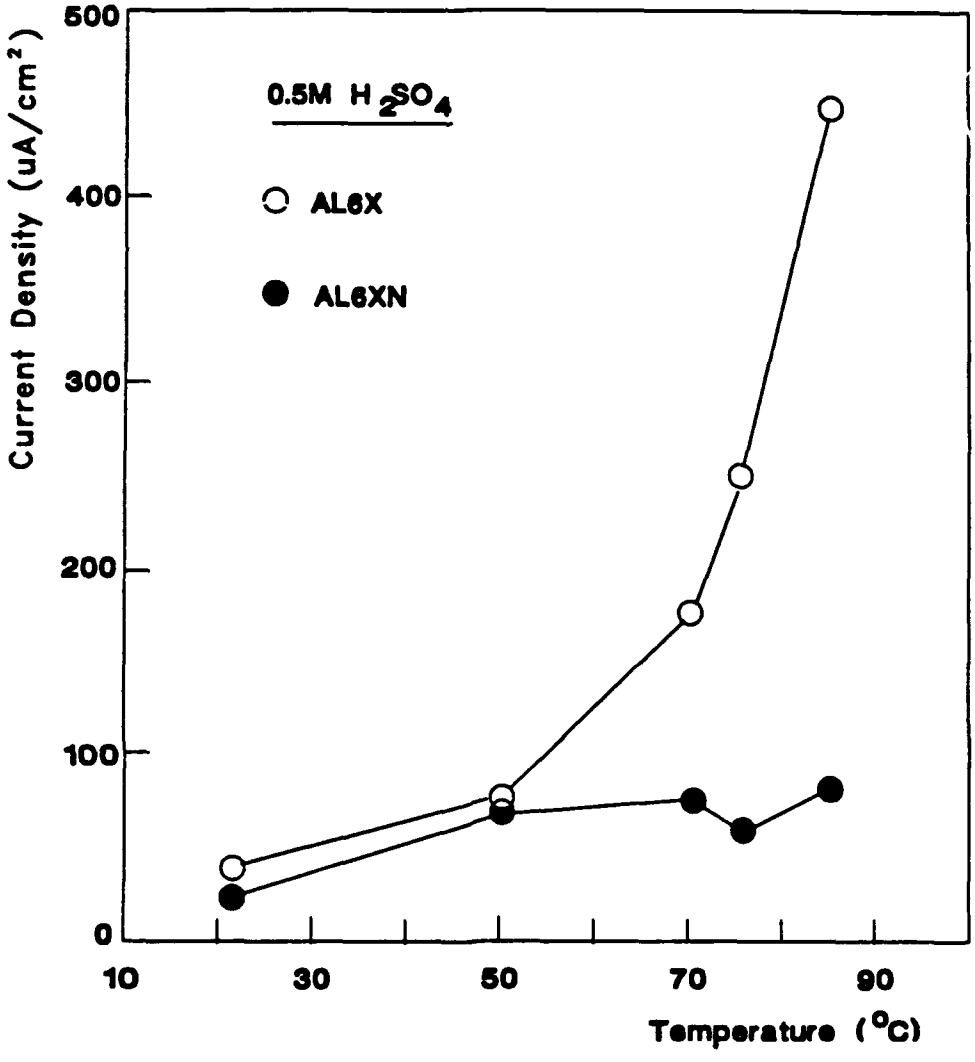
500
400
300
200
100
0
Current Density (uA/cm²)
0.5M H2SO4
AL6X
AL6XN
10
30
50
70
90
Temperature (°C)

Figure 8.2 (b)

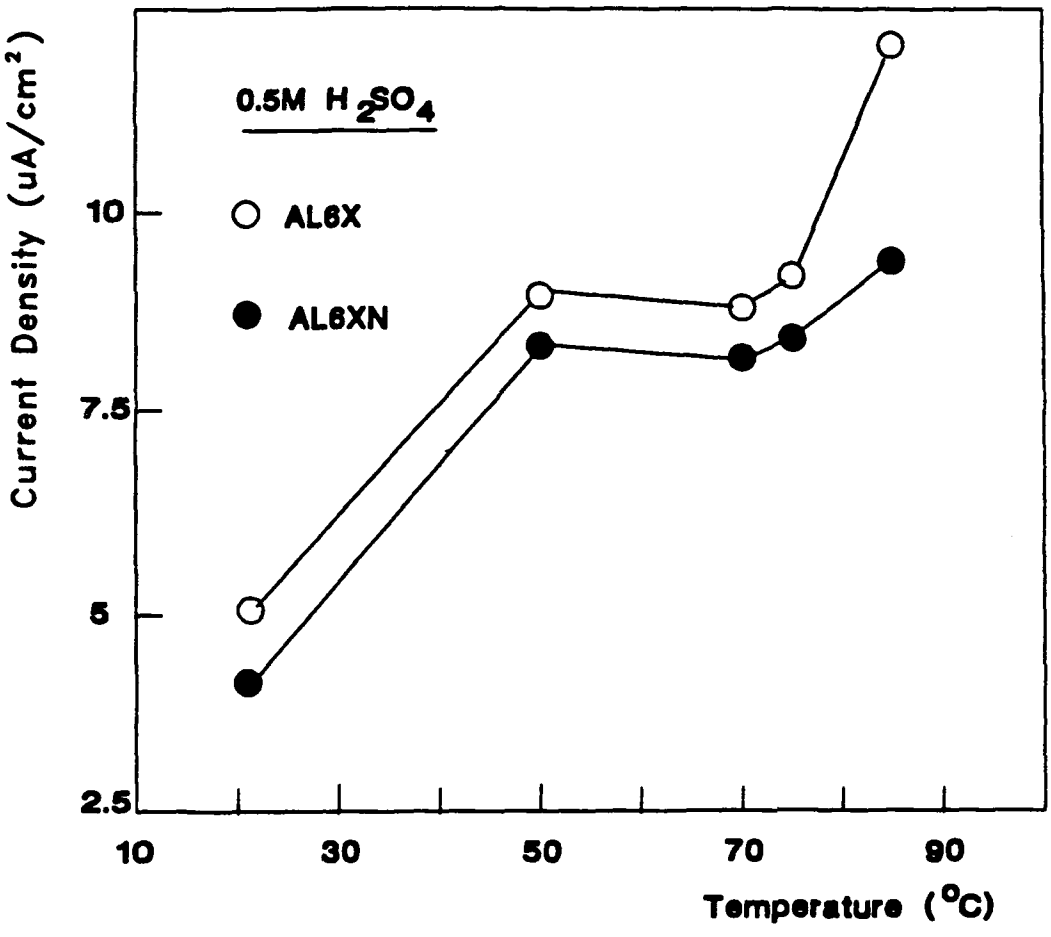

(c)

Figure 8.2 Salient electrochemical characteristics vs. temperature for AL6X and AL6XN alloys polarized in 0.5M H_2SO_4. (a) Potentials(E_{br}, E_{pp} and E_{ocp}), (b) Critical current density(I_{crit}) and (c) Passivation current density(I_{pass})